

Copyright
By
Stephen Wroe Foster
2010

The thesis committee for Stephen Wroe Foster
certifies that this is the approved version of the following thesis:

Reducing Top Mat Reinforcement in Bridge Decks

**APPROVED BY
SUPERVISING COMMITTEE:**

James O. Jirsa, Supervisor

Oguzhan Bayrak

Reducing Top Mat Reinforcement in Bridge Decks

by

Stephen Wroe Foster, B.S.Arch.E.

Thesis

Presented to the Faculty of the Graduate School of

The University of Texas at Austin

in Partial Fulfillment

of the Requirements

for the Degree of

Master of Science in Engineering

The University of Texas at Austin

May 2010

DEDICATION

To my excellent wife Jill, for her worth is far above jewels

ACKNOWLEDGEMENTS

I would like to thank the Texas Department of Transportation and the Center for Transportation Research for the financial opportunity to work on this research. The experience has been dear to me, and I hope this research project is valuable for the great state of Texas.

I would also like to thank Dr. Jirsa, Dr. Bayrak, and Dr. Klinger for their guidance and instruction throughout this research. It has been such a wonderful privilege to learn from each of you. I could not have asked for a more distinguished set of advisors.

I would like to show my sincere appreciation to the FSEL staff—Andrew Valentine, Eric Schell, Blake Stassney, Dennis Phillip, Mike Wason, Barbara Howard, and Jessica Hanten. This thesis and all the other work at FSEL is a result of your dedication to the students and faculty.

I would also like to express my gratitude to all the students at FSEL. I will miss the camaraderie and friendship between us all; the bond between students makes FSEL the best graduate school experience in the country.

I would especially like to thank James “Locksmith” Foreman for being the best research partner I could have asked for—“A-Team” for life!

Finally, I would like to thank my family for always supporting me and encouraging me throughout my time at the University of Texas. I can never truly express how much your love for Jill and I means to us both.

April 13, 2010

Reducing Top Mat Reinforcement in Bridge Decks

Stephen Wroe Foster, M.S.E.

The University of Texas at Austin, 2010

Supervisor: James O. Jirsa

The Texas Department of Transportation (TxDOT) uses precast, prestressed concrete panels (PCPs) as stay-in-place formwork for most bridges built in Texas. The PCPs are placed on the top flanges of adjacent girders and topped with a 4-in. cast-in-place (CIP) slab. This thesis is directed towards identifying and quantifying the serviceability implications of reducing the deck reinforcement across the interior spans of CIP-PCP decks. The goal of this research is to understand how the PCPs influence cracking and crack control in the CIP slab and to make recommendations to optimize the top mat reinforcement accordingly.

Several tests were conducted to evaluate the performance of different top mat reinforcement arrangements for ability to control crack widths across PCP joints. The longitudinal reinforcement was tested using a constant bending moment test, a point load test, and several direct tension tests. Because of difficulty with the CIP-PCP interface

during the longitudinal tests, direct tension tests of the CIP slab only were used to compare the transverse reinforcement alternatives. Prior to testing, various top mat design alternatives were evaluated through pre-test calculations for crack widths. Standard reinforcing bars and welded wire reinforcement were considered for the design alternatives.

During this study, it was found that the tensile strength of the CIP slab is critical to controlling transverse crack widths. The CIP-PCP interface is difficult to simulate in the laboratory because of inherent eccentricities that result from the test specimen geometry and loading conditions. Furthermore, the constraint and boundary conditions of CIP-PCP bridge decks are difficult to simulate in the laboratory. Based on the results of this testing program, it seems imprudent to reduce the longitudinal reinforcement across the interior spans of CIP-PCP decks. The transverse reinforcement, however, may be reduced using welded wire reinforcement across the interior spans of CIP-PCP decks without compromising longitudinal crack width control. A reduced standard reinforcing bar option may also be considered, but a slight increase in longitudinal crack widths should be expected.

TABLE OF CONTENTS

CHAPTER 1 INTRODUCTION	1
1.1 Background.....	1
1.1.1 Longitudinal and Transverse Directions.....	1
1.1.2 Motivation for Current Study.....	3
1.2 Research Objectives and Scope	4
CHAPTER 2 LITERATURE REVIEW	5
2.1 Strength of Bridge Decks.....	5
2.1.1 Arching Action in Concrete Slabs	5
2.1.2 Conservative Design of Bridge Decks.....	7
2.1.3 Significant Reserve Capacity at Interior Girders	7
2.2 Cracking of CIP-PCP Bridge Decks	10
2.2.1 Cracking Behavior	10
2.2.2 Methods for Crack Control	13
2.3 Composite Behavior of CIP-PCP Decks	15
2.3.1 Mechanical Shear Anchorage	15
2.3.2 Surface Condition of the PCPs	17
2.3.3 Delamination of PCPs.....	18
2.4 Research Significance.....	20
CHAPTER 3 CALCULATED CRACK WIDTHS	21
3.1 Purpose of Calculations	21
3.2 Simplifying Assumptions	21
3.2.1 Cross-Section Geometry	21
3.2.2 Loading Conditions.....	22
3.2.3 Welded Wire Reinforcement	22
3.3 Approach to Calculations.....	23
3.3.1 Gergely-Lutz Equation.....	24
3.3.2 CEB-FIP Equation	24
3.3.3 Flow Chart of Calculations	25

3.4	Results.....	25
3.5	Recommended Test Specimens	28
3.6	Flexibility of Top Mat Reinforcement.....	28
CHAPTER 4 LONGITUDINAL REINFORCEMENT TEST PROGRAM		31
4.1	Introduction.....	31
4.2	Constant Bending Moment Test	31
4.2.1	Test Setup.....	31
4.2.2	Material Properties.....	34
4.2.3	Results.....	35
4.3	Point Load Test with Pre-Crack.....	38
4.3.1	Pre-Cracking of Specimen	39
4.3.2	Test Setup.....	40
4.3.3	Material Properties.....	42
4.3.4	Results.....	42
4.4	Direct Tension Test of CIP-PCP Deck	44
4.4.1	Test Setup.....	44
4.4.2	Material Properties.....	47
4.4.3	Results.....	47
4.5	Direct Tension Test of CIP-PCP Deck with Saw-Cut	48
4.5.1	Test Setup.....	49
4.5.2	Material Properties.....	50
4.5.3	Results.....	50
4.6	Direct Tension Test of CIP Slab with Saw-Cut.....	51
4.6.1	Test Setup.....	52
4.6.2	Material Properties.....	54
4.6.3	Results.....	54
4.7	Direct Tension Test of CIP Slab	56
4.7.1	Test Setup.....	56
4.7.2	Material Properties.....	56
4.7.3	Results.....	56

4.8	Discussion of Longitudinal Reinforcement Test Results.....	57
4.8.1	Tensile Strength of Concrete	57
4.8.2	Composite Behavior of CIP Slab with PCPs	58
4.8.3	Reduction of Longitudinal Reinforcement	59
CHAPTER 5 TRANSVERSE REINFORCEMENT TEST PROGRAM		60
5.1	Introduction.....	60
5.2	Direct Tension Tests of CIP Slab.....	60
5.2.1	Test Setup.....	60
5.2.2	Material Properties.....	61
5.2.3	Results.....	61
5.3	Discussion of Transverse Reinforcement Test Results.....	65
5.3.1	Comparison to Crack Width Equations	65
5.3.2	Benefits of Welded Wire	67
5.3.3	Reduction of Transverse Reinforcement	67
CHAPTER 6 CONCLUSIONS AND RECOMMENDATIONS		70
6.1	Summary	70
6.2	Conclusions.....	70
6.3	Recommendations.....	71
APPENDIX A SAMPLE CRACK WIDTH CALCULATION		72
A.1	No. 5 @ 6-in. o.c., Transverse	72
A.2	D31 @ 6-in. o.c., Transverse	73
APPENDIX B STEEL REINFORCEMENT MATERIAL TESTS		75
B.1	A605 Reinforcing Bars	75
B.2	A706 Reinforcing Bars	76
B.3	A185 Welded Wire Reinforcement	79
REFERENCES.....		82
VITA		87

LIST OF TABLES

Table 2-1: Factors Affecting Cracking (Krauss & Rogalla, 1996).....	11
Table 3-1: Longitudinal Reinforcement Specimens	28
Table 3-2: Transverse Reinforcement Specimens	28
Table 3-3: Flexibility of Recommended Top Mat Specimens.....	30
Table 5-1: Transverse Reinforcement Test Specimens	60
Table 5-2: Cracking of Transverse Specimens	61

LIST OF FIGURES

Figure 1-1: Typical CIP-PCP Bridge Deck (adapted from Buth et al., 1972).....	1
Figure 1-2: CIP-PCP Bridge Deck Terminology.....	2
Figure 1-3: Longitudinal Section through PCP Butt Joint.....	2
Figure 1-4: Transverse Section through Girder Flange	3
Figure 2-1: Arching Action in Concrete Slabs	6
Figure 2-2: Tension Hoop around the Compression Field.....	6
Figure 2-3: Coselli (2004) CIP-PCP Deck Specimen.....	8
Figure 2-4: Load and Strain Gage Locations for Load Tests (Coselli, 2004).....	8
Figure 2-5: Results for (a) Interior and (b) Overhang Loading (Coselli, 2004)	9
Figure 2-6: Deck Cracking Observed by Folliard et al. (2003)	12
Figure 2-7: Anchorage of Cross-Wires for WWR (Ivy Steel & Wire, 2009).....	14
Figure 2-8: Mechanical Shear Connectors (Buth et al. 1972)	15
Figure 2-9: Dowel Bar across Panel Joint (Buth et al. 1972)	16
Figure 2-10: Delamination of Skewed PCP (Boswell, 2008).....	18
Figure 2-11: Comparison of Boswell (2008) and Donnelly (2009).....	19
Figure 2-12: Beginning of Flooding PCPs for Curing.....	19
Figure 3-1: Simplified Longitudinal Section	22
Figure 3-2: Simplified Transverse Section	22
Figure 3-3: Calculation Flow Chart	25
Figure 3-4: Transverse Crack Widths for (a) Gergely-Lutz and (b) CEB-FIP	26
Figure 3-5: Longitudinal Crack Widths for (a) Gergely-Lutz and (b) CEB-FIP	27
Figure 3-6: Measuring Flexibility of Recommended Specimens	29
Figure 3-7: Section Dimensions for Typical 8-in. Deck.....	29
Figure 4-1: PCPs Prior to Casting CIP Slab	32
Figure 4-2: Gap between PCPs.....	32
Figure 4-3: Constant Bending Moment Test Setup	33
Figure 4-4: Loading Beams for Constant Bending Moment Test.....	33
Figure 4-5: Instrumentation for Constant Bending Moment Test	34
Figure 4-6: Linear Potentiometer on CIP Slab across Expected Crack Location.....	34

Figure 4-7: Deflection Potentiometer	34
Figure 4-8: Delamination during Constant Bending Moment Test	36
Figure 4-9: First Crack due to Lead Wires	36
Figure 4-10: PCP Behavior during Constant Bending Moment Test	37
Figure 4-11: Cracking of the Constant Bending Moment Region	37
Figure 4-12: Results for Constant Moment Test.....	38
Figure 4-13: Casting of Point Load Specimen.....	39
Figure 4-14: Pre-Crack Test Setup	40
Figure 4-15: Pre-Crack of Point Load Specimen.....	40
Figure 4-16: Point Load Test Setup	41
Figure 4-17: Instrumentation for Point Load Test	41
Figure 4-18: Load vs. Crack Width Plot for Point Load Test.....	42
Figure 4-19: Crack Width at (a) Start and (b) End of Test	43
Figure 4-20: Results for Point Load Test.....	44
Figure 4-21: Concrete Saw used to Cut PCPs	45
Figure 4-22: Direct Tension Specimens Prior to Casting	45
Figure 4-23: Welded Plates in MTS Grip.....	46
Figure 4-24: CIP-PCP Tension Test Setup	46
Figure 4-25: Eccentric Loading during CIP-PCP Tension	47
Figure 4-26: Delamination of PCPs during Tension Test.....	48
Figure 4-27: Section of Saw-Cut CIP-PCP Specimen.....	48
Figure 4-28: Saw-Cut of CIP	49
Figure 4-29: Saw-Cut Specimen in MTS Machine.....	49
Figure 4-30: Delamination of Saw-Cut Specimen.....	50
Figure 4-31: Cracking Behavior of the Saw-Cut Specimen	51
Figure 4-32: First Crack at Surface of Saw-Cut Specimen.....	51
Figure 4-33: CIP Specimen Prior to Casting	52
Figure 4-34: CIP Section with Saw-Cut	53
Figure 4-35: CIP Slab with Saw-Cut Specimen	53
Figure 4-36: Load-Deflection Plot for CIP Tension Test	54
Figure 4-37: Cracking of CIP Specimen.....	55

Figure 4-38: Results for Tension Test of CIP with Saw-Cut.....	55
Figure 4-39: Sample CIP Section	57
Figure 4-40: Comparison of Cracking Load to Yield of Reinforcement.....	58
Figure 4-41: Shear Transfer across CIP-PCP Interface	59
Figure 5-1: Stress vs. Elongation for No. 5 and D31 Specimens	62
Figure 5-2: Stress vs. Elongation for No. 4 and D20 Specimens	62
Figure 5-3: Crack Widths for Test Specimen No. 5-1	63
Figure 5-4: Crack Width Results for No. 5 and D31 Specimens.....	64
Figure 5-5: Crack Width Results for No. 4 and D20 Specimens.....	64
Figure 5-6: Comparison of Crack Width Equations to No. 5 and D31 Specimens	66
Figure 5-7: Comparison of Crack Width Equations to No. 4 and D20 Specimens	66
Figure 5-8: Comparison of Stress vs. Elongation for Transverse Specimens.....	68
Figure 5-9: Comparison of Crack Widths for Transverse Specimens	68
Figure B-1: Stress-Strain for A605 Reinforcing Bars.....	75
Figure B-2: Stress vs. Total Deflection for A605 Reinforcing Bars.....	76
Figure B-3: Stress-Strain for No. 5 A706 Reinforcing Bars.....	77
Figure B-4: Stress-Strain for No. 4 A706 Reinforcing Bars.....	77
Figure B-5: Stress vs. Time for No. 5 A706 Reinforcing Bars.....	78
Figure B-6: Stress vs. Time for No. 4 A706 Reinforcing Bars.....	78
Figure B-7: Stress-Strain for D31 Reinforcement	79
Figure B-8: Stress-Strain for D20 Reinforcement	80
Figure B-9: Stress vs. Total Deflection for D31 Reinforcement	80
Figure B-10: Stress vs. Total Deflection for D20 Reinforcement	81

CHAPTER 1

INTRODUCTION

1.1 BACKGROUND

The Texas Department of Transportation (TxDOT) uses precast, prestressed concrete panels (PCPs) as stay-in-place formwork for most bridges built in Texas. The PCP system offers significant advantages in the speed, cost, and safety of constructing bridge decks. The PCPs are placed on the top flanges of adjacent girders and topped with a 4-in. cast-in-place (CIP) slab. Figure 1-1 shows a typical CIP-PCP bridge deck with a view of the PCPs, the top mat reinforcement, and the CIP slab.

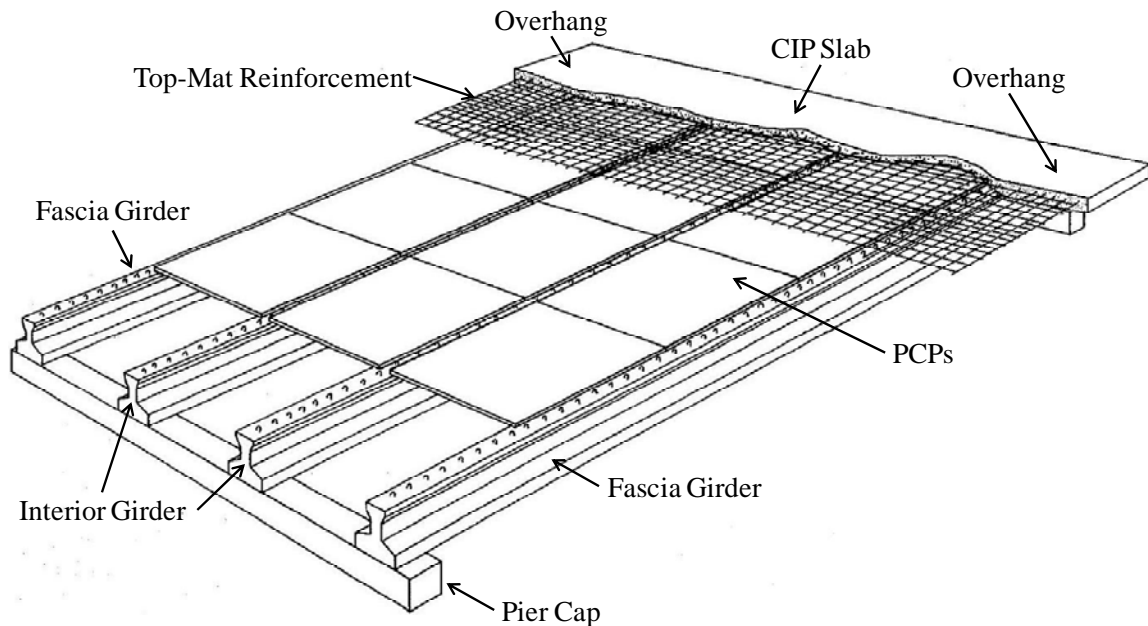


Figure 1-1: Typical CIP-PCP Bridge Deck (adapted from Buth et al., 1972)

1.1.1 Longitudinal and Transverse Directions

The terminology for CIP-PCP bridge decks used in this thesis is shown in Figure 1-2.

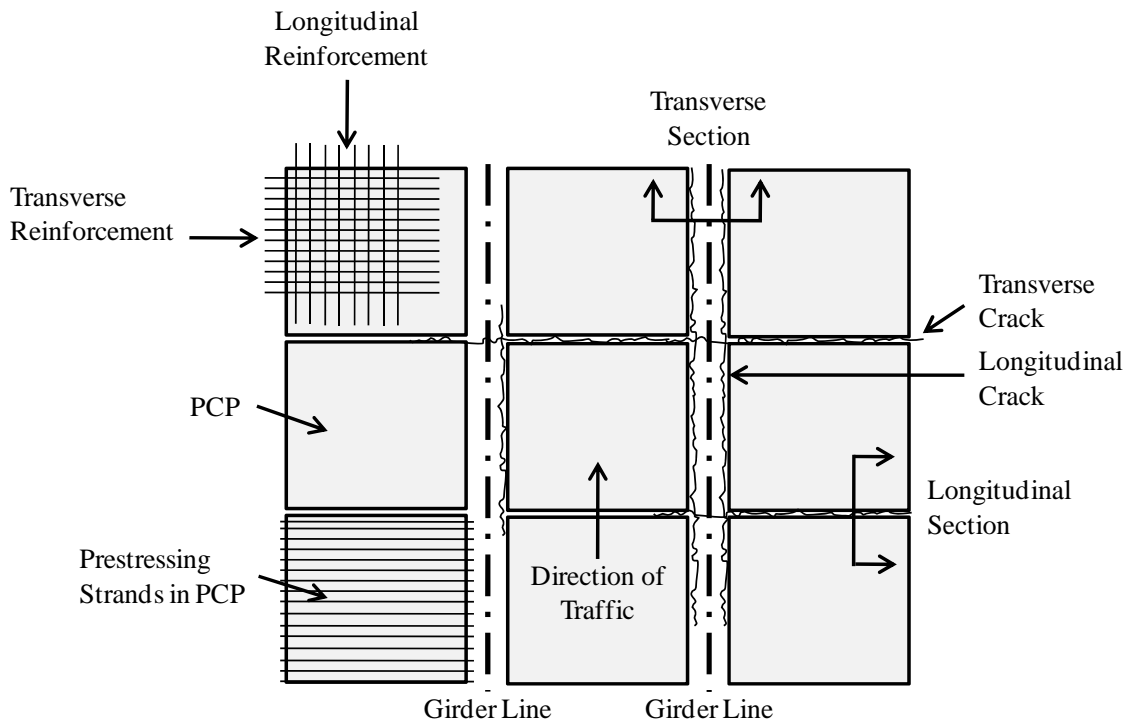


Figure 1-2: CIP-PCP Bridge Deck Terminology

The longitudinal reinforcement runs parallel to the girders and controls the transverse crack widths, as shown in the longitudinal section through the panel-to-panel butt joint in Figure 1-3. The transverse reinforcement runs perpendicular to the girders and controls the longitudinal crack widths, as shown in the transverse section through the girder flange in Figure 1-4. The transverse reinforcement is also needed to provide negative-moment capacity of the deck across the girders.

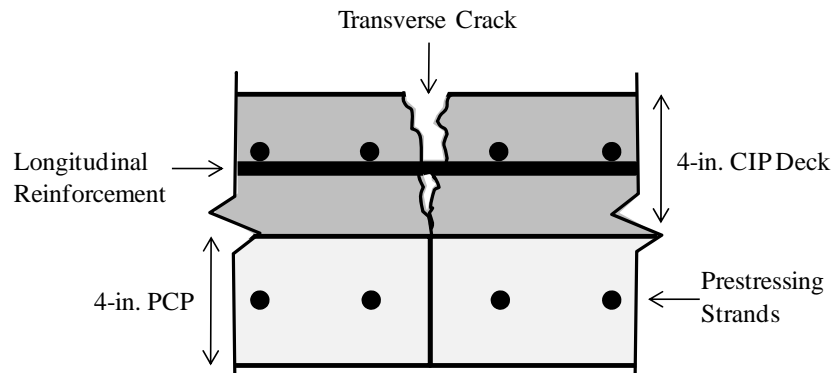


Figure 1-3: Longitudinal Section through PCP Butt Joint

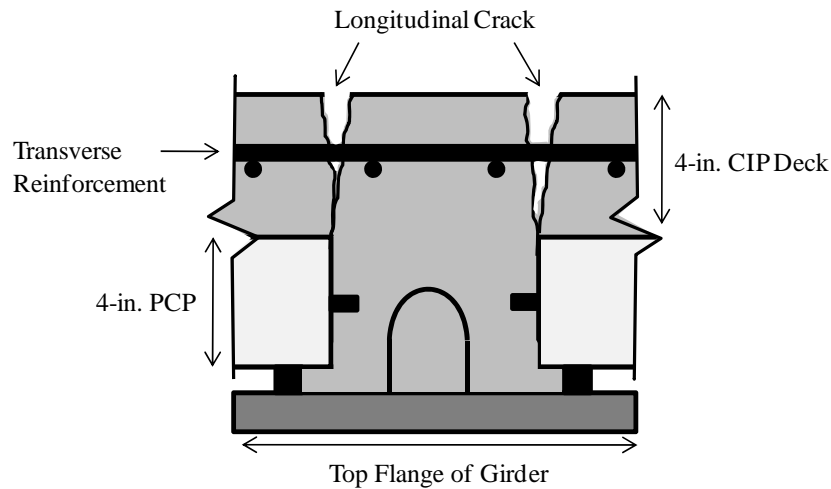


Figure 1-4: Transverse Section through Girder Flange

The current longitudinal reinforcement in TxDOT standard details for the CIP topping slab is No. 4 standard reinforcing bars spaced 9 in. on-center (No. 4 @ 9-in. o.c.), and the current transverse reinforcement is No. 5 standard reinforcing bars spaced 6 in. on-center (No. 5 @ 6-in. o.c.).

1.1.2 Motivation for Current Study

The CIP-PCP bridge decks have performed well. Coselli et al. (2006) have shown the apparent factor of safety is well above 4-5 for interior spans of the bridge (see Chapter 2 for a discussion of this study). No other element in a typical bridge is believed to have such great reserve capacity. Because of this reserve strength, reduction of the transverse reinforcement may be possible.

The longitudinal and transverse reinforcement is necessary to control crack widths under service conditions. These cracks form due to restrained shrinkage of the CIP slab and creep of the PCPs below. These cracks occur at the edges of the PCPs and are referred to as “reflective cracking” because the cracks reflect the layout of the PCPs, as seen in Figure 1-2. A complete discussion of cracking of CIP-PCP bridge decks is presented in Chapter 2.

1.2 RESEARCH OBJECTIVES AND SCOPE

In this thesis, the first phase of TxDOT Project 0-6348: Controlling Cracking in Prestressed Concrete Panels and Optimizing Bridge Deck Reinforcing Steel is presented. The top mat reinforcement portion of TxDOT Project 0-6348 is directed towards identifying and quantifying the serviceability implications of reducing the deck reinforcement across the interior spans of CIP-PCP decks. The goal of the research project is to understand how the PCPs influence cracking and crack control in the CIP slab and to make recommendations to optimize the top mat reinforcement accordingly.

In this thesis, design options for the top mat reinforcement were developed through tests of alternate reinforcement arrangements in the CIP slab. Various top mat design alternatives were evaluated through pre-test calculations for crack widths reported in the literature and in the design codes. Standard reinforcing bars and welded wire reinforcement were considered for the design alternatives in this phase of the project. Therefore, tests were conducted to identify and quantify the crack control benefits of welded wire reinforcement. Steel fibers were not studied as design alternatives for the top mat reinforcement in this phase of Project 0-6348.

CHAPTER 2

LITERATURE REVIEW

2.1 STRENGTH OF BRIDGE DECKS

In this section, some of the reported research showing the reserve strength of decks is summarized.

2.1.1 Arching Action in Concrete Slabs

The significant reserve capacity of reinforced concrete slabs was first reported by Ockleston (1955) after testing a three-storey, reinforced concrete building in South Africa in 1952. The ultimate strengths of the lightly reinforced slabs were six times greater than the design strength. Ockleston (1958) ruled out tensile strength and strain hardening as viable reasons to describe the excess strength and proposed that the presence of compressive membrane action, also referred to as arching action, could account for the discrepancy between predicted and observed strength. Although he could not predict how much load arching action could carry, Ockleston (1958) was the first to describe the phenomenon:

As a result vertical deflection of the slabs would tend to cause outward horizontal displacements at the periphery of the panels. The tendency to spread would be prevented by the slabs which completely surrounded the loaded panels and formed extremely stiff diaphragms for forces in the plane of the floor. Consequently compressive membrane stresses would be developed and the carrying capacity of the slabs would...be increased by the resulting arching action. (p. 198)

Many other researchers have since confirmed the effect of arching action in reinforced concrete slabs, including Christiansen (1963), Park (1965), Liebeberg (1966), Gamble, Sozen, and Seiss (1969), Brotchie and Holly (1971), Black (1975), Desayi and

Kulkarni (1977), and others. Detailed mechanics procedures now exist to predict the forces from arching action in concrete slabs (Park & Gamble, 2000).

Arching action is shown in Figures 2-1 and 2-2 below. Once flexural cracking occurs, a compression field originating from the load point spreads to the restraining supports, as shown in Figure 2-1. Section equilibrium is maintained by a tension hoop around the compression field, shown in Figure 2-2, as well as by bottom reinforcement in the slab that acts as tension ties. The extent of arching action depends on a number of factors, including lateral restraint of the supports, material properties, slab thickness, and plan extent. Full lateral restraint of the supports is not required to develop arching action, although the slab must be thick enough for the arching action forces to develop.

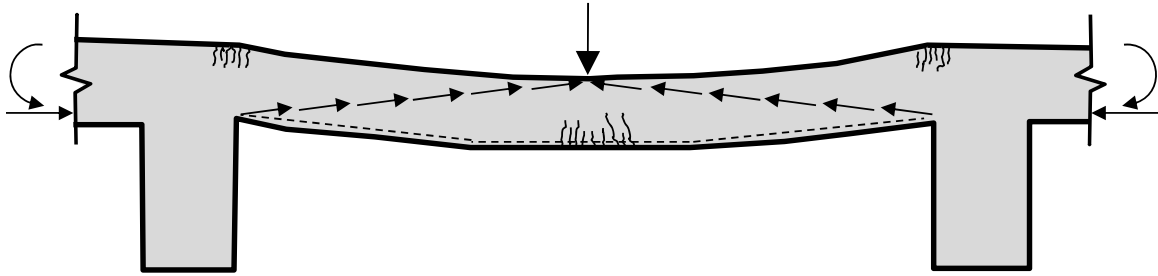


Figure 2-1: Arching Action in Concrete Slabs

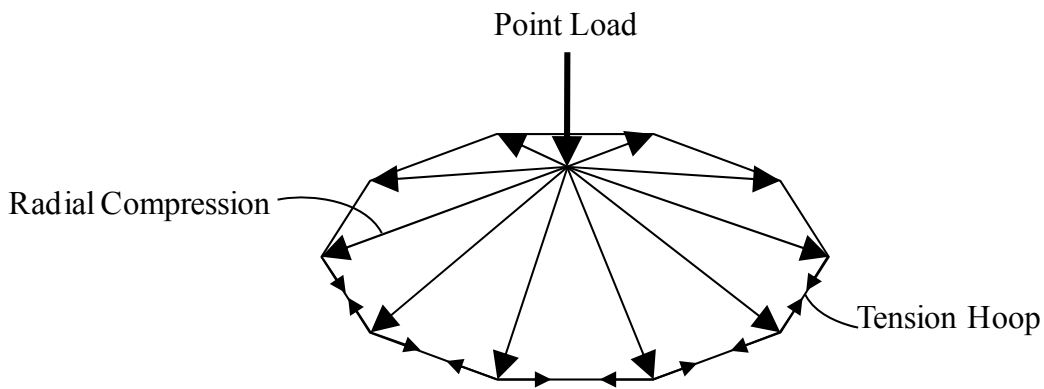


Figure 2-2: Tension Hoop around the Compression Field

2.1.2 Conservative Design of Bridge Decks

After arching action was identified in reinforced concrete slabs, specific research on the strength of bridge decks followed. The Ontario Ministry of Transportation and Communications sponsored research in the 1960s that focused on the associated reserve strength of arching action in bridge decks. Batchelor and Hewitt (1976) tested several scale models as part of that research and found that bridge deck capacity significantly exceeded calculated flexural strength. The flexural capacity of the decks was as much as six times the design strength; the failure mode of nearly all the decks was punching shear, not flexure. Decks without isotropic reinforcement were still able to carry twice the design load. Batchelor and Hewitt (1976) recommended using 0.2% isotropic reinforcement in a seven-inch deck, equivalent to the American Association of State Highway and Transportation Officials (AASHTO) minimum temperature and shrinkage reinforcement. Csagoly, Holowka, and Dorton (1978) verified the experimental results of Batchelor and Hewitt (1976) by testing forty full-scale, in-service bridges in Ontario. Csagoly et al. (1978) agreed that arching action increased the flexural capacity of bridge decks and that punching shear was the governing failure mode.

Several other researchers have confirmed the reserve capacity of bridge decks and the conservative nature of the governing design codes, including Kuang and Morely (1992), Miller, Aktan, and Shahrooz (1994), Azad et al. (1994), Ebeido and Kennedy (1996), Graddy et al. (2002), Hon, Taplan, and Al-Mahaidi (2005), Taylor et al. (2007), and others.

2.1.3 Significant Reserve Capacity at Interior Girders

More recent studies by Coselli et al. (2006) have shown the significant reserve capacity of the current transverse reinforcement across interior girders of bridges. Coselli (2004) built a full-scale CIP-PCP bridge and performed several different load tests across the deck. A picture of the specimen prior to casting is shown in Figure 2-3. Two of the tests, an interior and overhang loading condition, along with the corresponding strain gage locations are shown in Figure 2-4.



Figure 2-3: Coselli (2004) CIP-PCP Deck Specimen

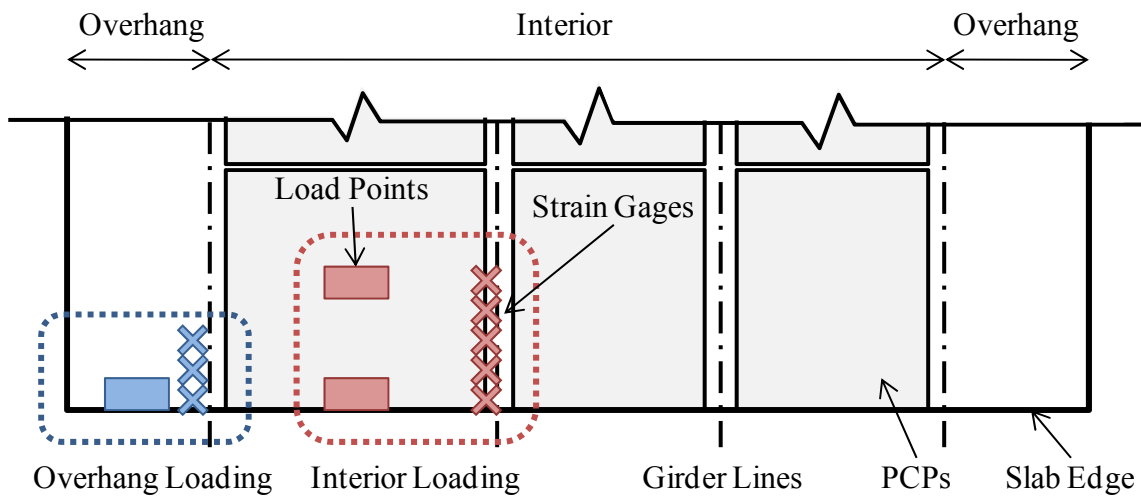


Figure 2-4: Load and Strain Gage Locations for Load Tests (Coselli, 2004)

Comparing strain readings for the interior and overhang loading conditions shows the significant reserve capacity in the current top mat reinforcement. Figure 2-5 shows the strain data collected for the (a) interior and (b) overhang loading conditions.

reported failure loads above 5 times the HS-25 loading tandem (Coselli, 2004, p. 152-153, 183). For the overhang loading condition, however, the deck was able to carry 3.05 times the HS-25 load, and the reinforcement reached yield strain.

The significant reserve capacity in the top mat reinforcement at the interior girder is due to the benefits of arching action. No arching action is present in the overhang because of the lack of restraint at the edge. Based on these studies, it would appear that current reinforcement ratios can be reduced across interior spans without violating serviceability or safety requirements.

2.2 CRACKING OF CIP-PCP BRIDGE DECKS

Because the task addressed in this research study was to optimize the reinforcing steel used to control crack widths, cracking behavior of CIP-PCP bridge decks must be understood. Cracking in any concrete structure is random by nature and difficult to research; cracking must be expected and cannot be eliminated without severely affecting the economy of CIP-PCP bridge decks. Therefore, crack spacing and crack widths must be controlled in a good design. This section summarizes some of the major research on the cracking behavior of bridge decks, focusing on CIP-PCP decks in particular, and the various methods used to control the cracks.

2.2.1 Cracking Behavior

Cracking occurs when tensile stresses in the deck exceed the tensile strength of the concrete. These stresses can be caused by temperature changes in the concrete, concrete shrinkage, and loading from self-weight and traffic. Several different factors influence the probability of cracking. Krauss and Rogalla (1996) conducted a comprehensive study to determine the contributing factors affecting cracking of bridge decks. Table 2-1 shows the results of their study. Undoubtedly, concrete properties affect deck cracking more than any other factors. Although quantity of reinforcement and reinforcing bar size, the focus of this thesis, were found to have a “minor” effect on influencing crack occurrence, they play a much greater role in controlling crack widths once cracks occur. This study is focused on controlling crack widths.

Table 2-1: Factors Affecting Cracking (Krauss & Rogalla, 1996)

Factors	Effect			
	Major	Moderate	Minor	None
Design				
Restraint	✓			
Continuous/simple spans		✓		
Deck thickness		✓		
Girder type		✓		
Girder size		✓		
Alignment of top and bottom reinforcement bars		✓		
Form type			✓	
Concrete cover			✓	
Girder spacing			✓	
Quantity of reinforcement			✓	
Reinforcement bar sizes			✓	
Dead-load deflections during casting			✓	
Stud spacing			✓	
Span length			✓	
Bar type--epoxy coated			✓	
Skew			✓	
Traffic volume				✓
Frequency of traffic-induced vibrations				✓
Materials				
Modulus of elasticity	✓			
Creep	✓			
Heat of hydration	✓			
Aggregate type	✓			
Cement content and type	✓			
Coefficient of thermal expansion		✓		
Paste volume--free shrinkage		✓		
Water-cement ratio		✓		
Shrinkage-compensating cement		✓		
Silica fume admixture		✓		
Early compressive strength			✓	
HRWRAs			✓	
Accelerating admixtures			✓	
Retarding admixtures			✓	
Aggregate size			✓	
Diffusivity			✓	
Poisson's ratio			✓	
Fly ash				✓
Air content				✓
Water content				✓
Construction				
Weather	✓			
Time of casting	✓			
Curing period and method		✓		
Finishing procedures		✓		
Vibration of fresh concrete			✓	
Pour length and sequence			✓	
Construction loads				✓
Traffic-induced vibrations				✓

Looking at Table 2-1, restraint is the only design factor to have a “major” affect on cracking. For CIP-PCP decks, the PCPs provide significant restraint to the CIP slab. Accordingly, cracking of CIP-PCP bridge decks is largely influenced by the interaction of the CIP slab and the PCPs. Some of the earliest research on CIP-PCP decks describes cracking at the joints of the PCPs, including Jones & Furr (1970), Buth, Furr, and Jones (1972), and others. More recently, Merrill (2002) and Folliard et al. (2003) have documented the cracking behavior of CIP-PCP. To better understand how the information presented by Krauss and Rogalla (1996) related to CIP-PCP bridges in Texas, Folliard et al. (2003) conducted field evaluations of two CIP-PCP bridge decks that were experiencing deck cracking. Figure 2-6 shows the typical crack pattern that was observed at the interior of the deck. Section views of typical transverse and longitudinal cracking are shown in Figure 1-3 and Figure 1-4, respectively. This crack pattern is often referred to as “reflective cracking” because the cracks in the CIP slab reflect the PCP edge below.

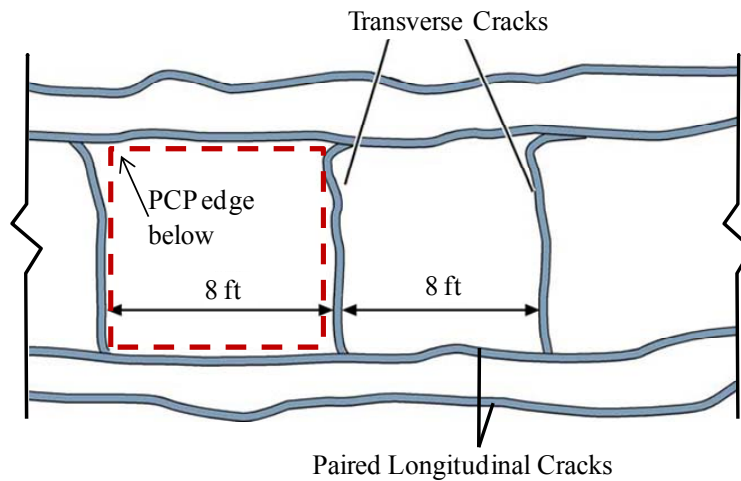


Figure 2-6: Deck Cracking Observed by Folliard et al. (2003)

Transverse cracking is caused by the shrinkage of the CIP slab, the restraint provided by the PCPs, and the joint between adjacent panels (Merrill, 2000). In addition to these factors, longitudinal cracking is also caused by creep of the PCPs due to the sustained prestressing force. Historically, longitudinal cracking has also been caused by poor bedding strip details, but the problem has since been resolved (Merrill, 2000).

2.2.2 Methods for Crack Control

Crack spacing is already determined in CIP-PCP decks because of the PCP layout. Therefore, crack widths are the only factor to consider for design of the reinforcement. The range of acceptable crack widths can vary widely. Typical recommendations range from 0.004 to 0.008 in. for corrosive conditions and 0.008 to 0.012 in. for non-corrosive conditions (Broms, 1965 and Krauss & Rogalla, 1996).

The most significant way to control cracks is to reduce the probability of cracks from occurring. As shown in Table 2-1, the best approach to preventing cracks is to optimize the concrete materials to reduce the potential for cracking. Folliard et al. (2003) conducted significant research into the use of concrete materials to control shrinkage cracking of CIP-PCP decks across panel joints. Folliard et al. (2003) recommended using innovative materials mixtures of shrinkage reducing admixtures, calcium-sulfoaluminate admixtures, fibers, and high-volume fly ash.

Once cracks form across the PCP joints, the crack width is controlled by the steel reinforcement crossing the crack. Typically, deformed reinforcing bars or welded wire reinforcement (WWR) are used to control cracking.

There has been significant research on controlling crack widths with deformed reinforcing bars, although the exact behavior of a section with PCPs and CIP slab is still largely unknown. Stress in the reinforcement, bar spacing, bar diameter, and depth of the bars all influence crack widths to some extent. There have been several methods developed to understand and calculate crack widths, including Broms (1965), Nawy (1968), Gergely and Lutz (1968), CEB-FIP (1978), Frosch (2001), DeStefano et al. (2003), Beeby (2004), Tammo and Thelandersson (2009), and others. The following conclusions are generally agreed on: (i) higher stresses produce higher strains and, therefore, larger crack widths, (ii) for the same area of steel, a larger number of narrower cracks will form as the bar spacing is reduced, (iii) having the reinforcement as close to the surface as possible is best for controlling crack widths at the surface, although large clear cover is desirable to prevent corrosion.

There has been much less research on crack control using welded wire reinforcement. Studies by Atlas, Siess, and Kesler (1965), Lloyd, Rejali, and Kesler (1969), and Lee et al. (1987) have been reported. Welded wire reinforcement is often considered to better control crack widths due to the higher strength of the steel and the improved anchorage provided by the welded cross-wires, which are shown in Figure 2-7 (Atlas et al., 1965).

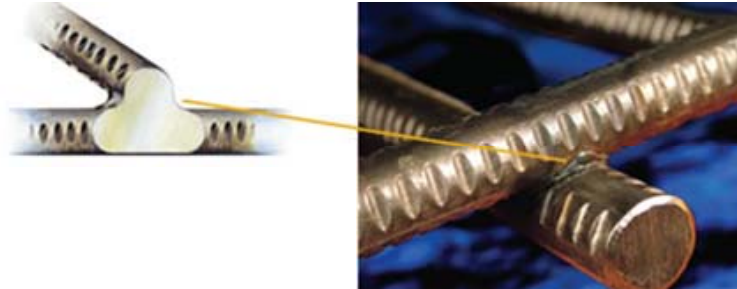


Figure 2-7: Anchorage of Cross-Wires for WWR (Ivy Steel & Wire, 2009)

Early research by Lloyd et al. (1969), however, showed that deformed reinforcing bars and deformed WWR control crack spacing and crack widths equally well. It was later found that welded wire provides better crack control than conventional reinforcement only if the spacing of the transverse cross wires (S_t) is restricted, depending on the transfer length (L_t'). The transfer length is the distance from a crack that the strain in the steel and concrete are equal. Lee et al. (1987) reported the following: (i) when $S_t < L_t'$, crack spacing is governed by S_t , (ii) when $L_t' < S_t < 2L_t'$, crack spacing will vary from S_t to $(S_t - L_t')$, (iii) when $S_t > L_t'$, crack spacing is independent of S_t . Lee et al. (1987) concluded, “If the spacing of transverse wires approaches L_t' or $2L_t'$ from the lower end, or if it exceeds $2L_t'$, WWR acts as ordinary reinforcement, as far as maximum crack spacing and width are concerned” (p. 488). For a transfer length of 6.5-in., for example, the ideal transverse wire spacings would be less than 5.5-in. or between 6.5-in. and 12-in. Any other transverse spacing would not benefit the cracking behavior.

Based on previous research, it is clear that optimizing the reinforcement will help control crack widths. The benefits of welded wire reinforcement, although largely undocumented, are worth studying due to the potential for increased construction productivity.

2.3 COMPOSITE BEHAVIOR OF CIP-PCP DECKS

As described earlier, the interaction of the CIP slab with the surface of the PCPs is important to understanding the cracking behavior of CIP-PCP decks. It is also important to understanding the overall performance of these decks. Field studies of some of the earliest CIP-PCP decks were conducted by Jones and Furr (1970) to study the composite behavior of the CIP slab and PCPs. The study included soundings to detect delamination between the CIP slab and the PCPs. Cores were also taken to observe any delamination or cracking between the CIP and PCP. Load tests were conducted on in-service bridges to verify the monolithic behavior of the bridge. No evidence of significant delamination was found, and the CIP slab and PCPs acted as a unit during the load tests.

Several issues regarding the CIP-PCP interface have since been researched, including mechanical shear anchorage, surface condition of the PCP surface, and delamination concerns during loading.

2.3.1 Mechanical Shear Anchorage

Buth, Furr, and Jones (1972) conducted a series of static and fatigue tests to evaluate the capability of PCPs to act compositely with the CIP topping slab to distribute wheel loads. Two different mechanical shear connectors (Z-bars and V-bars) and grouting of the CIP surface were tested to determine if they would improve the behavior of the CIP-PCP interface. The Z-bar and V-bar detail is shown in Figure 2-8. Additional dowel bars across the longitudinal butt joints of the panels were also used in some areas of the deck to determine if they would assist in transferring load across the joint. Grout was also applied to the PCP surface in some areas of the deck to serve as an additional bonding agent. The dowel bar detail is shown in Figure 2-9.

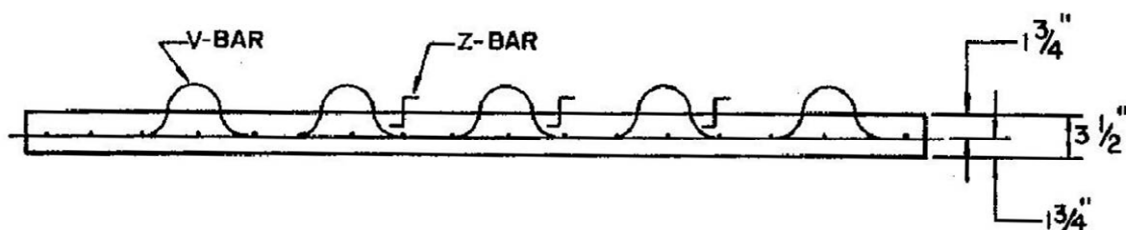


Figure 2-8: Mechanical Shear Connectors (Buth et al. 1972)

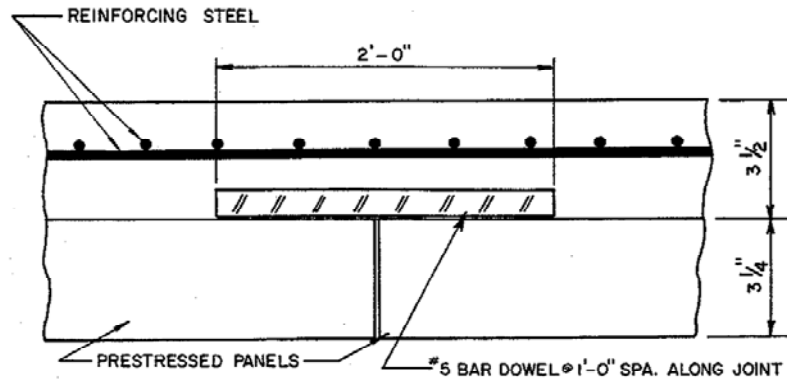


Figure 2-9: Dowel Bar across Panel Joint (Buth et al. 1972)

The load tests indicated that none of these details provided any measureable improvement in the performance of bond or load transfer. In fact, the highest failure loads were in areas of the bridge with no grout, Z-bars, or dowels. Buth et al. (1972) concluded that bond across the interface between the PCPs and the CIP was sufficient for composite action.

Barnoff and Rainey (1974) investigated composite behavior for the Pennsylvania Transportation Institute. They studied panels without any mechanical shear anchors across the CIP-PCP interface and concluded that only a roughened top surface of the PCP was needed to develop full composite action.

Barker (1975) also investigated the effect of shear studs as mechanical anchors between the CIP and PCPs. Tests were conducted using PCPs with shear studs protruding from the top surface and others with only raked surface finishes. Barker (1975) reported that adequate panel surface roughness provided sufficient shear transfer, eliminating the need for shear reinforcement between the panel and the topping slab. It was also noted that the performance of the CIP-PCP deck system was not affected by the joints between the precast panels.

Kluge and Sawyer (1975) performed four series of tests to determine if mechanical anchors were needed across the CIP-PCP interface. The first series of tests were simple beam tests to evaluate the reliability of the bond between the CIP and PCPs. For one of the specimens, the top surface of the PCP was oiled prior to casting the topping slab. For the second series of tests, shear strength across the PCP butt joints was

tested by comparing specimens with and without joints. In the third series of tests, the effect of cracks over the PCP butt joints on the flexural strength of the deck was evaluated. In the last series of tests, the punching shear of the composite section was evaluated. Overall, Kluge and Sawyer (1975) concluded that there was sufficient bond between the CIP and PCPs without any mechanical connectors. They also observed that a clean PCP surface was necessary to achieve full strength since the oiled specimen failed at a load 40% lower than the clean specimens. No adverse effects of joints between the PCPs were found.

Although primarily researching the effect of the PCP strand extensions, Bieschke and Klingner (1982) also evaluated the effects of U-bars, (similar to the V-bars used by Buth et al. shown in Figure 2-8), on the performance of CIP-PCP decks. The researchers confirmed that U-bars did not have any effect on the structural performance of the deck.

2.3.2 Surface Condition of the PCPs

In addition to studying transfer length and slip of the prestressing strands in PCPs, Abendroth (1994) studied the composite action between the CIP slab and PCPs with a raked top finish. Abendroth (1994) found that the first interface slip occurred at loads greater than twice the design wheel load amplified for impact. Furthermore, after the initial slip occurred, the specimens demonstrated significant reserve capacity, indicating that a rake finish provided sufficient surface roughness to allow horizontal shear transfer between the CIP slab and the PCPs.

Merrill (2002) discussed many aspects of the use of CIP-PCP bridges in Texas. Of particular importance, he noted that the moisture content of the PCP surface prior to placing the CIP slab is significant because the PCPs will draw moisture out of the CIP slab, resulting in drying shrinkage cracking. Although previous researchers had not explicitly mentioned moisture content as an area of importance, several of the projects did ensure the PCP surface was moist prior to placing the CIP. For instance, Buth et al. (1972) notes that the PCPs were “thoroughly cleansed with water from a hose and nozzle and then damp dried shortly before placement of the cast-in-place concrete” (p. 20).

Dowell and Smith (2006) studied the relationship between shear transfer and surface roughness conditions of the PCPs. “Coarse broom,” “medium broom,” and “carpet drag” finishes were applied to PCPs prior to the concrete curing. Dowell and Smith (2006) observed no sign of shear slip in any of the finishes and concluded that any PCP roughening technique will work to prevent shear slip across the CIP-PCP interface.

2.3.3 Delamination of PCPs

Boswell (2008) investigated the structural performance of skewed PCP systems as part of TxDOT Project 0-5367. Although the primary objective of Boswell (2008) is not in the scope of this research, the performance of the CIP-PCP interface during his testing is relevant. While testing skewed panels for a load applied at midspan, failure occurred due to delamination of the CIP slab with the PCP surface. Figure 2-10 shows some of the delamination that occurred during testing. The specimen had a very smooth surface finish and was not moistened as described by Merrill (2002).



Figure 2-10: Delamination of Skewed PCP (Boswell, 2008)

As a result of the delamination, Donnelly (2009) re-evaluated the skewed PCPs following careful procedures for surface texture and moisture conditions. These panels did not delaminate and experienced significantly higher strengths than the panels Boswell (2008) tested. A comparison of applied load to compressive strains is shown in Figure 2-11. Donnelly (2009) made the following conclusions: (i) a rake finish of approximately $\frac{1}{4}$ in. should be provided to maintain adequate surface roughness conditions, (ii) the

surface roughness may be reduced by flooding of the prestressing bed during curing, as shown in Figure 2-12, and (iii) the PCPs should be wet to a saturated surface dry condition to prevent the PCPs from drawing water out of the CIP topping slab. It should be noted that Boswell's tests had rather smooth PCP surface finish, a factor that may be more important than a moist surface.

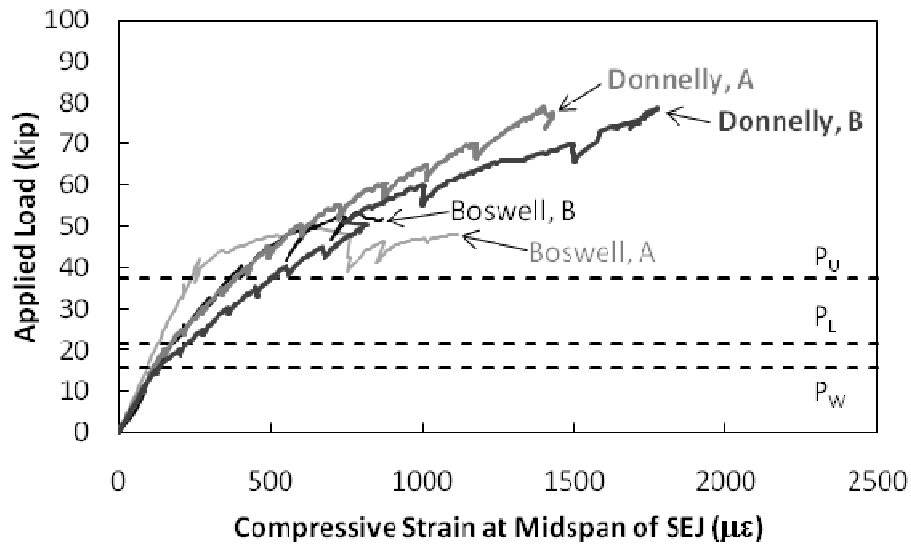


Figure 2-11: Comparison of Boswell (2008) and Donnelly (2009)



Figure 2-12: Beginning of Flooding PCPs for Curing

2.4 RESEARCH SIGNIFICANCE

A reduction in the reinforcement in CIP-PCP bridge decks in Texas could lead to further economy in bridge construction. Valuable information regarding the behavior of the CIP-PCP interface is provided, especially the influence on cracking in the CIP slab.

CHAPTER 3

CALCULATED CRACK WIDTHS

3.1 PURPOSE OF CALCULATIONS

Crack width calculations were performed considering top mat reinforcement currently used by TxDOT and alternative arrangements. The results were used to develop specimens for the experimental program.

3.2 SIMPLIFYING ASSUMPTIONS

As described in Chapter 2, cracking in reinforced concrete is difficult to predict. It is random by nature, and crack widths in structural members generally show large scatter. Although there is strong documentation on the cracking tendency at the joints of PCPs (see Chapter 2), there is no literature on how the joints between PCPs with a CIP overlay affect crack width predictions. Therefore, simplifying assumptions had to be made so that the reinforcing alternatives could be evaluated in terms of crack width control.

3.2.1 Cross-Section Geometry

Due to the difficulty of determining crack widths for the field conditions shown in Figure 1-3 and Figure 1-4, the crack widths were estimated using the simplified cross-sections shown in Figure 3-1 and Figure 3-2. The deck was modeled as an 8-in. deep, 12-in. wide strip, with the various steel alternatives modeled at a depth corresponding to 2-in. clear cover. This model was only used as a basis for comparing the various reinforcement alternatives and was not considered an accurate representation of the composite deck with PCPs shown in Figure 1-3 and Figure 1-4. Nevertheless, the model allowed a comparison of the effects of varying bar sizes and spacing in an idealized condition.

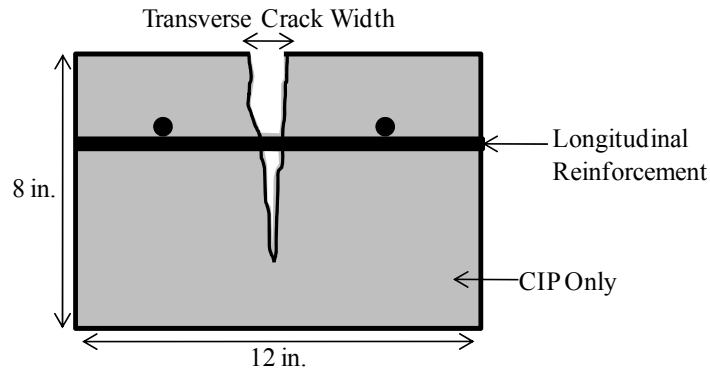


Figure 3-1: Simplified Longitudinal Section

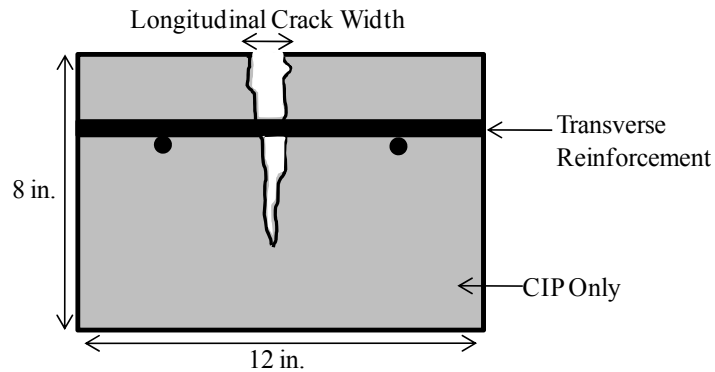


Figure 3-2: Simplified Transverse Section

3.2.2 Loading Conditions

In addition to removing the panels from the idealized cross section, the loading was simplified. In the field, a combination of shrinkage, creep, temperature, dead weight, and traffic loads cause the cracks to form. In order to estimate and compare crack widths, the loading was simplified as a pure bending moment. This moment created tension in the reinforcement and allowed for a simple and direct comparison of the crack widths for the various reinforcing alternatives.

3.2.3 Welded Wire Reinforcement

The improved anchorage of the welded wire reinforcement is also difficult to model. Therefore, a simplified approach was taken for the purposes of these calculations. The anchorage of welded wire reinforcement was modeled by improving the tension-

stiffening factor when analyzing the section. Tension stiffening factors are typically 0.7 for smooth bars, wires, and strands and 1.0 for deformed bars. A tension stiffening factor of 1.3 was used for the welded wire reinforcement.

This modification was determined by comparing two ratios: (i) the development length of standard reinforcing bars to the development length of the welded wire reinforcement, and (ii) the development length of the welded wire reinforcement to the distance between the cross-wires. These ratios provide a rough estimate for the increased anchorage that is associated with welded cross-wires. For the current TxDOT reinforcement, these ratios ranged between 1.5 and 2. Based on these comparisons and lack of data in the literature, a conservative assumption of 1.3 was used to model the improved anchorage performance of the welded cross-wires.

3.3 APPROACH TO CALCULATIONS

The simplified sections were analyzed for each of the reinforcing alternatives using the sectional analysis program RESPONSE (Felber, 1990). As a basis for comparison, the crack widths were estimated for a particular bending moment, which was taken as 1.5 times the initial cracking moment of the current TxDOT reinforcement. This value was used to represent the service conditions of CIP-PCP decks. Using a concrete strength of 4,000 psi for the sections shown Figure 3-1 and Figure 3-2, this value was 7.91 k-ft for the transverse reinforcement and 7.66 k-ft for the longitudinal reinforcement. This approach allowed direct comparisons to be made between all of the reinforcing alternatives.

The strain profile at this bending moment from RESPONSE was used to calculate the expected crack widths. By modifying the tension-stiffening factor, the strain values changed for the welded wire reinforcement. RESPONSE does not allow the use of a tension-stiffening factor greater than one; therefore, a similar sectional analysis program developed by Quinn (2009) was used to obtain strain values for the welded wire reinforcement.

Because of the complexity of estimating crack widths, and for the purposes of establishing a comparative platform for discussion, two different equations were used to calculate the crack widths for each of the reinforcing alternatives.

3.3.1 Gergely-Lutz Equation

Crack widths were calculated using the Gergely-Lutz (1968) equation, which is the basis for crack control requirements in ACI 318. The maximum crack width is calculated based on three primary factors: the steel strain at the crack, concrete cover, and the area of concrete around each bar (Collins & Mitchell, 1997). The equation relating these factors is as follows:

$$w_{max} = 2.2 \beta \varepsilon_s (d_c A)^{1/3} \quad \text{Equation 3-1}$$

Where:

- w_{max} = maximum crack width
- β = factor accounting for strain gradient
- ε_s = strain in steel
- d_c = distance from top of slab to the reinforcement
- A = effective area of concrete surrounding each bar/wire

3.3.2 CEB-FIP Equation

CEB-FIP (1978) crack widths are calculated using estimated average crack spacing. The crack spacing is calculated based on clear cover, bar diameter, and maximum spacing between the bars. The equation relating these factors is as follows:

$$s_m = 2 (c + s/10) + k_1 k_2 (d_b/\rho_{ef}) \quad \text{Equation 3-2}$$

Where:

- s_m = average crack spacing
- c = clear cover
- s = maximum spacing between bars (limited to $15d_b$)
- k_1 = bond properties of bars (0.4 for deformed bars)
- k_2 = coefficient accounting for strain gradient
- d_b = diameter of bar/wire
- ρ_{ef} = area of steel / area of effective embedment zone of concrete

The average crack spacing is then multiplied by the strain at the top of the deck (at the critical moment $1.5 M_{cr}$) to determine an average crack width. To find the maximum crack width, the average crack width was then multiplied by 1.7 (Collins & Mitchell, 1997).

3.3.3 Flow Chart of Calculations

A flow chart summarizing the approach to calculating the crack widths is shown in Figure 3-3. A sample calculation for the standard reinforcing bars and welded wire reinforcement is shown in Appendix A.

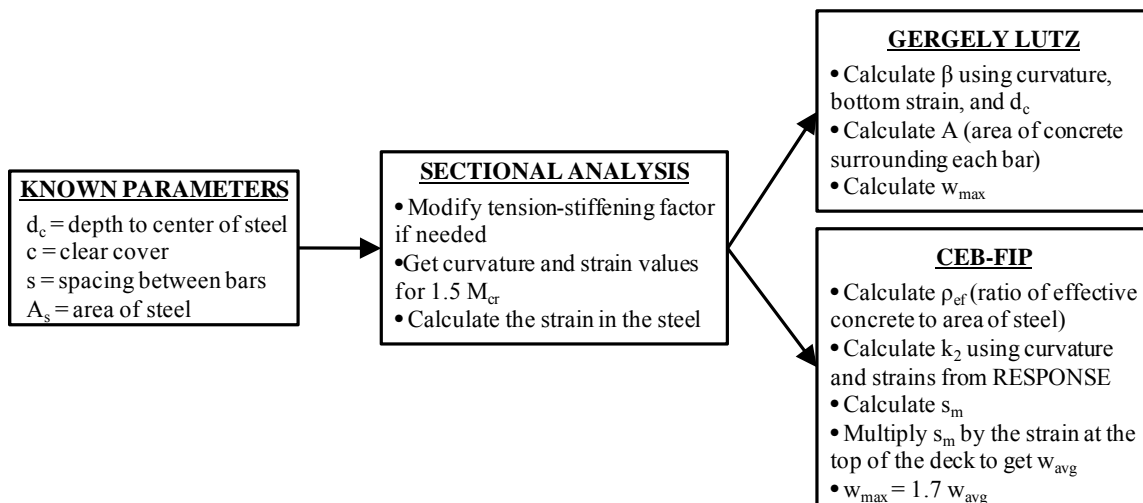
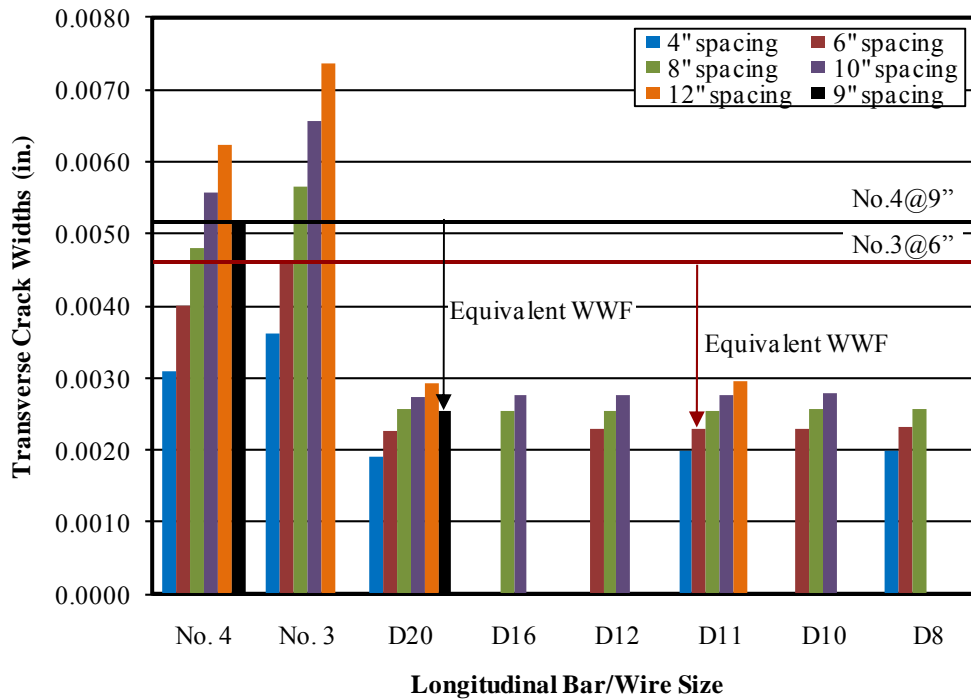


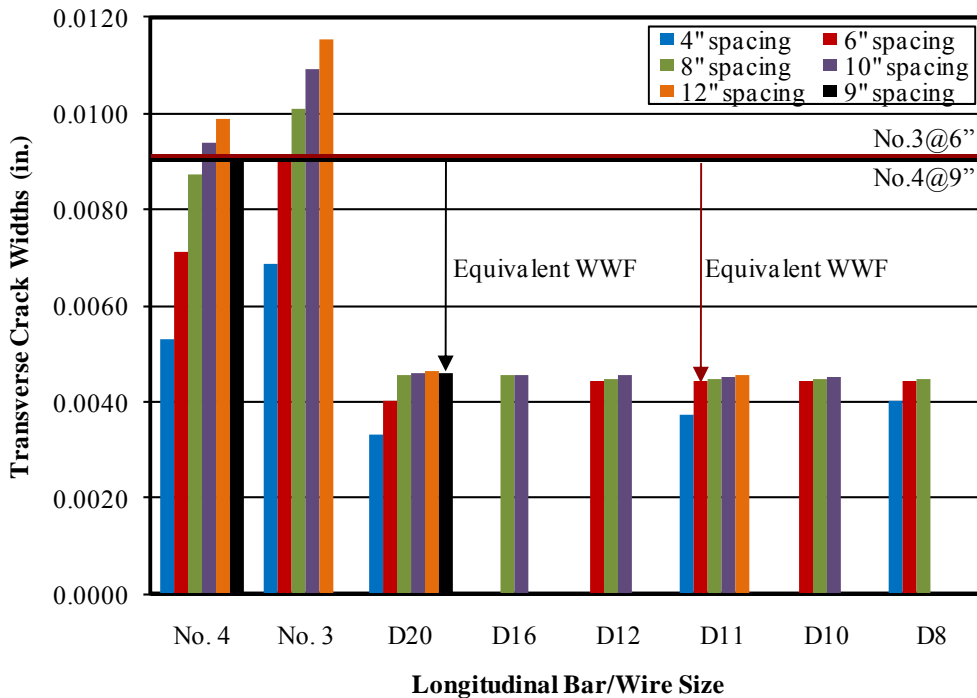
Figure 3-3: Calculation Flow Chart

3.4 RESULTS

The calculated crack widths showed all of the expected trends. For a given bar size, crack widths increase as the bar spacing increases. Similarly, for a given bar spacing, crack widths decrease as the area of steel increases. This behavior is expected because the bar stresses are less for the given moment ($1.5 M_{cr}$) as the steel area increases. The anchorage from the welded wire reinforcement also reduces the crack widths. The significant improvement of the welded wire, however, is largely dependent on the tension stiffening factor that was assumed in the calculations. Figure 3-4 and Figure 3-5 show the results for the transverse and longitudinal crack widths, respectively.

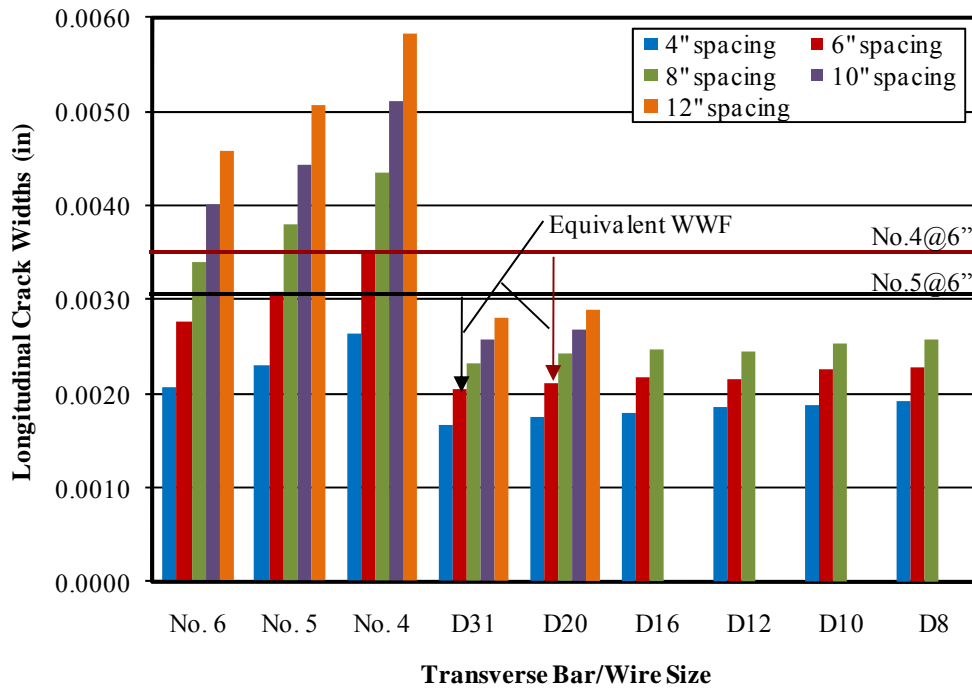


(a) Gergely-Lutz Equation

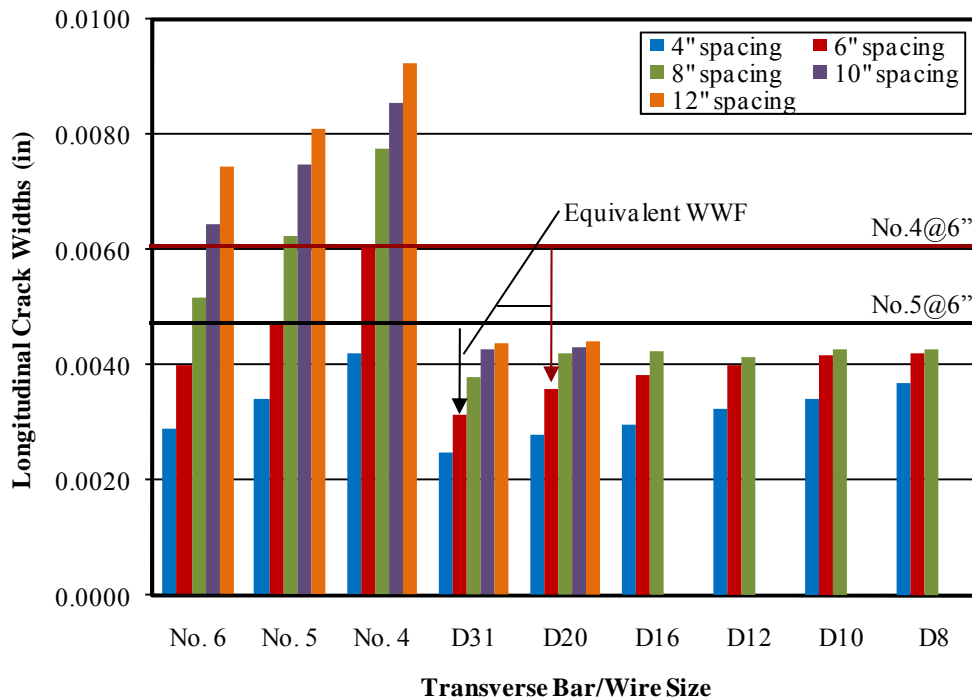


(b) CEB-FIP Equation

Figure 3-4: Transverse Crack Widths for (a) Gergely-Lutz and (b) CEB-FIP



(a) Gergely-Lutz Equation



(b) CEB-FIP Equation

Figure 3-5: Longitudinal Crack Widths for (a) Gergely-Lutz and (b) CEB-FIP

3.5 RECOMMENDED TEST SPECIMENS

Based on these calculations, an initial series of eight test specimens, four longitudinal specimens and four transverse specimens, were selected. The test specimens that were selected and the corresponding crack widths (for the theoretical case described earlier) are shown in Table 3-1 and Table 3-2 for the longitudinal and transverse reinforcement, respectively.

Table 3-1: Longitudinal Reinforcement Specimens

Specimen	Area of Steel (in ² /ft)	CEB-FIP Crack Width (in)	Gergely-Lutz Crack Width (in)
1. No. 4 @ 9 in.	0.27	0.0091	0.0052
2. No. 3 @ 6 in.	0.22	0.0091	0.0046
3. D20 @ 9 in.	0.27	0.0046	0.0025
4. D11 @ 6 in.	0.22	0.0044	0.0023

Table 3-2: Transverse Reinforcement Specimens

Specimen	Area of Steel (in ² /ft)	CEB-FIP Crack Width (in.)	Gergely-Lutz Crack Width (in.)
1. No. 5 @ 6 in.	0.62	0.0048	0.0031
2. No. 4 @ 6 in.	0.40	0.0061	0.0035
3. D31 @ 6 in.	0.62	0.0032	0.0020
4. D20 @ 6 in.	0.40	0.0036	0.0021

These specimens represent current TxDOT reinforcement (Specimen 1), a reduced rebar option (Specimen 2), and the corresponding welded wire equivalents (Specimen 3 and Specimen 4). These initial test specimens were selected to provide a comparison between welded wire and standard reinforcing bars and to compare different options for reducing the top mat reinforcement.

3.6 FLEXIBILITY OF TOP MAT REINFORCEMENT

Because of concerns raised by TxDOT regarding work men walking on No. 3 bars, the relative flexibility of the proposed top mat specimens was investigated. To compare the stiffness of each of these options, an 8-ft. by 8-ft. mat was constructed and placed on 1.5-in. chairs spaced 3-ft. on center. The deflection of the mat was measured as

one, 190-lb. man stood at the center of the chairs, as shown in Figure 3-6. The selected chair size and spacing ensured all of the options would deflect without touching the floor.



Figure 3-6: Measuring Flexibility of Recommended Specimens

This setup allowed the relative flexibility of the proposed specimens to be compared, but does not reflect the in-situ conditions of walking on the mat. For example, the most the reinforcement mat would deflect in the field would be $7/8$ in. at which point the reinforcement would rest on the PCPs. The section dimensions for a typical 8-in. deck are shown in Figure 3-7. Furthermore, the TxDOT specifications allow for the top mat reinforcement to rest even closer to the panels, sometimes even directly on the PCPs (TxDOT, 2006).

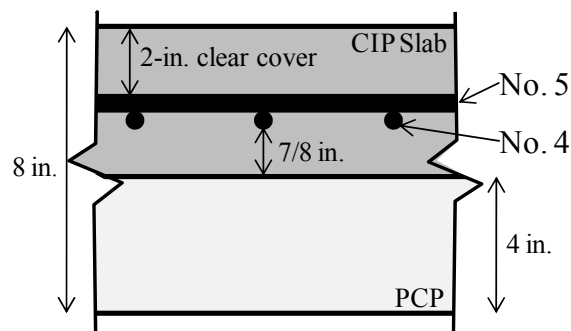


Figure 3-7: Section Dimensions for Typical 8-in. Deck

It is also important to note that the length of the rebar placed in a bridge deck will be much longer; therefore, the counter-weight of the mat would increase, the boundary conditions would change, and the mat would deflect less.

Table 3-3 shows the measured deflections of each of the proposed specimens. The current TxDOT reinforcement deflected 1/2 in. The reduced rebar option deflected significantly more, but always returned to its original position without any permanent deformation. The welded options showed significant improvements in stiffness. The reduced welded wire option (Specimen 4) behaved similarly to the current TxDOT reinforcement (Specimen 1).

Table 3-3: Flexibility of Recommended Top Mat Specimens

Specimen 1	Specimen 2	Specimen 3	Specimen 4
1/2 in	1- 3/16 in	3/8 in	5/8 in

Based on these results, the Specimens 1, 3, and 4 are comparably stiff. While Specimen 2 is more flexible, the additional flexibility may not be a concern considering that in the field the top mat does not deflect much before resting on the PCPs, as described earlier.

CHAPTER 4

LONGITUDINAL REINFORCEMENT TEST PROGRAM

4.1 INTRODUCTION

A series of tests were performed to study transverse cracking at PCP butt joints with different longitudinal steel arrangements. Because of the difficulty simulating the PCP boundary conditions, several tests with different boundary and loading conditions were performed to study the performance of a section at transverse PCP butt joints.

4.2 CONSTANT BENDING MOMENT TEST

First, a constant bending moment test was conducted across the butt joint between two 8-ft. by 8-ft. PCPs. The objective of this test was to develop tension across the butt joint similar to that produced by shrinkage or temperature in a typical bridge deck, but in a much shorter time than would be needed for a laboratory restrained shrinkage test. Although the loading conditions in the field are not pure bending stresses, this test induces tension across the PCP joint and cracking in the CIP slab at the butt joint. The intent was to study longitudinal reinforcement alternatives by comparing the observed crack widths at comparable strains or stresses in the reinforcement.

4.2.1 Test Setup

Two 8-ft. by 8-ft. PCPs were topped with a 4-in. CIP slab. A photograph of the PCPs prior to casting is shown in Figure 4-1. The standard TxDOT reinforcement (No. 5 @ 6-in. o.c. transverse, No. 4 @ 9-in. o.c. longitudinal) was used throughout the topping slab. Rather than butt the PCPs against each other at the joint, a 1.5-in. gap was cast between the PCPs to ensure uniform compression under bending across the joint, as shown in Figure 4-2. No photographs were taken during casting for this specimen, although this cast was similar to the cast for point load test specimen, which is shown in Figure 4-13.



Figure 4-1: PCPs Prior to Casting CIP Slab



Figure 4-2: Gap between PCPs

The test setup for the constant bending moment test is shown in Figure 4-3. The deck was centered and supported by rollers on top of two support beams four feet apart. One of the rollers was welded in place and the other was free. The ends of the deck were loaded with hydraulic rams on top of steel loading beams that distributed the load across the transverse length of the deck, as shown in Figure 4-4.

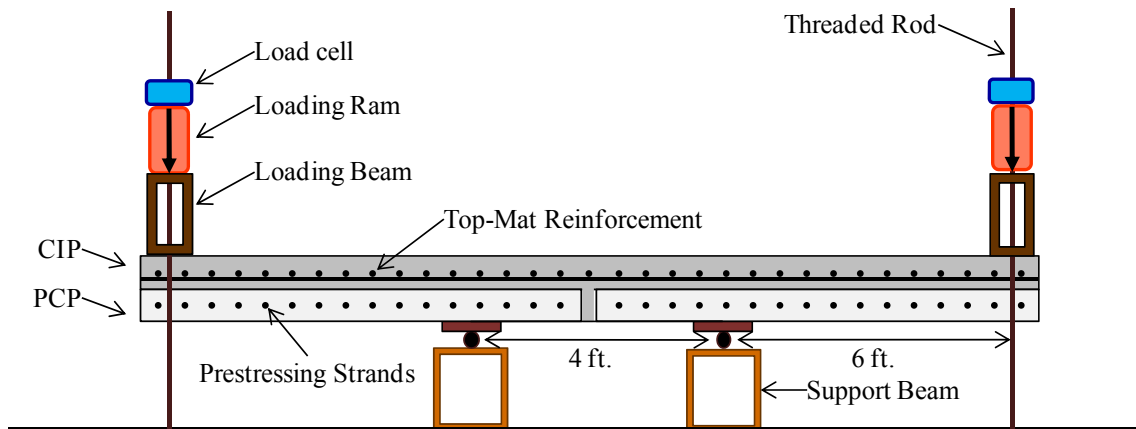


Figure 4-3: Constant Bending Moment Test Setup

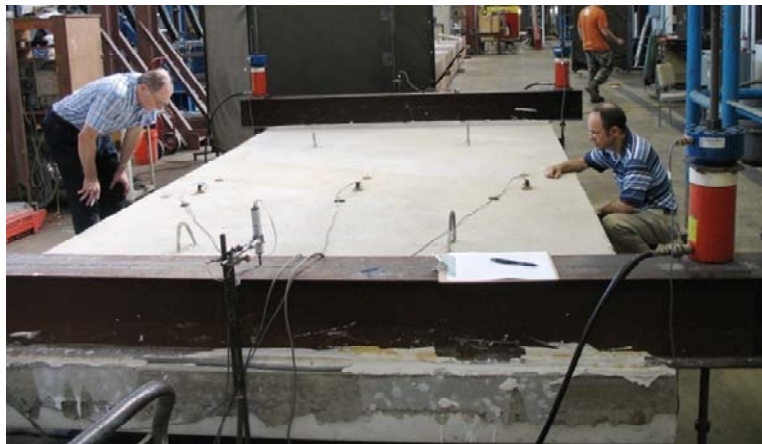


Figure 4-4: Loading Beams for Constant Bending Moment Test

Instrumentation was provided to record strains in the reinforcement, loads, the deflections at each end of the deck, and crack widths across the butt joint between the PCPs. A total of thirteen strain gages were placed on the No.4 bars that crossed the joint between the PCPs. Three linear potentiometers were attached to the surface of the deck to record the crack width across the PCP joint. Load cells were placed at each load location. One linear potentiometer was provided at the center of each loading beam to record the end deflections. Figure 4-5 shows a layout of all the instrumentation used during the constant bending moment test. Figure 4-6 and Figure 4-7 show the crack and deflection potentiometers, respectively.

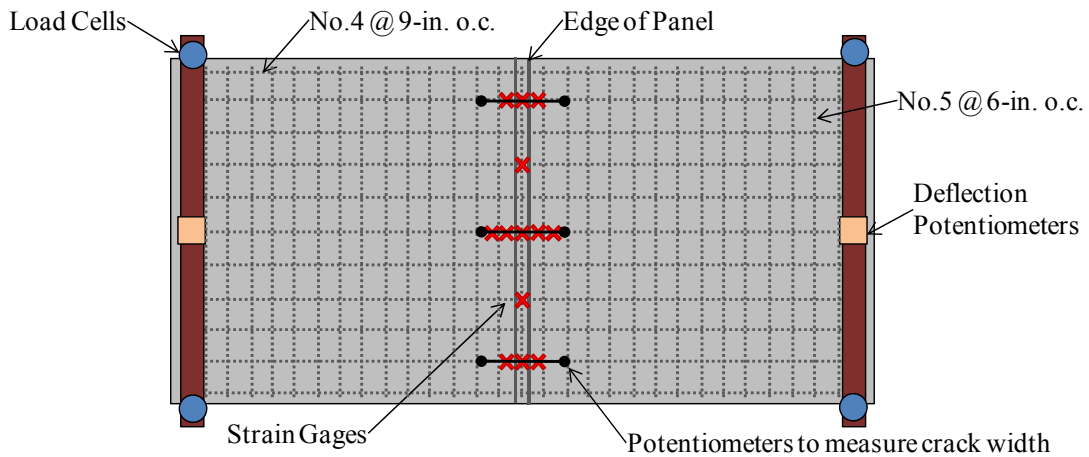


Figure 4-5: Instrumentation for Constant Bending Moment Test



Figure 4-6: Linear Potentiometer on CIP Slab across Expected Crack Location



Figure 4-7: Deflection Potentiometer

4.2.2 Material Properties

To reflect field conditions of the concrete, typical TxDOT Class S concrete mix was used for this specimen. The typical concrete mix design used by the ready mix provider consisted of the following:

- 3760 lbs of sand
- 5920 lbs of 1-in. river gravel

- 1370 lbs of cement
- 560 lbs of fly ash
- 38.5 gallons of water
- 6 oz. of air
- 27 oz. of retarder
- 91 oz. of water reducer

Several 4-in. by 8-in. cylinders were cast to monitor the compressive strength of the concrete. The 7-day strength was 4,270 psi, and the 28-day strength was 5,400 psi.

ASTM A605 reinforcing bars were used for the longitudinal and transverse reinforcement throughout the specimen. The yield strength of the reinforcement was 63 ksi with an ultimate strength of 92 ksi. The complete material test information for the reinforcement is shown in Appendix B.

4.2.3 Results

Several problems occurred during the constant bending moment test. First, several of the data acquisition instruments failed to record data. This was due to loss of strain gages during casting, improper hookup of the wiring, and/or faulty equipment. Therefore, no deflection data was gathered and only one surface potentiometer recorded crack widths.

Second, unexpected delamination of the CIP slab and PCPs was observed. The delamination cracks formed before any surface cracks in the CIP formed and worsened as the test progressed. A photo of the delamination is shown in Figure 4-8.



Figure 4-8: Delamination during Constant Bending Moment Test

Third, the first crack in the CIP slab did not form at the PCP joint. The first crack occurred at the section where the strain gage lead wires exited the CIP slab. Figure 4-9 shows a photo of the crack and the lead wires exiting the slab. The measured crack width was 0.01 in.



Figure 4-9: First Crack due to Lead Wires

The delamination between the CIP slab and the PCPs may have been exacerbated by the moment applied to the specimen. As the ends were loaded there was a tendency for the stiffer PCP to pry upward on the CIP slab, as shown in Figure 4-10. As a result, the location of first cracking was not controlled.

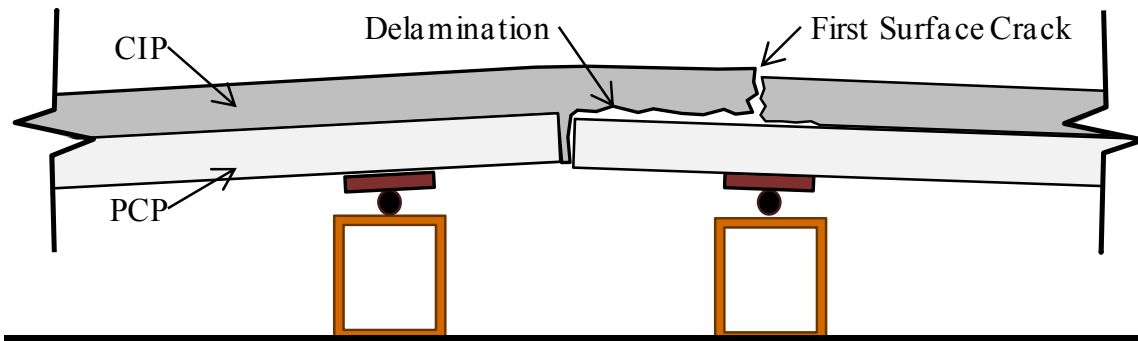


Figure 4-10: PCP Behavior during Constant Bending Moment Test

Furthermore, as the loading increased, several other cracks opened across the constant moment region, as opposed to a single crack at the PCP joint. A crack at the PCP joint did eventually form, and, as the loading progressed beyond yield of the reinforcement, this crack opened significantly. Figure 4-11 shows the distribution of surface cracks throughout the constant moment region.

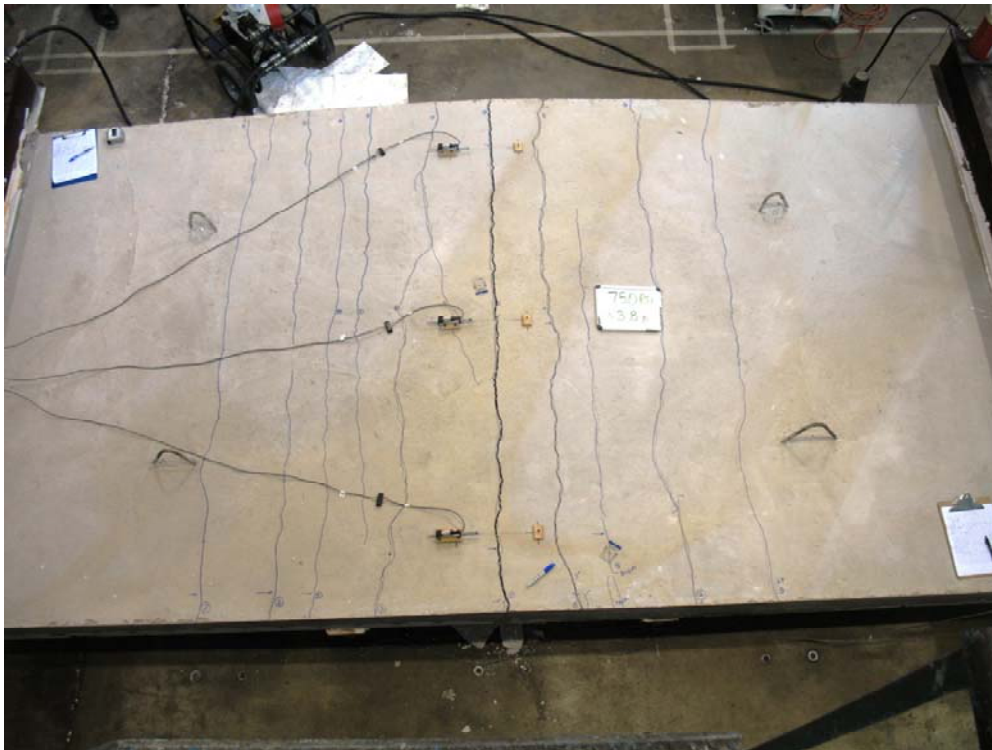


Figure 4-11: Cracking of the Constant Bending Moment Region

Lastly, when the crack did form over the butt joint, the strain in the reinforcement immediately exceeded yield. In Figure 4-12, strain in the reinforcement is plotted against measured crack width. The plot shows the measured readings for the only functioning surface potentiometer and the corresponding strain gage in the reinforcement directly beneath the potentiometer. Hand measurements taken with a crack comparator are shown as well. When the crack did form over the butt joint, the tensile force needed to form the crack exceeded the yield capacity of the CIP slab reinforcement. Because the specimen was subjected to a controlled load, the crack opened until the force was balanced by either lowering the applied load or the steel reaching strain hardening.

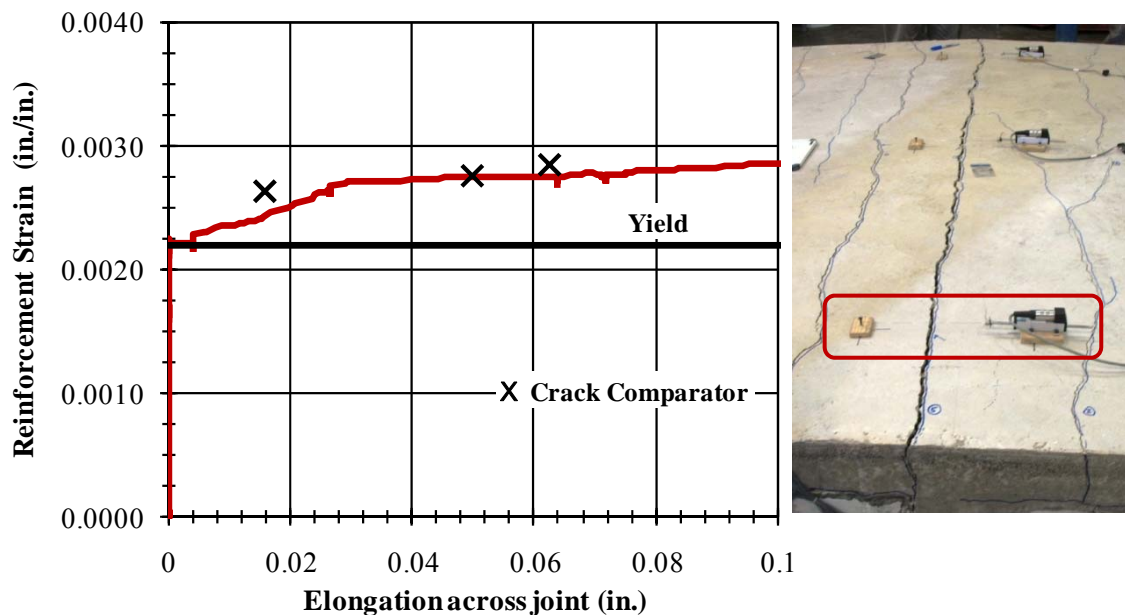


Figure 4-12: Results for Constant Moment Test

4.3 POINT LOAD TEST WITH PRE-CRACK

Because of the difficulties experienced with the constant bending moment test, the loading condition was modified in two ways. First, a single support at the PCP joint was used to increase the likelihood of one crack forming at the PCP joint and avoid the “prying” problem. Second, the deck was pre-cracked by loading the deck in the opposite

direction to reduce the tensile capacity of the CIP slab and help control the energy release in the deck when cracking was reached.

4.3.1 Pre-Cracking of Specimen

Similar to the constant bending moment test, two 8-ft. by 8-ft. PCPs placed 1.5-in. apart were topped with a 4-in. CIP slab. Instead of using the current TxDOT reinforcement, the second top mat reinforcement option (No. 4 @ 6-in. o.c. transverse, No. 3 @ 6-in. o.c. longitudinal) was used throughout the topping slab. A photograph during casting of the specimen is shown in Figure 4-13.



Figure 4-13: Casting of Point Load Specimen

Figure 4-14 shows the test setup for the pre-crack loading. One end of the deck was loaded with hydraulic rams beneath a steel loading beam that distributed the load across the deck. Another steel beam was placed on top of the deck at the PCP joint. Temporary jacks were used to support the opposite end of the deck because load information was not needed at that location.

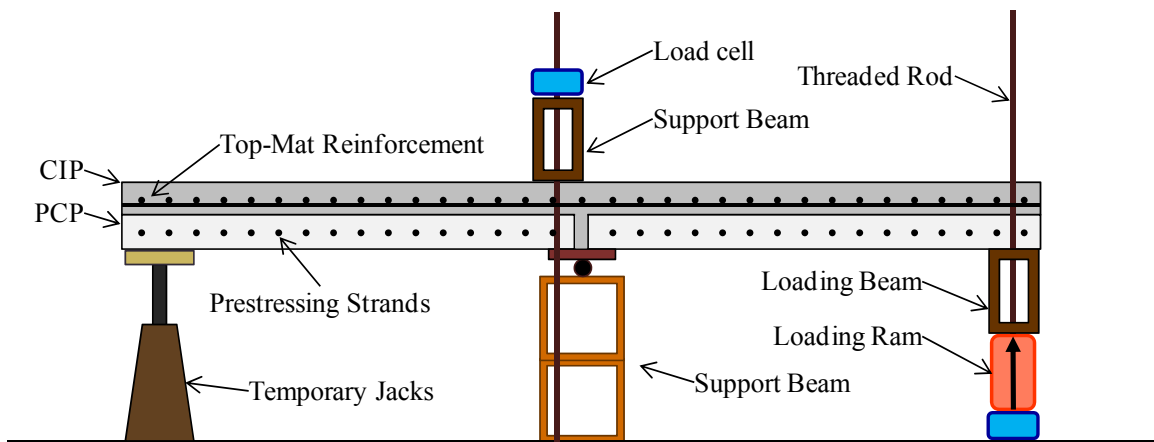


Figure 4-14: Pre-Crack Test Setup

The goal of this pre-crack test was to form a crack in the bottom half of the deck that would extend into the CIP slab to a location at or near the longitudinal reinforcement of the deck, shown as the ideal pre-crack in Figure 4-15. The pre-crack loading progressed as expected and the CIP slab was cracked to a depth near the reinforcement. Unfortunately, the loading was removed too quickly and the self-weight of the deck caused the crack to propagate all the way to the surface of the CIP. The measured crack at the surface was 0.009 in. Nonetheless, the pre-crack loading reduced the effective cracking capacity of the deck and the crack formed at the PCP joint.

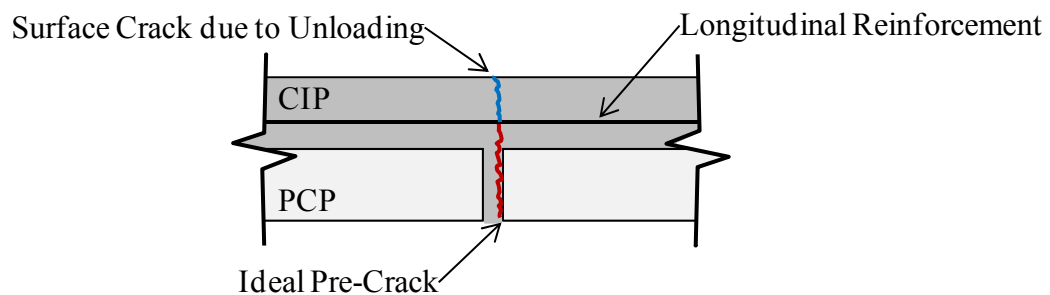


Figure 4-15: Pre-Crack of Point Load Specimen

4.3.2 Test Setup

Once the deck was pre-cracked, the loading beam was placed on top of the deck. The test setup for the point load test is shown in Figure 4-16.

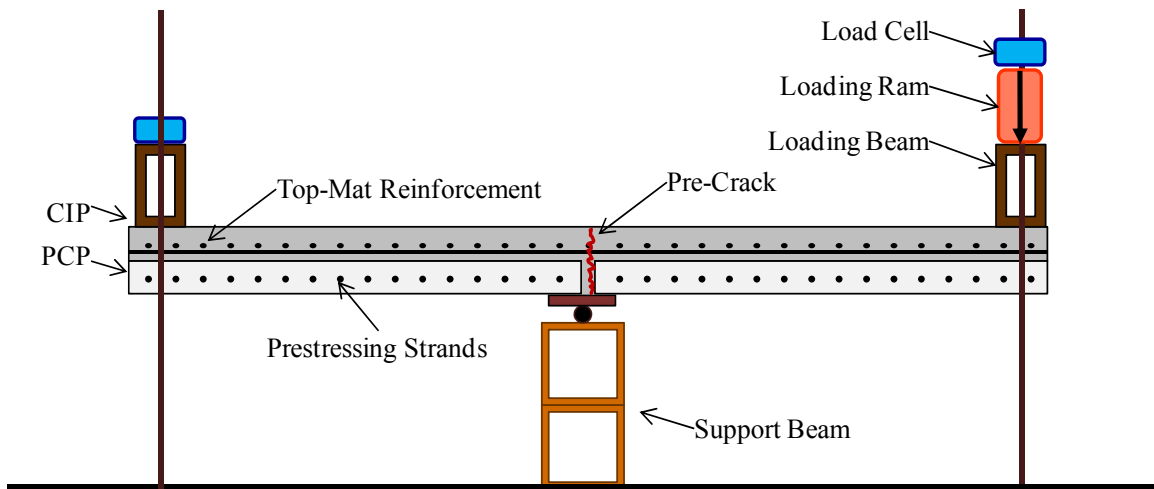


Figure 4-16: Point Load Test Setup

Instrumentation was provided to gather data on the strain in the reinforcement, the applied load, the deck deflection, and the crack width across the PCP joint. A total of twenty strain gages were placed on the No. 3 bars that crossed the joint between the PCPs. Three linear potentiometers were attached to the surface of the deck to record the growth of the crack width. Load cells were placed at each load location. One linear potentiometer was provided at the center of the loading beam to record the end deflection. Figure 4-17 shows a layout of all the instrumentation for the point load test.

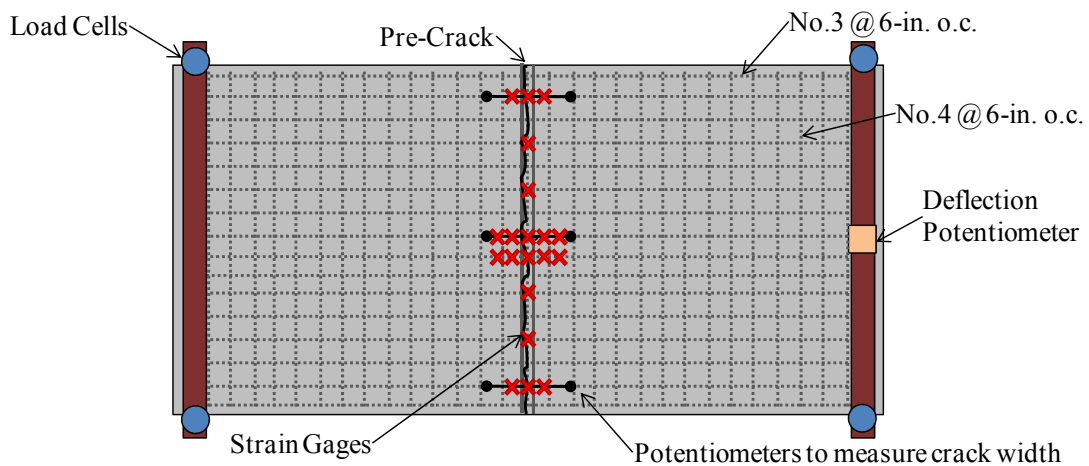


Figure 4-17: Instrumentation for Point Load Test

4.3.3 Material Properties

The concrete mix and steel reinforcement properties were the same as the constant bending moment test. TxDOT Class S concrete was used, and the reinforcement was from the same heat as the constant bending moment specimen (63 ksi yield, 92 ksi ultimate). The 7-day strength was 4,780 psi and the 28-day strength was 6,400 psi.

4.3.4 Results

A plot showing the growth of the pre-crack during the point load test is shown in Figure 4-18. The load was increased as the surface crack of the CIP slab grew from 0.009 in. to 0.06 in., as shown in Figure 4-19. The loading was paused throughout the test to measure crack widths by hand with a crack comparator.

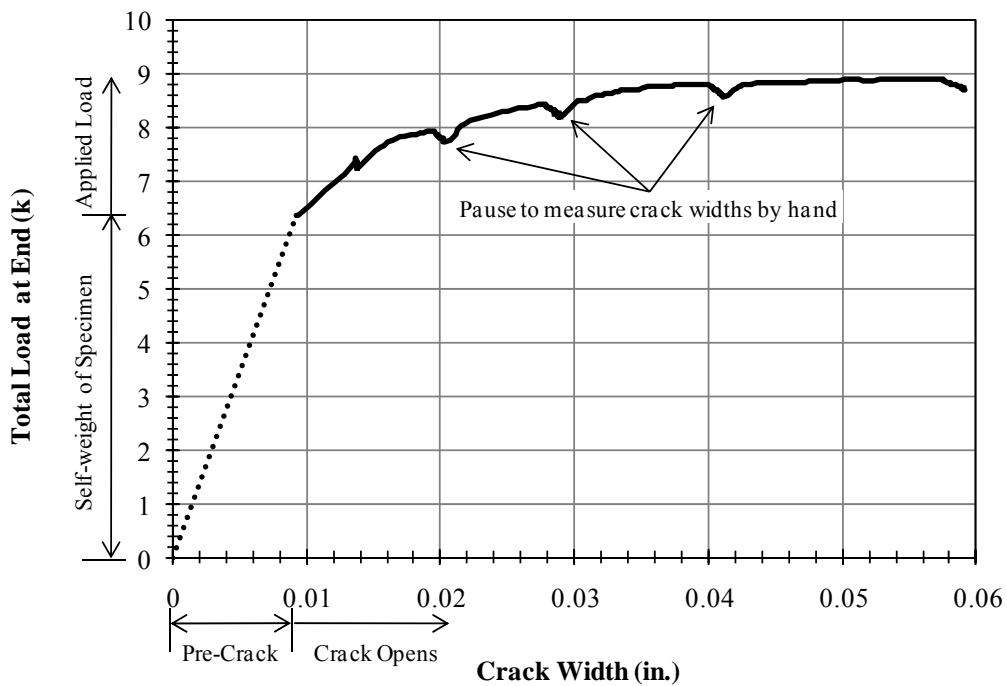
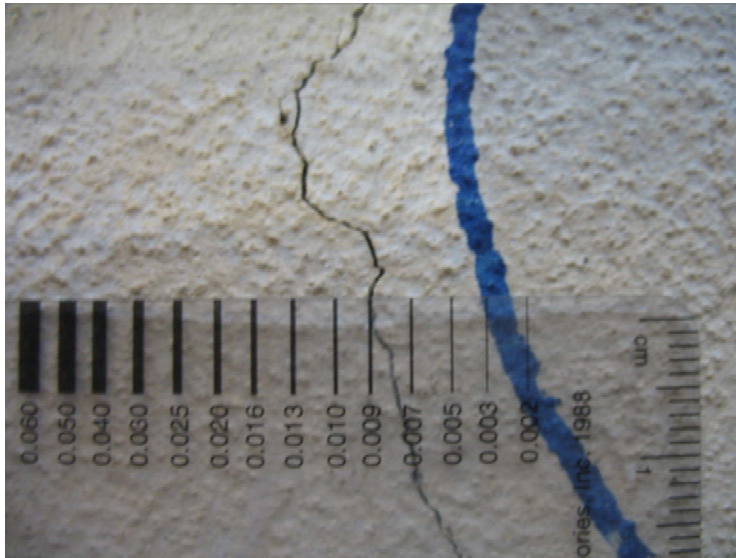


Figure 4-18: Load vs. Crack Width Plot for Point Load Test



(a) Start of Test



(b) End of Test

Figure 4-19: Crack Width at (a) Start and (b) End of Test

A plot of strain in the reinforcement versus crack width for the three surface potentiometers across the deck is shown in Figure 4-20. The strain in the reinforcement was roughly 0.0015 in./in. at the start of the test due to the pre-crack loading. The reinforcement yielded very early in the test as the crack width increased to about 0.015-in.

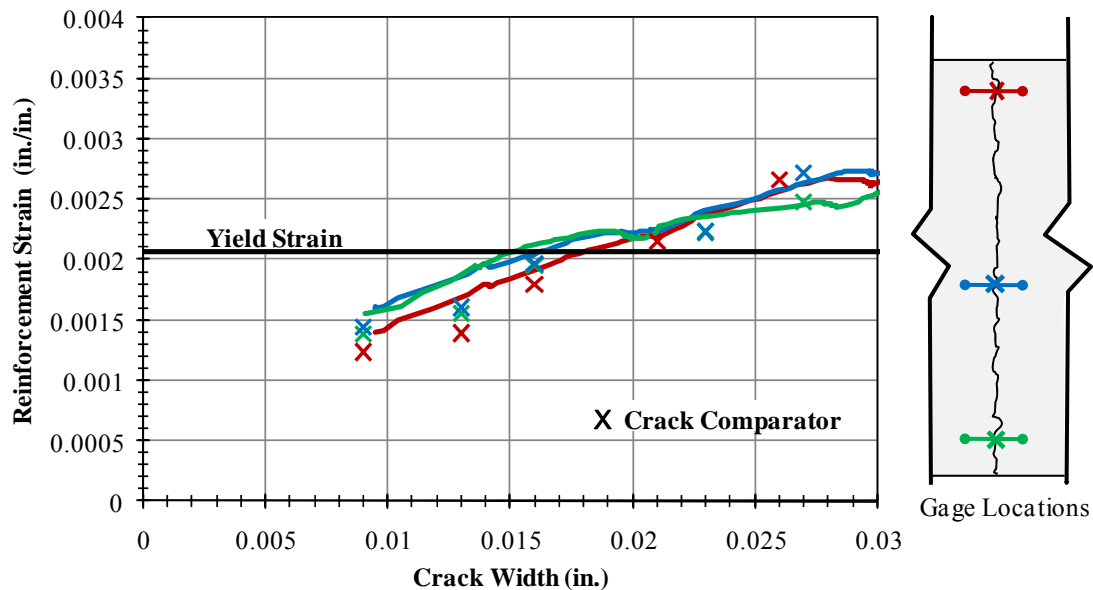


Figure 4-20: Results for Point Load Test

Overall, this test was more successful than the constant bending moment test. The instrumentation worked properly and a single crack formed at the PCP joint. However, it was still difficult to control the energy release at cracking. In this case, a crack formed through the CIP slab under the weight of the specimen prior to the application of load. There was also some minor delamination observed during the point load test; however, a photograph was not taken.

4.4 DIRECT TENSION TEST OF CIP-PCP DECK

Because the energy release was difficult to control and a more repeatable test was desired without the need for pre-cracking, a direct tension test of the CIP-PCP deck was performed under controlled deformation.

4.4.1 Test Setup

In order to fit the specimen into a MTS machine that could be operated in deformation or load control, two 18-in. by 24-in. PCP sections were topped with a 4-in. CIP slab. These PCP sections were cut from an 8-ft. by 8-ft. panel using the concrete saw shown in Figure 4-21. Three No. 3 reinforcing bars, spaced six inches apart, were placed

in the CIP topping slab, as shown in Figure 4-22. Unlike the previous test specimens, the PCPs were butted against each other similar to field conditions.



Figure 4-21: Concrete Saw used to Cut PCPs

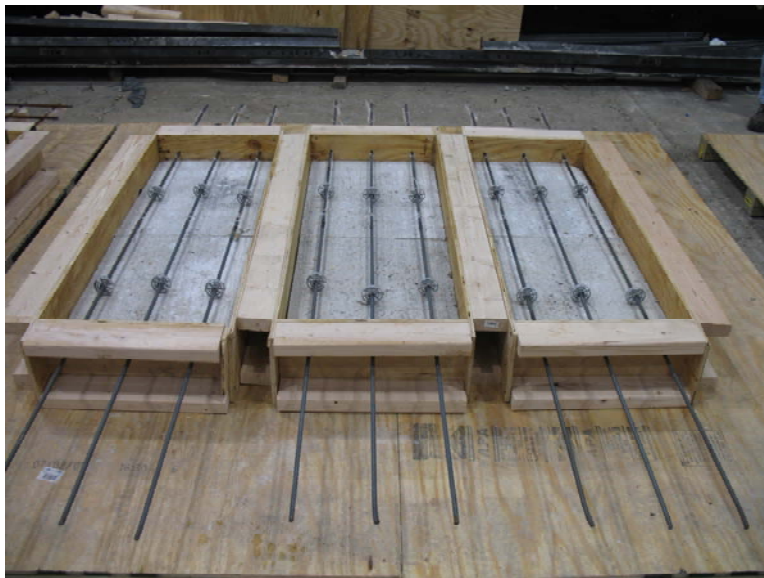


Figure 4-22: Direct Tension Specimens Prior to Casting

To grip the specimen during loading, 5/8-in. thick plates were welded to the reinforcing bars. These plates extended six inches beyond the length of the bars and were

gripped in the MTS test machine. Figure 4-23 shows the welded plate in the MTS machine grips, and Figure 4-24 shows the direct tension test setup for the CIP-PCP deck.



Figure 4-23: Welded Plates in MTS Grip

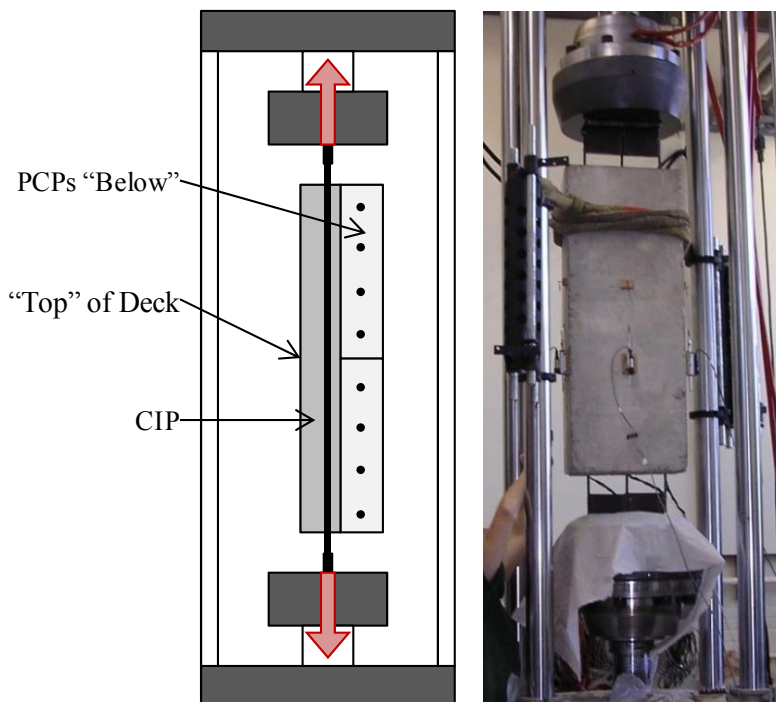


Figure 4-24: CIP-PCP Tension Test Setup

A potentiometer was installed on the CIP surface across the PCP joint to record crack width data. A surface potentiometer was also installed on each of the other three faces of the specimen to determine if any eccentric loading was occurring. The MTS

machine recorded load and deflection of the loading piston. Strain gages were not used because the simplicity of the loading allowed for direct conversion of load to strain.

4.4.2 Material Properties

The concrete mix and steel reinforcement properties were the same as the previous tests. TxDOT Class S concrete was used and had a 28-day strength of 6,600 psi. The A605 reinforcing bars were from the same heat as the previous specimens (63 ksi yield, 92 ksi ultimate).

4.4.3 Results

Because the longitudinal reinforcement is not centered in the CIP slab (see Figure 3-7 for complete dimensions), the loading caused significant eccentricity in the specimen. As a result, the specimen was again subjected to bending and the PCP sections completely delaminated. The crack extended into the CIP slab from the CIP-PCP interface instead of the exposed surface (top of deck). Furthermore, the crack did not occur at the joint of the PCP sections. In Figure 4-25, a schematic representation of the eccentric loading is shown. A photograph of the delaminated PCP section is shown in Figure 4-26.

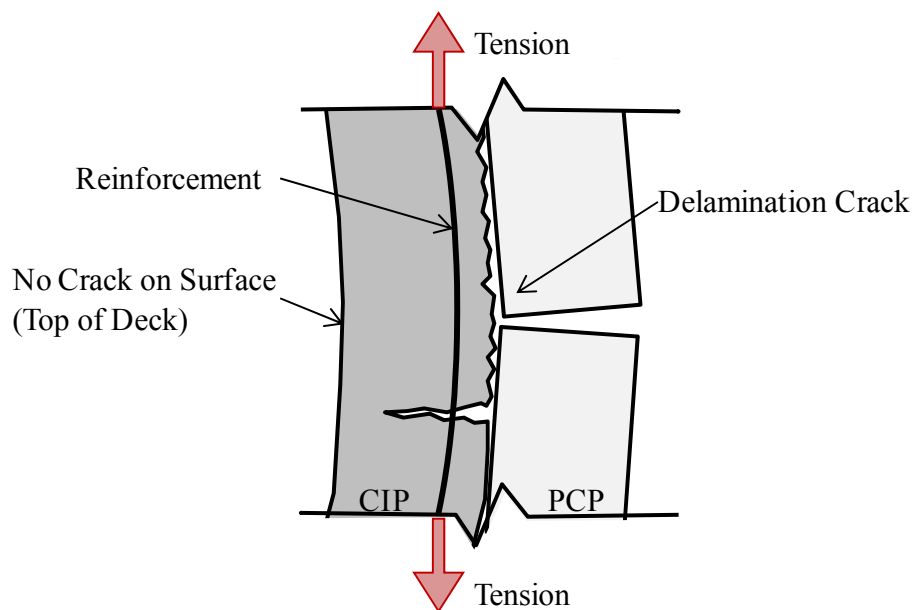


Figure 4-25: Eccentric Loading during CIP-PCP Tension



Figure 4-26: Delamination of PCPs during Tension Test

4.5 DIRECT TENSION TEST OF CIP-PCP DECK WITH SAW-CUT

In an attempt to reduce the eccentricity and delamination observed in the first direct tension test, another tension test was performed with a groove cut into the CIP topping slab, as shown in Figure 4-27. The groove was cut to a depth such that the longitudinal reinforcement was centered across the cut section. The groove was placed directly above the PCP joint in an effort to force the crack to form at the joint. A photograph of the saw-cut is shown in Figure 4-28.

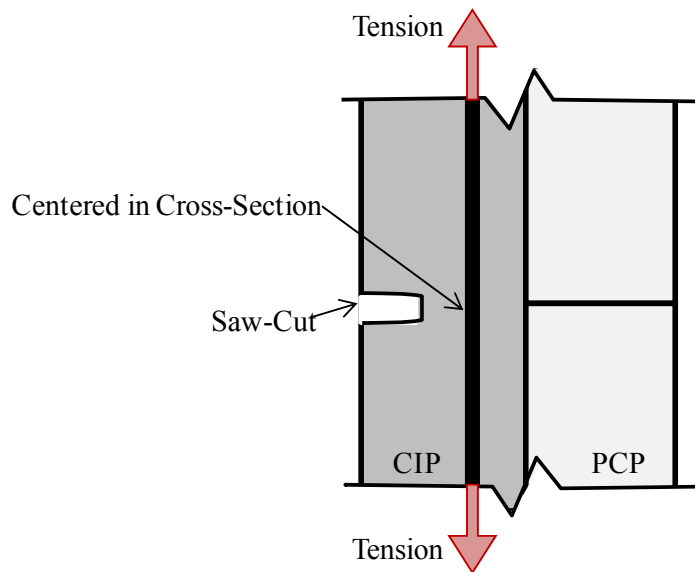


Figure 4-27: Section of Saw-Cut CIP-PCP Specimen



Figure 4-28: Saw-Cut of CIP

4.5.1 Test Setup

The test setup was the same as the previous direct tension test of the CIP-PCP deck except two No. 4's @ 9-in. o.c. were placed in the topping slab instead of three No.3's @ 6-in. o.c. Figure 4-29 shows the saw-cut specimen in the MTS machine. The instrumentation was also the same as the previous CIP-PCP direct tension test; surface potentiometers were installed on all four sides of the specimen.



Figure 4-29: Saw-Cut Specimen in MTS Machine

4.5.2 Material Properties

This specimen was cast at the same time as the direct tension specimen without the saw cut. The 28-day strength of the TxDOT Class S mix was 6,600 psi and the yield strength of the A605 steel reinforcement was 63 ksi (same heat as previous reinforcement).

4.5.3 Results

As a result of the saw-cut, the eccentricity of the load was slightly reduced. Delamination was not eliminated. Figure 4-30 shows the delamination crack that was observed during testing. Although there was less eccentricity of load at the butt joint section, bending over the rest of the specimen was largely unchanged and the same problem persisted.

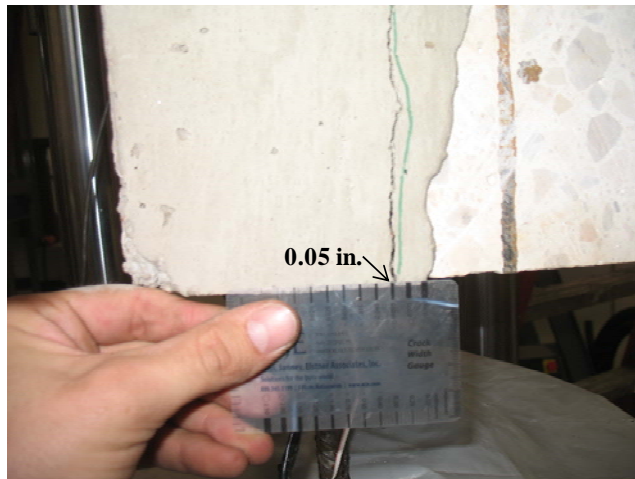


Figure 4-30: Delamination of Saw-Cut Specimen

A crack did form on the top surface of the CIP slab, but only after the crack formed on the bottom face of the CIP slab. Figure 4-31 shows the cracking behavior of the saw-cut specimen. The crack on the bottom was wider than the crack on the top surface due to the eccentricity. Figure 4-32 shows the observed cracking when the crack first propagated to the surface of the CIP.

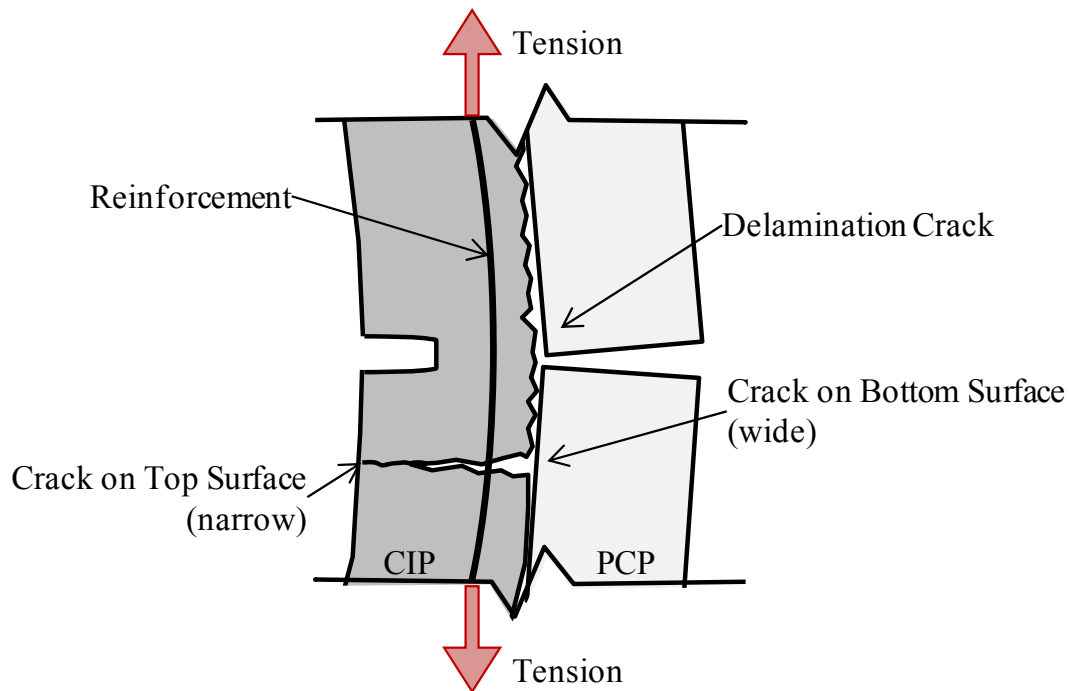


Figure 4-31: Cracking Behavior of the Saw-Cut Specimen

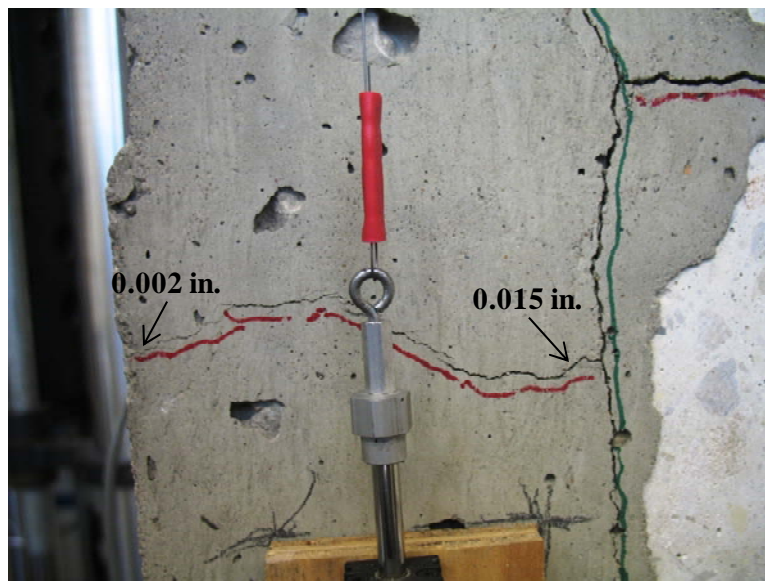


Figure 4-32: First Crack at Surface of Saw-Cut Specimen

4.6 DIRECT TENSION TEST OF CIP SLAB WITH SAW-CUT

To eliminate the delamination problems and the resulting non-composite behavior of the CIP slab and the PCPs, a direct tension test of a CIP-only section was conducted to

find a testing approach that would allow for simple and direct comparison of the various top mat reinforcement alternatives.

4.6.1 Test setup

A 4-ft. long by 18-in wide by 4-in. deep slab with two No.4's @ 9-in. o.c. placed in the center of the cross-section was tested in the MTS machine. Placing the bars at the center of the cross-section, not at field-condition depth, prevented the loading from being eccentric. A photo of the formwork and reinforcement prior to casting is shown in Figure 4-33.

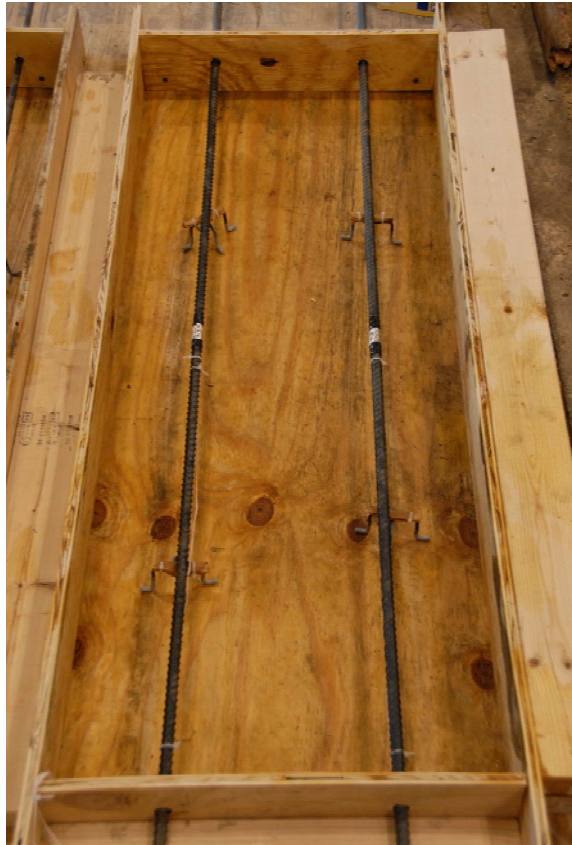


Figure 4-33: CIP Specimen Prior to Casting

Furthermore, a groove was cut on either side of the specimen to reduce the energy release at cracking and ensure that the reinforcement would not yield prior to cracking. The cross-section details are shown in Figure 4-34, and a photograph of the specimen is shown in Figure 4-35.

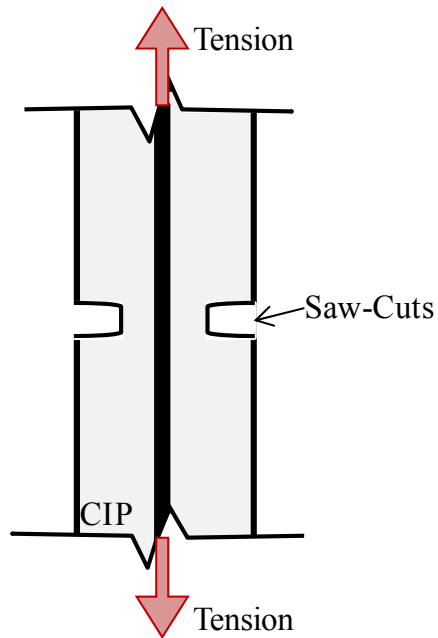


Figure 4-34: CIP Section with Saw-Cut



Figure 4-35: CIP Slab with Saw-Cut Specimen

Because of the difficulty predicting where the cracks would form (even with the saw-cuts), the surface potentiometers were placed to measure deformation over the entire length of the specimen. Otherwise, the instrumentation remained unchanged.

4.6.2 Material Properties

A high early strength mix that was being used for another research project was used for this specimen. The concrete mix had a design strength of 6,000 psi and consisted of the following properties:

- Type III low-alkali cement
- Water-to-cement ratio of 0.52
- $\frac{3}{4}$ -in. crushed limestone

The specimen was tested when the concrete was 14 days old. The compressive strength at the time of testing was 5,500 psi. The same A605 reinforcing bars with a yield strength of 63 ksi and an ultimate strength of 92 ksi were used for this specimen.

4.6.3 Results

Two cracks formed during the CIP direct tension test. The first formed across the saw-cut at a load well below the yield load of the two No.4 bars. The second crack formed across the full section just prior to reaching yield in the reinforcement. The load-deflection plot in Figure 4-36 shows the load at which the two cracks formed. A photograph of the two cracks is shown in Figure 4-37.

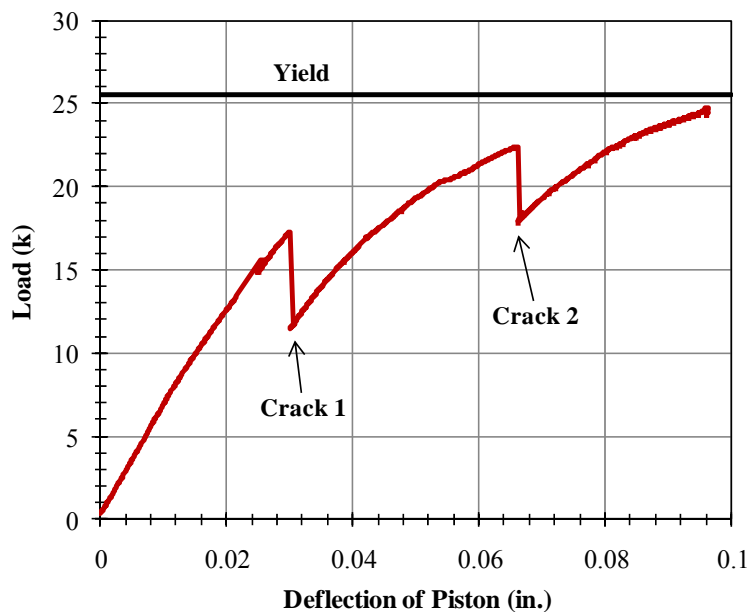


Figure 4-36: Load-Deflection Plot for CIP Tension Test

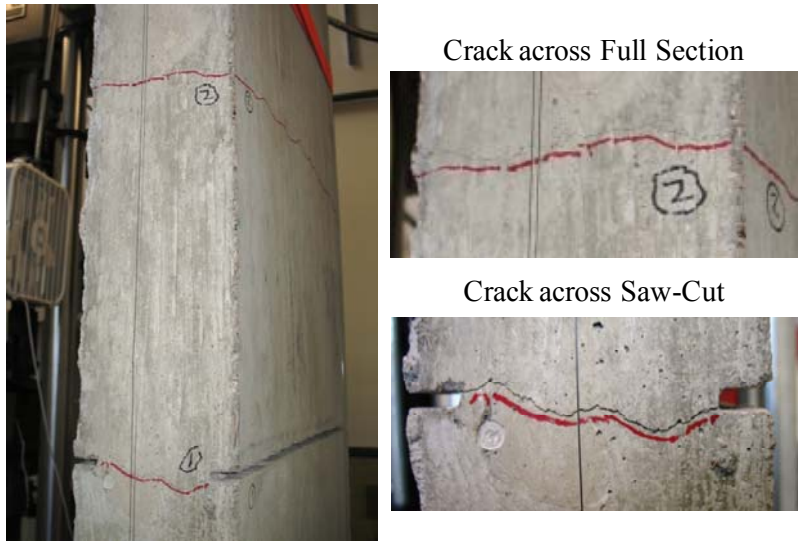


Figure 4-37: Cracking of CIP Specimen

The measured crack widths are shown in Figure 4-38. Notice the crack across the saw-cut opens at a considerably lower stress than the crack across the full-section. The crack widths increase rapidly as the stress in the reinforcement reaches yield.

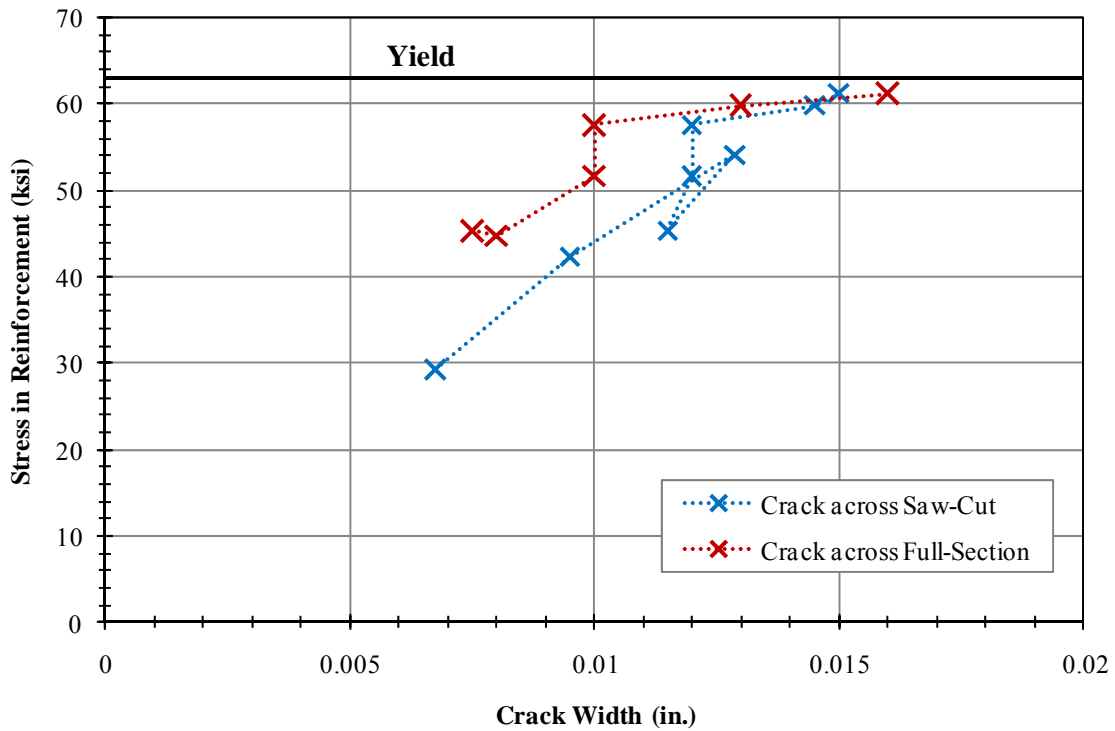


Figure 4-38: Results for Tension Test of CIP with Saw-Cut

4.7 DIRECT TENSION TEST OF CIP SLAB

Because of the success of the direct tension test of the CIP slab with the saw-cut and the repeatability of the test procedure, the direct tension test of the CIP slab appeared to provide the best way to evaluate the various reinforcement arrangements. Therefore, another direct tension test was conducted using typical longitudinal reinforcement, No. 4 @ 9-in. o.c.

4.7.1 Test Setup

The test setup and instrumentation were the same as the previous CIP direct tension test; however, no cut was made across the section. The saw-cut was removed to better reflect the in-service conditions of the CIP slab.

4.7.2 Material Properties

To promote cracking at lower stress levels, a concrete mix with a design strength of 3,000 psi was used for this specimen. The concrete mix consisted of the following properties:

- 4-1/4 sack (a measure of how much portland cement to include)
- 25% fly ash
- 3/4-in. maximum aggregate size
- 6 to 8-in. slump

The concrete had a 7-day strength of 3,000 psi and a 28-day strength of 3,980 psi.

ASTM A706 reinforcing bars were used to help promote welding of the bars to the 5/8-in. plate. The yield strength of the reinforcement was 65 ksi with an ultimate strength of 100 ksi. The complete material test information for the reinforcement is shown in Appendix B.

4.7.3 Results

The concrete never cracked prior to reaching yield of the reinforcement. The test was stopped after the reinforcement reached yield because crack widths immediately reach levels not likely under service conditions. Because the concrete never cracked prior

to yielding the two No. 4 bars, it was decided that further tests of specimens with longitudinal reinforcement less than is currently used was not a feasible solution.

4.8 DISCUSSION OF LONGITUDINAL REINFORCEMENT TEST RESULTS

Significant knowledge on the behavior of CIP-PCP decks and the current longitudinal reinforcement was gained. Based on this test program, three findings were made: (i) the tensile strength of the CIP slab is critical to controlling transverse crack widths, (ii) the composite behavior of the CIP slab and the PCPs is difficult to simulate in the laboratory due to delamination issues associated with boundary and loading conditions in the tests, and (iii) it is unlikely that the current longitudinal reinforcement can be reduced while controlling transverse crack widths.

4.8.1 Tensile Strength of Concrete

TxDOT specifies a minimum 28-day compressive strength of 4,000 psi for CIP slabs on PCPs (TxDOT Class S Mix). The actual strength, however, is frequently higher than specified; typical values during this testing program were higher than 6,000 psi. Because the strength of the CIP slab was higher than anticipated, the top mat reinforcement was at a higher stress than anticipated when the CIP slab cracked.

Pre-cracking and saw-cutting were used to help alleviate this problem during the test program, but it is clear that strength of the CIP slab is critical to controlling crack widths in the field. Higher concrete strengths lead to larger stresses in the reinforcement at cracking. Accordingly, higher strength concretes will have wider crack widths for a given reinforcing arrangement. To illustrate the point, consider the 18-in. by 4-in. CIP section shown in Figure 4-39. In Figure 4-40, the cracking load is plotted against the strength of concrete for this section. The load values corresponding to yield of various reinforcing arrangements are also shown.

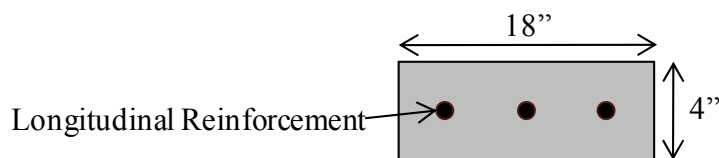


Figure 4-39: Sample CIP Section

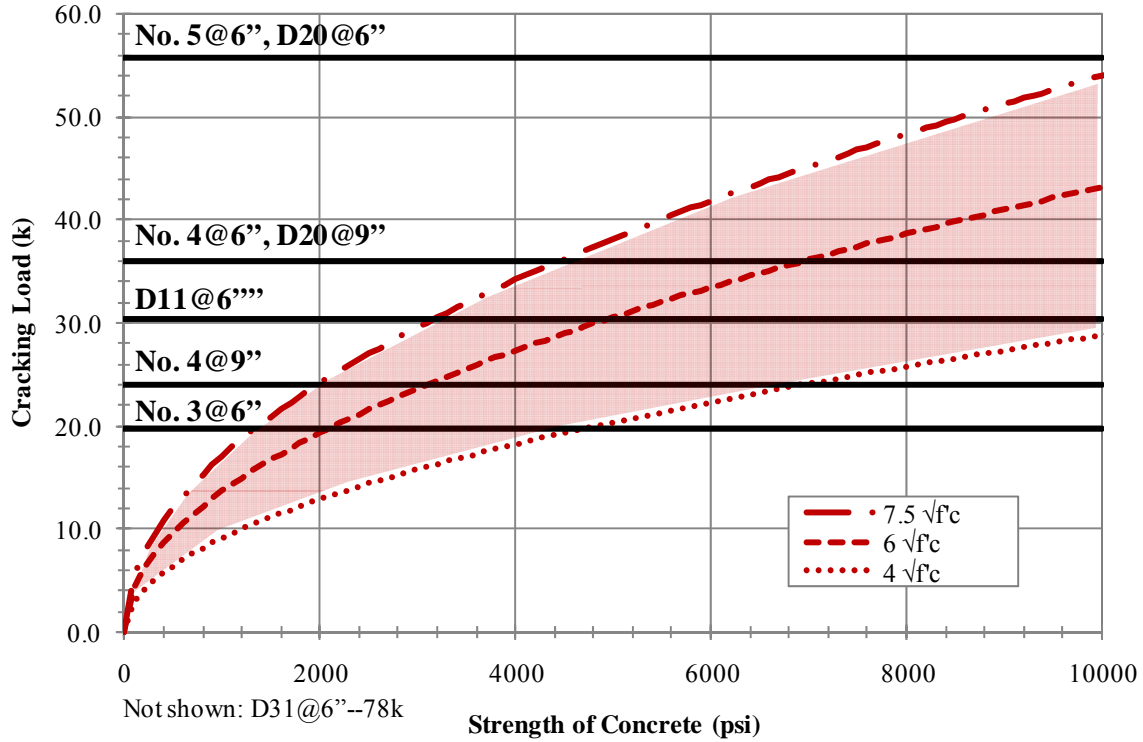


Figure 4-40: Comparison of Cracking Load to Yield of Reinforcement

Note that No. 3 @ 6-in. o.c. will yield just after 4,000 psi concrete reaches $4\sqrt{f'_c}$. If the tensile strength of the concrete is any higher than $4\sqrt{f'_c}$ or the concrete strength is any higher than 4,000 psi, then No. 3 @ 6-in. o.c. will yield as cracking of the concrete occurs. Comparing the cracking loads of the successful direct tension tests that were performed for the transverse reinforcement (described in Chapter 5), first cracking was between 6.25 and $6.6\sqrt{f'_c}$ for the direct tension tests. Therefore, the only longitudinal specimen that would crack before yielding would be D20 @ 9-in. o.c.

4.8.2 Composite Behavior of CIP Slab with PCPs

Delamination was observed during all of the tests that were performed with a CIP slab on top of PCPs. The surface condition of the PCPs was broom finished and flooded during construction as seen in Figure 2-12. The moisture content of the surface of the PCPs was not confirmed to be saturated, surface dry, however. This may have contributed to the delamination cracking that was observed. Regardless, it was apparent

after the direct tension test of the CIP-PCP deck (see Section 4.1.3) that shear transfer from the CIP to PCP crossing the interface was limited. The ideal shear transfer for the direct tension test is shown in Figure 4-41. This behavior was clearly not accomplished otherwise the observed delamination cracking and eccentricity of the load would not have occurred.

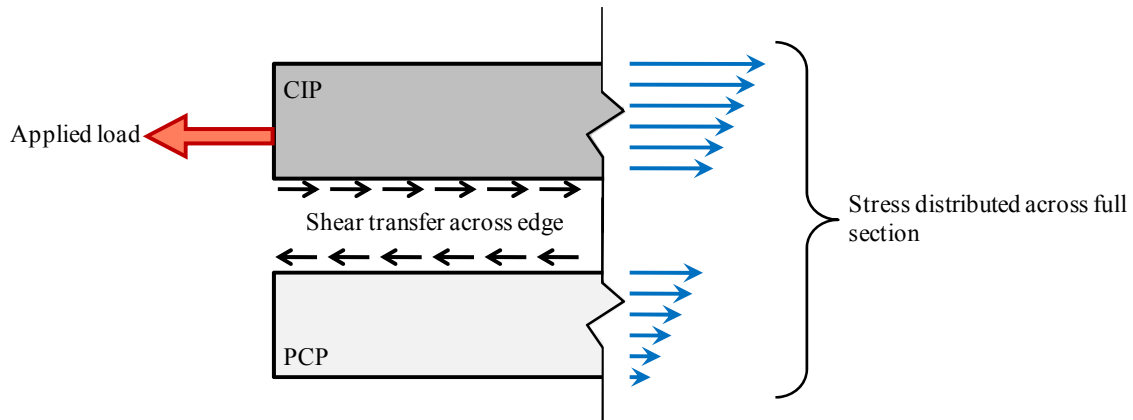


Figure 4-41: Shear Transfer across CIP-PCP Interface

4.8.3 Reduction of Longitudinal Reinforcement

Overall, a reduction in longitudinal reinforcement does not appear to be warranted without sacrificing crack width control. Because the yield strength of the current longitudinal reinforcement detail is already at or near the cracking strength of the concrete, reducing the steel would reduce the likelihood of controlling crack widths. The D20 @ 9-in. o.c. could control crack widths better than the No.4 @ 9-in. o.c., but it is expected that increased cost of the welded wire reinforcement could not be offset by reducing the area of steel.

CHAPTER 5

TRANSVERSE REINFORCEMENT TEST PROGRAM

5.1 INTRODUCTION

Based on the results of the longitudinal reinforcement test program, several direct tension tests of the CIP slab were conducted to evaluate transverse reinforcement alternatives. Since typical transverse steel reinforcement involves larger bars than typical longitudinal reinforcement, it is likely that the concrete will crack prior to yielding.

5.2 DIRECT TENSION TESTS OF CIP SLAB

Two direct tension tests of the CIP slab were conducted for each of the transverse reinforcement alternatives shown in Table 5-1. The deformed bars and welded wire options have the same area but different yield stresses.

Table 5-1: Transverse Reinforcement Test Specimens

Specimen	Area of Steel (in ² /ft)	Yield Stress (ksi)
1. No. 5 @ 6 in.	0.62	62
2. No. 4 @ 6 in.	0.40	65
3. D31 @ 6 in.	0.62	84
4. D20 @ 6 in.	0.40	92

5.2.1 Test Setup

Four foot long by 12-in wide by 4-in. deep slabs with the reinforcing alternatives placed in the center of the cross-section were tested in the MTS machine. Placing the bars at the center of the cross-section, instead of field-condition depth, prevented the loading from being eccentric. The instrumentation was the same as was used in the longitudinal reinforcement tests of Chapter 4. No saw-cuts were made.

5.2.2 Material Properties

These specimens were cast using the same concrete mix as direct tension test of the CIP slab for the longitudinal reinforcement (Section 4.7). The 28-day strength of the mix was 3,980 psi.

ASTM A706 reinforcing bars were used for the standard reinforcing options to help promote welding of the bars to the 5/8-in. plate. The yield strength of the No. 5 bars was 62 ksi with an ultimate strength of 96 ksi. The yield strength of the No. 4 bars was 65 ksi with an ultimate strength of 100 ksi.

ASTM A185 deformed welded wire reinforcement was used for the welded wire alternatives. The yield strength of the D31 welded wire was 84 ksi with an ultimate strength of 94 ksi. The yield strength of the D20 welded wire was 92 ksi with an ultimate strength of 103 ksi. The complete material test information is shown in Appendix B.

5.2.3 Results

Cracking was observed prior to yielding for all of the tests. Table 5-2 shows the total number of cracks and the spacing between the cracks for each test.

Table 5-2: Cracking of Transverse Specimens

Reinforcement	Specimen	Number of Cracks	Spacing between Cracks (in.)
No. 5	No. 5-1	6	5-3-5-9-7.5
	No. 5-2	7	6-5.5-5.5-8-5-5.5
No. 4	No. 4-1	6	5.5-6-9.5-6-6.5
	No. 4-2	7	7.5-5-5-6.5-8-3.5
D31	D31-1	4	9-9-9*
	D31-2	4	9-9-9*
D20	D20-1	4	12-12-6.5 ⁺
	D20-2	4	6-8-10 ⁺

*Cross-wires spaced at 9-in. o.c., ⁺Cross-wires spaced at 6-in. o.c.

The stress vs. elongation plots for the No. 5 and D31 specimens and the No. 4 and D20 specimens are shown in Figure 5-1 and Figure 5-2, respectively. The reported elongation was taken by averaging the four linear potentiometers. The jagged peaks at the start of the test represent each of the cracks forming; the specimens cracked between 6.25

and $6.6\sqrt{f'_c}$. The plotted elongation provides an indication of the total growth of the crack widths across the specimen as the stress increases.

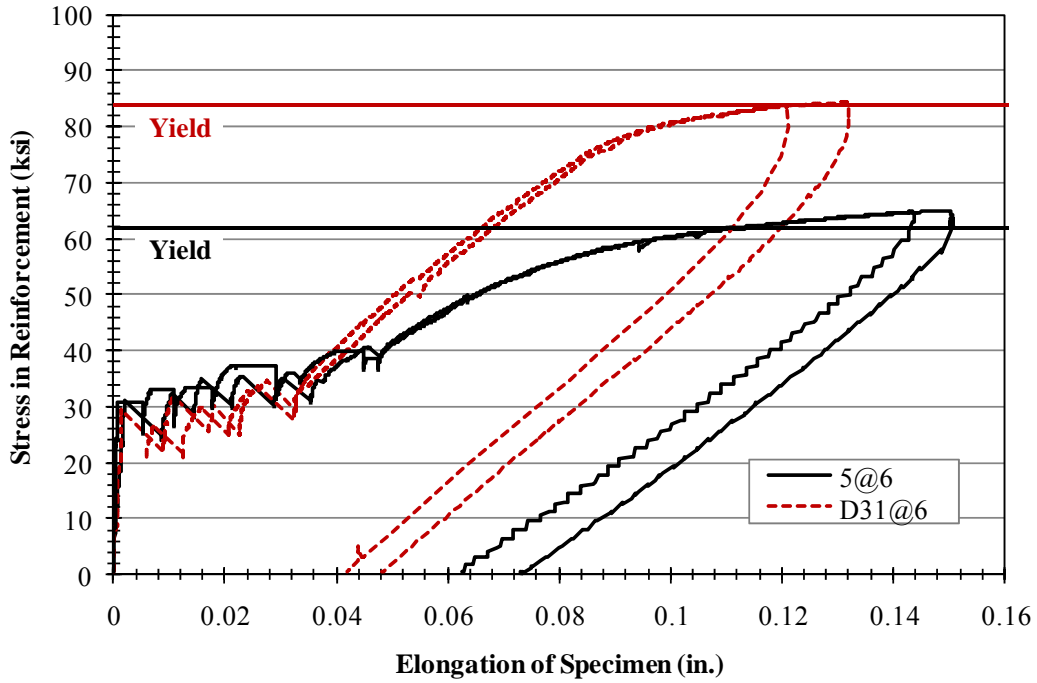


Figure 5-1: Stress vs. Elongation for No. 5 and D31 Specimens

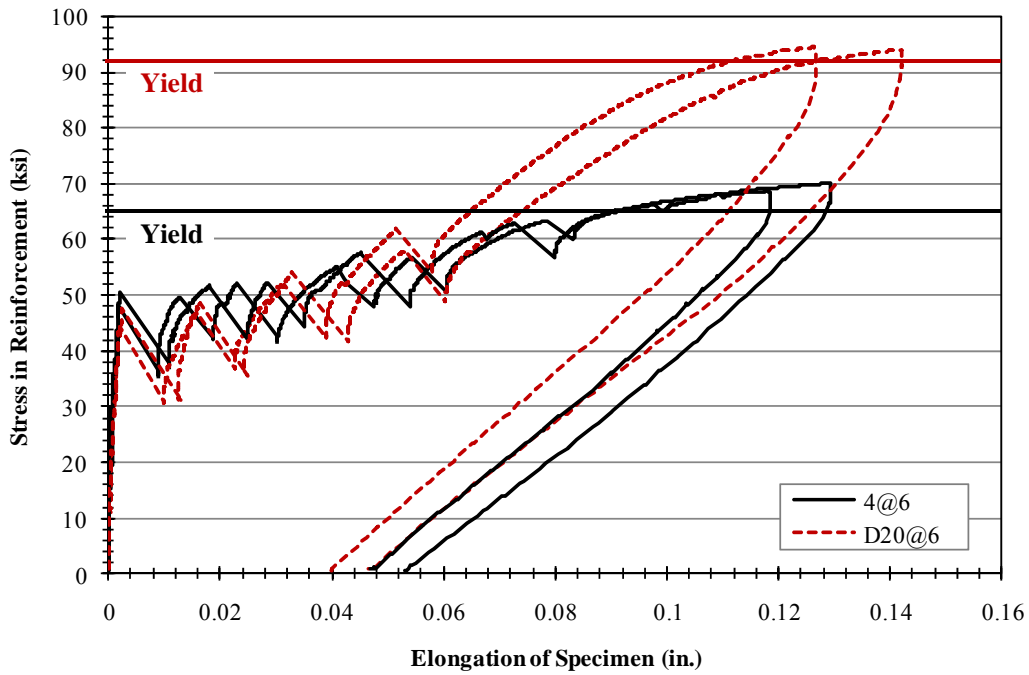


Figure 5-2: Stress vs. Elongation for No. 4 and D20 Specimens

The measured crack widths (crack comparator) for test specimen No. 5-1 are shown in Figure 5-3. Although Table 5-2 reports six total cracks for this specimen, only five cracks opened across the full cross-section. Because the concrete still has some capacity across a section that is not fully cracked, the stress in the reinforcement is unknown at that section. Therefore, the crack that did not open on both sides of the specimen is not presented in Figure 5-3. For the remaining five cracks, if there was any variation in crack width between faces, the average crack width is reported.

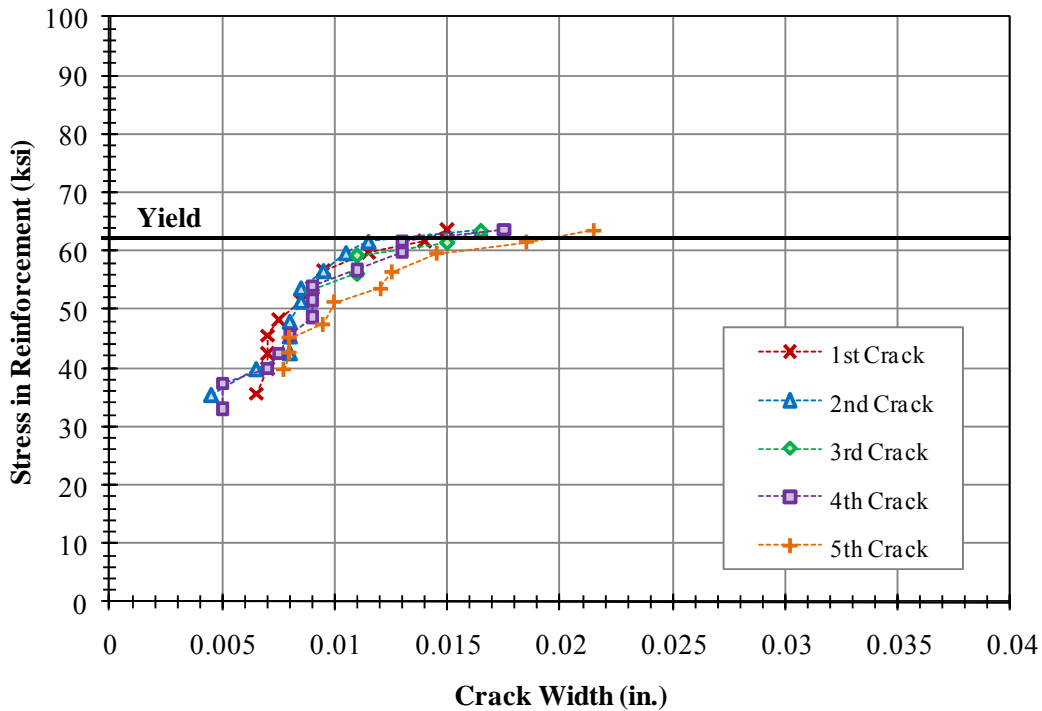


Figure 5-3: Crack Widths for Test Specimen No. 5-1

The complete crack width results for the No. 5 and D31 specimens and the No. 4 and D20 specimens are shown in Figure 5-4 and Figure 5-5, respectively. These plots follow the same procedure that was described for Figure 5-3. The crack width data collected for both test specimens for each reinforcement alternative is shown.

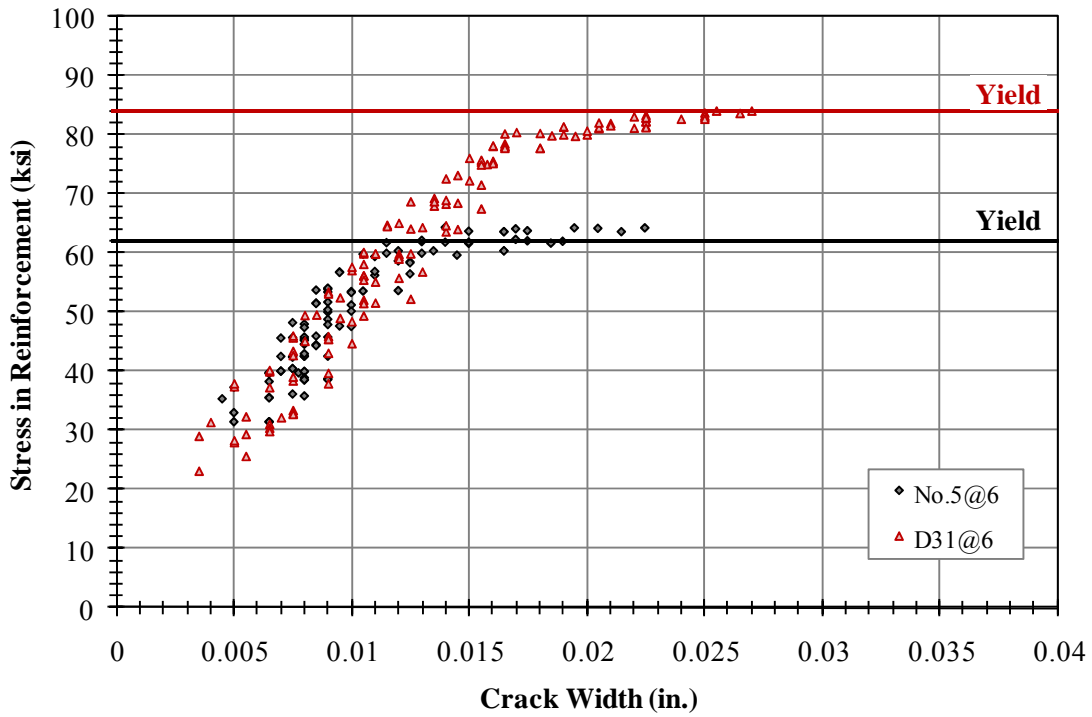


Figure 5-4: Crack Width Results for No. 5 and D31 Specimens

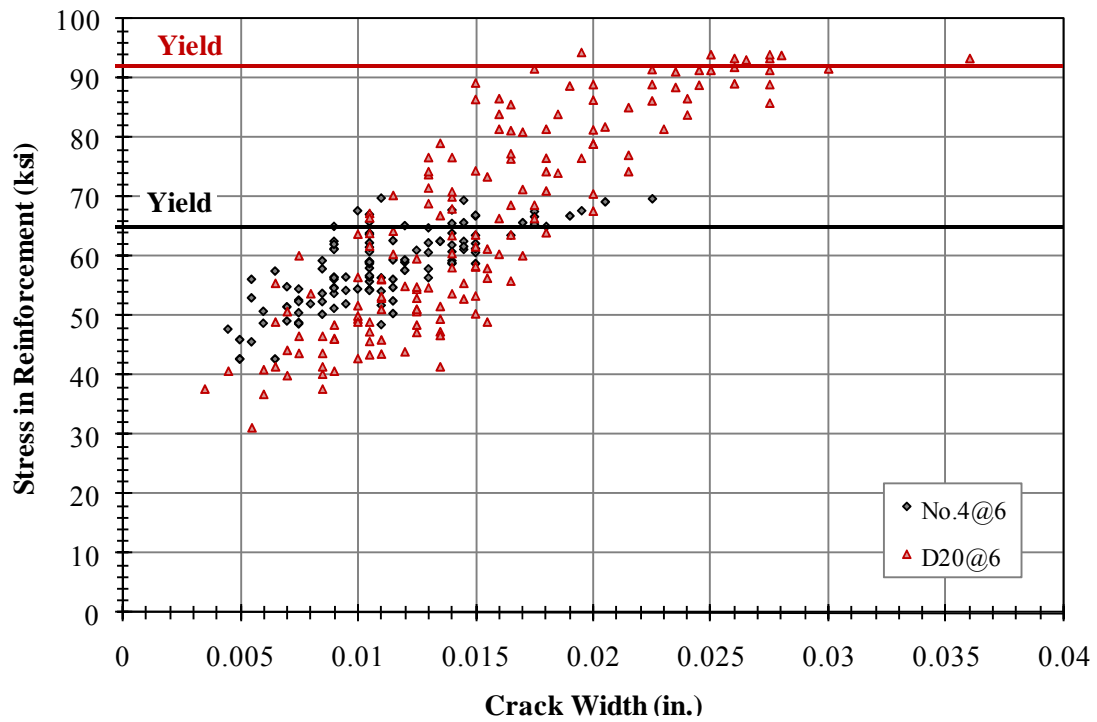


Figure 5-5: Crack Width Results for No. 4 and D20 Specimens

5.3 DISCUSSION OF TRANSVERSE REINFORCEMENT TEST RESULTS

As expected, the test results from the transverse test program were consistent and informative. First, because the transverse reinforcement involves larger bars, the specimens cracked prior to yield of the reinforcement. Second, a concrete mix with a 28-day strength of 3,980 psi lowered the cracking strength of the concrete. Third, the undesirable behavior of the CIP-PCP interface was avoided by testing the CIP slab only.

These tests allowed direct comparison of the transverse reinforcement alternatives. The results provide information in determining the usefulness of the crack width equations used in Chapter 3, the benefits of using welded wire reinforcement, and the ability to reduce the transverse reinforcement.

5.3.1 Comparison to Crack Width Equations

Because the testing program changed from a section under bending stresses to a section under pure tension, the equations of Chapter 3 were re-calculated using a uniform strain gradient. The uniform tension results of the Gergely-Lutz and CEB-FIP equations of Chapter 3 are shown in Figure 5-6 and Figure 5-7. Comparing the results of the transverse test program to the crack width equations, it is clear that the calculations are conservative. The calculated crack widths are larger than the experimental results for a given stress in the reinforcement. The Gergely-Lutz and CEB-FIP equations are based on maximum crack widths and were calibrated to be conservative. The Gergely-Lutz equation provides a reasonable, slightly conservative estimate of the crack widths of these tests.

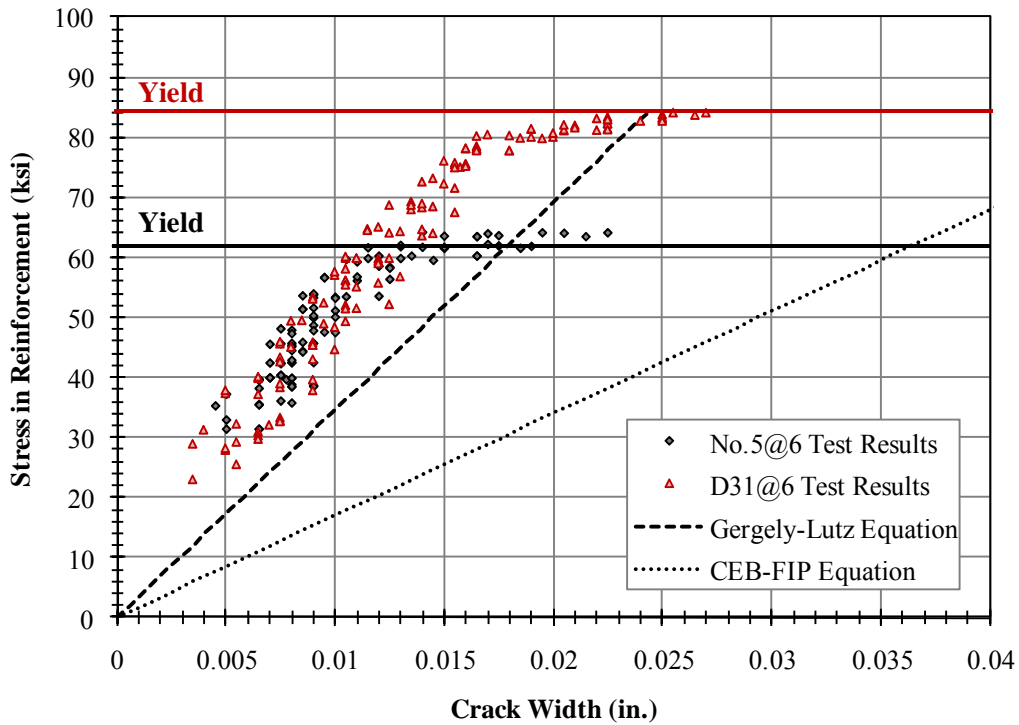


Figure 5-6: Comparison of Crack Width Equations to No. 5 and D31 Specimens

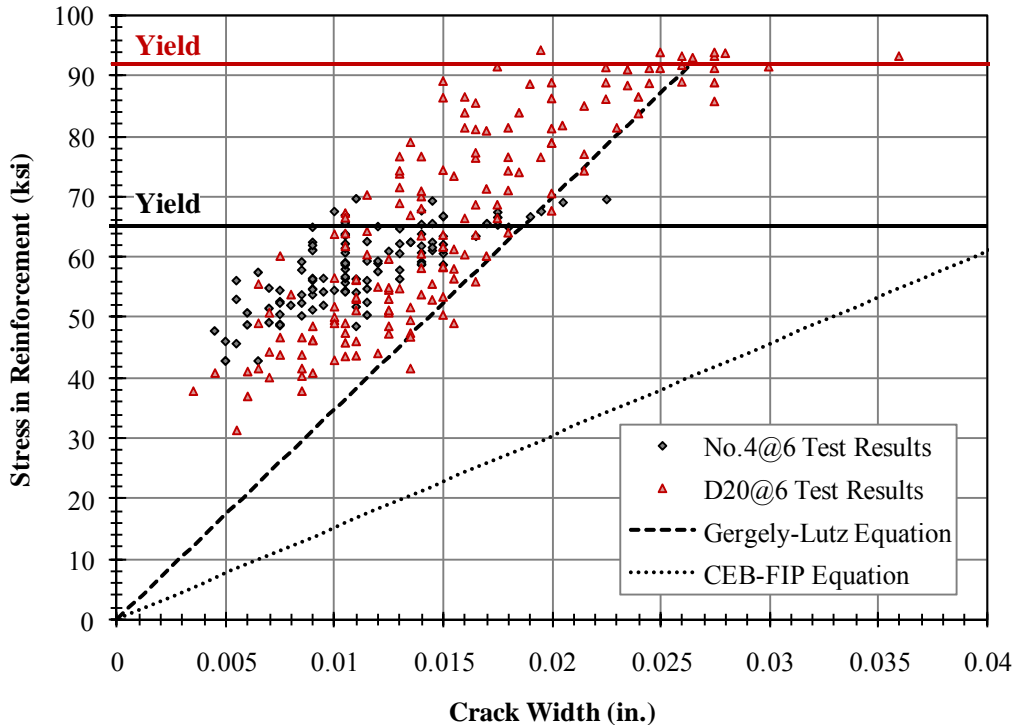


Figure 5-7: Comparison of Crack Width Equations to No. 4 and D20 Specimens

5.3.2 Benefits of Welded Wire

Based on these tests, the welded wire reinforcement is beneficial in two ways. First, the cross-wires increase the overall crack control performance. Looking at Figure 5-1 and Figure 5-2, the slope of the data after cracking provides an indication of crack control performance. A steeper slope indicates less total elongation (crack opening) at a given stress. Comparing the No. 5 and No. 4 bars to the welded wire equivalents, the welded wire controls the total crack opening much better. This benefit is difficult to see in Figure 5-4 and Figure 5-5 because there are fewer total cracks for the welded wire specimens. The widths of each crack may be similar, but there are significantly fewer cracks across the welded wire specimens.

Second, welded wire provides better crack width control at higher stresses. Looking at Figure 5-4, the No. 5 and D31 specimens exhibit similar crack widths up to 55 to 60 ksi, at which point the No. 5 bars reach yield and the crack widths increase rapidly while the D31 alternate remains linear up to nearly 80 ksi. Although the data is more scattered, similar behavior can be seen in Figure 5-5 for the No. 4 and D20 specimens.

5.3.3 Reduction of Transverse Reinforcement

Each of the transverse reinforcement alternatives appears to be a viable option for controlling longitudinal crack widths. A comparison of the four transverse reinforcement alternatives is shown in Figure 5-8 and Figure 5-9.

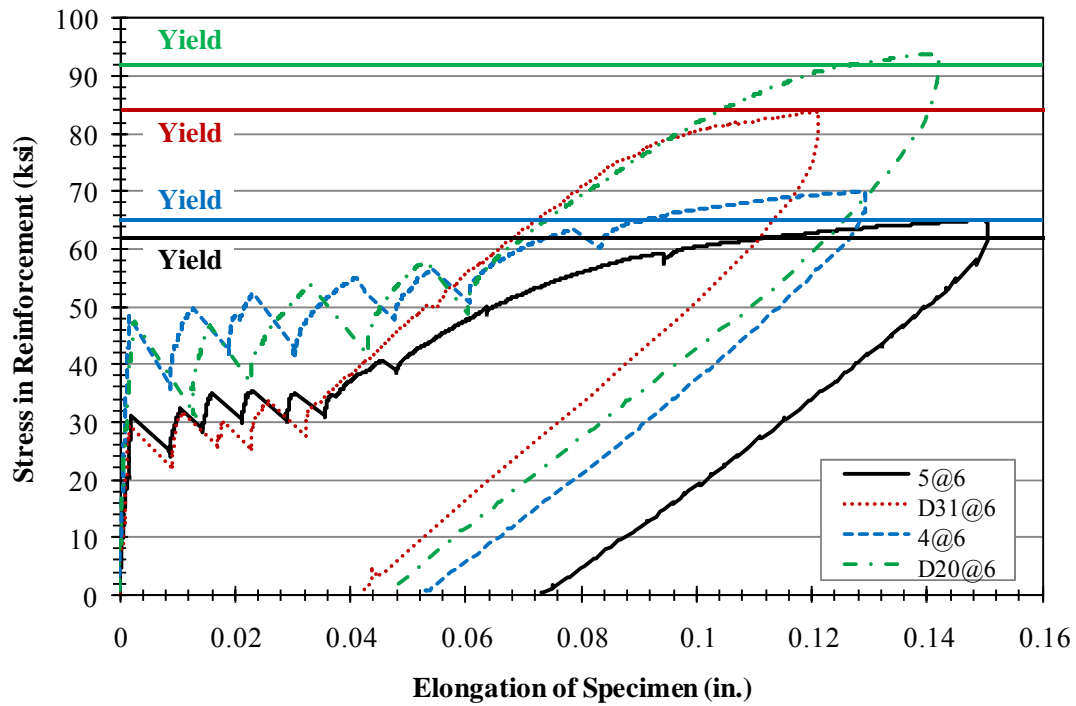


Figure 5-8: Comparison of Stress vs. Elongation for Transverse Specimens

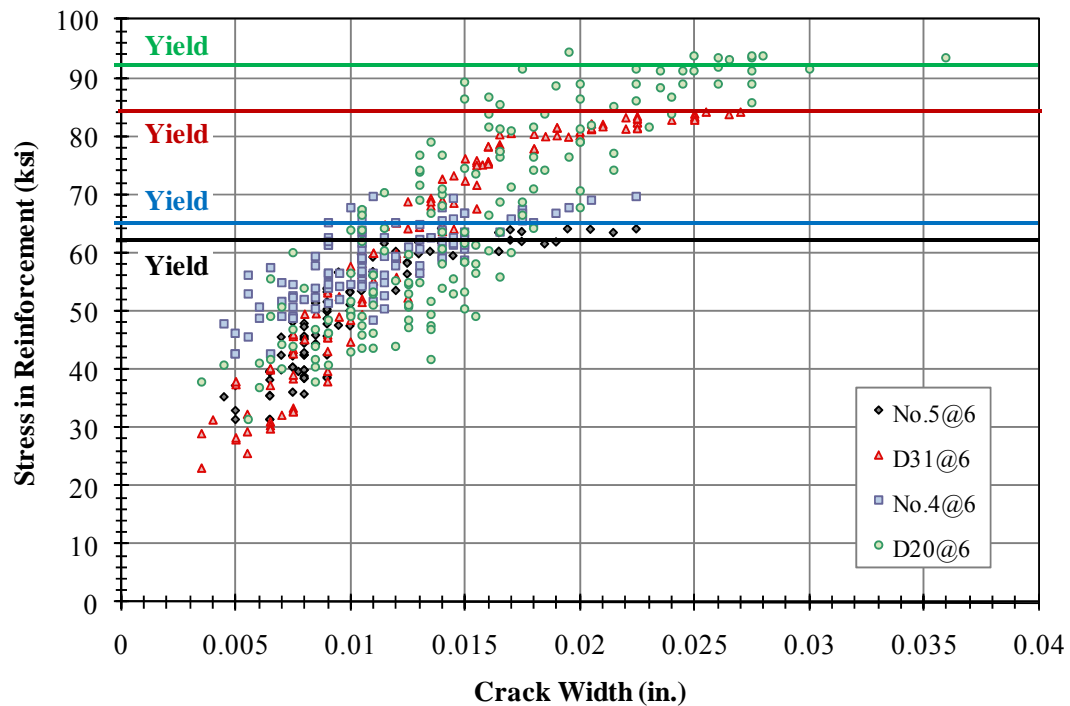


Figure 5-9: Comparison of Crack Widths for Transverse Specimens

The alternatives with the larger bar diameters (No. 5 bars and D31 welded wire) clearly control crack widths better than the smaller diameter alternatives (No. 4 bars and D20 welded wire). The crack widths for the No. 5 and D31 specimens are much less scattered, and the No. 5 and D31 reinforcement is at significantly lower stresses when cracking first occurs.

Of the two reduced steel options, the D20 option seems to be best for reducing the steel while controlling crack widths. First cracking occurs at a relatively low stress level (40 ksi cracking, 92 ksi yield), the crack control benefits are similar to the D31 welded wire (slope of the line after cracking), and the strength of the welded wire allows for crack control at higher stresses. The No. 4 bars yield soon after initial cracking (50 ksi cracking, 65 ksi yield), so there is relatively little reserve crack control capacity.

CHAPTER 6

CONCLUSIONS AND RECOMMENDATIONS

6.1 SUMMARY

Several tests were conducted to evaluate the performance of different top mat reinforcement arrangements for ability to control crack widths across PCP joints. The longitudinal reinforcement was tested using a constant bending moment test, a point load test, and several direct tension tests. Because of difficulty with the CIP-PCP interface during the longitudinal tests, direct tension tests of the CIP slab only were used to compare the transverse reinforcement alternatives. Prior to testing, various top mat design alternatives were evaluated through pre-test calculations for crack widths. Standard reinforcing bars and welded wire reinforcement were considered for the design alternatives.

6.2 CONCLUSIONS

The following conclusions are based on the results of the testing program conducted in this thesis:

- The tensile strength of the CIP slab is critical to controlling transverse crack widths.
- The CIP-PCP interface is difficult to simulate in the laboratory because of inherent eccentricities that result from the test specimen geometry and loading conditions.
- The constraint and boundary conditions of CIP-PCP bridge decks are difficult to simulate in the laboratory.
- Given the current TxDOT specifications for concrete strength, it would be imprudent to reduce the longitudinal reinforcement across the interior spans of CIP-PCP decks.

- The transverse reinforcement may be reduced using welded wire reinforcement across the interior spans of CIP-PCP decks without compromising longitudinal crack width control.

6.3 RECOMMENDATIONS

The following recommendations were developed based on the results of the testing program conducted in this thesis:

- Because of the difficulties simulating the constraint and boundary conditions with an applied load in the laboratory, field studies of the various reinforcement alternatives should be conducted either on-site or in a large restrained shrinkage test similar to those conducted in Folliard et al. (2003) or both.
- The only longitudinal reinforcement alternative from this test program that should be considered is D20 @ 9-in. o.c.
- For the transverse reinforcement, D20 @ 6-in. o.c. seem to be the most likely candidate for reducing the steel while maintaining longitudinal crack control. No. 4 @ 6-in. o.c. may also be considered, but a slight increase in longitudinal crack widths should be expected.

APPENDIX A

SAMPLE CRACK WIDTH CALCULATION

The crack width calculations were performed in Excel spreadsheets using the approach described in Chapter 3. This Appendix shows the complete calculation for two of the transverse reinforcement options, No.5 @ 6-in. o.c. and D31 @ 6-in. o.c.

A.1 NO. 5 @ 6-IN. O.C., TRANSVERSE

Output taken from RESPONSE:

Strain in reinforcement (at 7.91 k-ft) = 0.172×10^{-3} in./in.

Strain in concrete at top of deck (at 7.91 k-ft) = 0.353×10^{-3} in./in.

Gergely-Lutz Calculation:

$$w_{\max} = 2.2 \beta \epsilon_s (d_c A)^{1/3}$$

w_{\max} = maximum crack width

β = factor accounting for strain gradient = 2.05
 = h_2 / h_1 (from RESPONSE)

h_2 = distance from extreme tension fiber to neutral axis = 4.51 in.

h_1 = distance from reinforcement to neutral axis = 2.196 in.

ϵ_s = strain in steel (taken from RESPONSE) = 0.172×10^{-3} in./in.

d_c = distance from top of slab to the reinforcement = 2.31 in.
 = 2 in. + 0.625 in. / 2 = 2.31 in.

A = effective area of concrete surrounding each bar/wire = 27.04 in.²
 = 6 in. x 4.51 in. = 27.04 in.²

$$w_{\max} = 2.2 \times 2.05 \times 0.172 \times 10^{-3} \times (2.31 \times 27.04)^{1/3} = \mathbf{0.0031 \text{ in.}}$$

CEB-FIP Calculation:

$$s_m = 2 (c + s/10) + k_1 k_2 (d_b/\rho_{ef})$$

s_m = average crack spacing

c = clear cover = 2 in.

s = maximum spacing between bars (limited to $15d_b$) = 6 in.
 k_1 = bond properties of bars (0.4 for deformed bars)
 k_2 = factor for strain gradient (calculated using RESPONSE output)
 $= 0.25 \times (\epsilon_{\max} \text{ in embedment zone} + \epsilon_{\min}) / (2 \times \epsilon_{\max})$
 $= 0.25 \times (0.353 \times 10^{-3} + 0) / (2 \times 0.353 \times 10^{-3}) = 0.125$
 d_b = diameter of bar/wire = 0.625 in.
 ρ_{ef} = area of steel / area of effective embedment zone of concrete
 $= 0.62 \text{ in.}^2 / (12 \text{ in.} \times 4.51 \text{ in.}) = 0.0115$
 $s_m = 2 (2 + 6/10) + 0.4 \times 0.125 \times 0.625/0.0115 = 7.93 \text{ in.}$
 $w_{\text{avg}} = s_m \times \text{strain at top of deck} = 7.93 \text{ in.} \times 0.353 \times 10^{-3} \text{ in./in.} = 0.0028 \text{ in.}$
 $w_{\text{max}} = 1.7 \times w_{\text{avg}} = \mathbf{0.0048 \text{ in.}}$

A.2 D31 @ 6-IN. O.C., TRANSVERSE

Output taken from RESPONSE:

Strain in reinforcement (at 7.91 k-ft) = $0.105 \times 10^{-3} \text{ in./in.}$

Strain in concrete at top of deck (at 7.91 k-ft) = $0.241 \times 10^{-3} \text{ in./in.}$

Gergely-Lutz Calculation:

$$w_{\text{max}} = 2.2 \beta \epsilon_s (d_c A)^{1/3}$$

w_{max} = maximum crack width

β = factor accounting for strain gradient = 2.30
 $= h_2 / h_1$ (from RESPONSE)

h_2 = distance from extreme tension fiber to neutral axis = 4.10 in.

h_1 = distance from reinforcement to neutral axis = 1.78 in.

ϵ_s = strain in steel (taken from RESPONSE) = $0.105 \times 10^{-3} \text{ in./in.}$

d_c = distance from top of slab to the reinforcement = 2.31 in.
 $= 2.5 \text{ in.} + 0.625 \text{ in.} / 2 = 2.31 \text{ in.}$

A = effective area of concrete surrounding each bar/wire = 24.6 in.^2
 $= 6 \text{ in.} \times 4.10 \text{ in.} = 24.6 \text{ in.}^2$

$$w_{\text{max}} = 2.2 \times 2.3 \times 0.105 \times 10^{-3} \times (2.31 \times 24.6)^{1/3} = \mathbf{0.00204 \text{ in.}}$$

CEB-FIP Calculation:

$$s_m = 2 (c + s/10) + k_1 k_2 (d_b/\rho_{ef})$$

s_m = average crack spacing

c = clear cover = 2 in.

s = maximum spacing between bars (limited to $15d_b$) = 6 in.

k_1 = bond properties of bars (0.4 for deformed bars)

k_2 = factor for strain gradient (calculated using RESPONSE output)

$$= 0.25 \times (\epsilon_{\max} \text{ in embedment zone} + \epsilon_{\min}) / (2 \times \epsilon_{\max})$$

$$= 0.25 \times (0.241 \times 10^{-3} + 0) / (2 \times 0.241 \times 10^{-3}) = 0.125$$

d_b = diameter of bar/wire = 0.625 in.

ρ_{ef} = area of steel / area of effective embedment zone of concrete

$$= 0.62 \text{ in.}^2 / (12 \text{ in.} \times 4.10 \text{ in.}) = 0.0126$$

$$s_m = 2 (2 + 6/10) + 0.4 \times 0.125 \times 0.625/0.0126 = 7.68 \text{ in.}$$

$$w_{\text{avg}} = s_m \times \text{strain at top of deck} = 7.68 \text{ in} \times 0.241 \times 10^{-3} \text{ in/in} = 0.00185 \text{ in.}$$

$$w_{\text{max}} = 1.7 \times w_{\text{avg}} = \mathbf{0.00315 \text{ in.}}$$

APPENDIX B

STEEL REINFORCEMENT MATERIAL TESTS

B.1 A605 REINFORCING BARS

ASTM A605 reinforcing bars from the same heat of steel were used for the entire longitudinal reinforcement test program in Chapter 4 except the last CIP-only test (Section 4.7). The stress-strain curve for the A605 reinforcement is shown in Figure B-1. In Figure B-2, the stress is plotted against total deflection of the loading head. The yield stress of the A605 reinforcing bars was 63 ksi and the ultimate stress was 92 ksi.

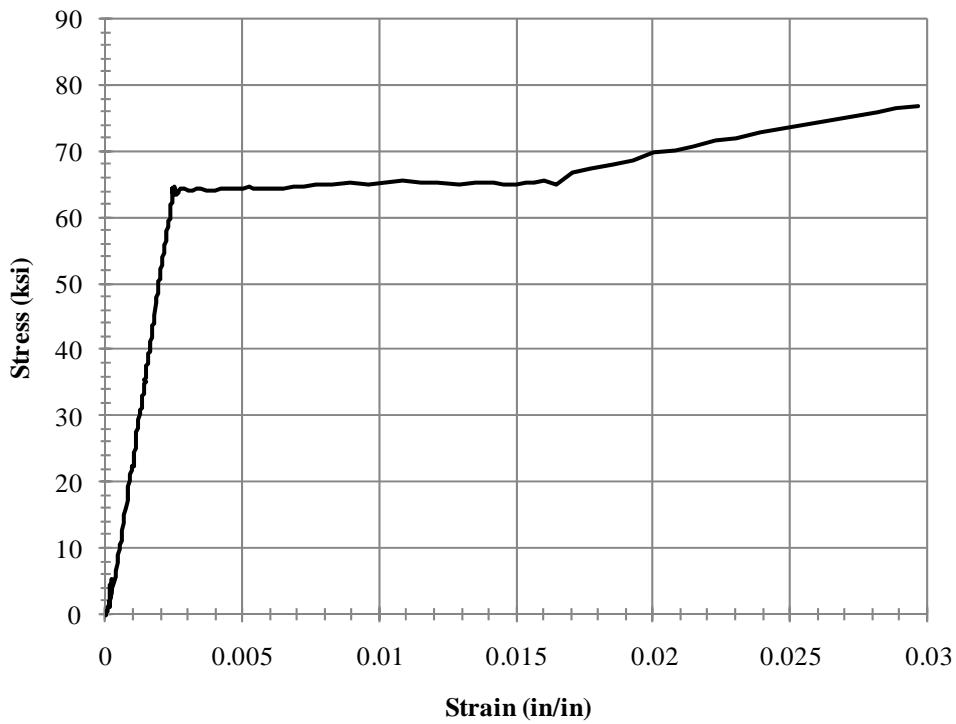


Figure B-1: Stress-Strain for A605 Reinforcing Bars

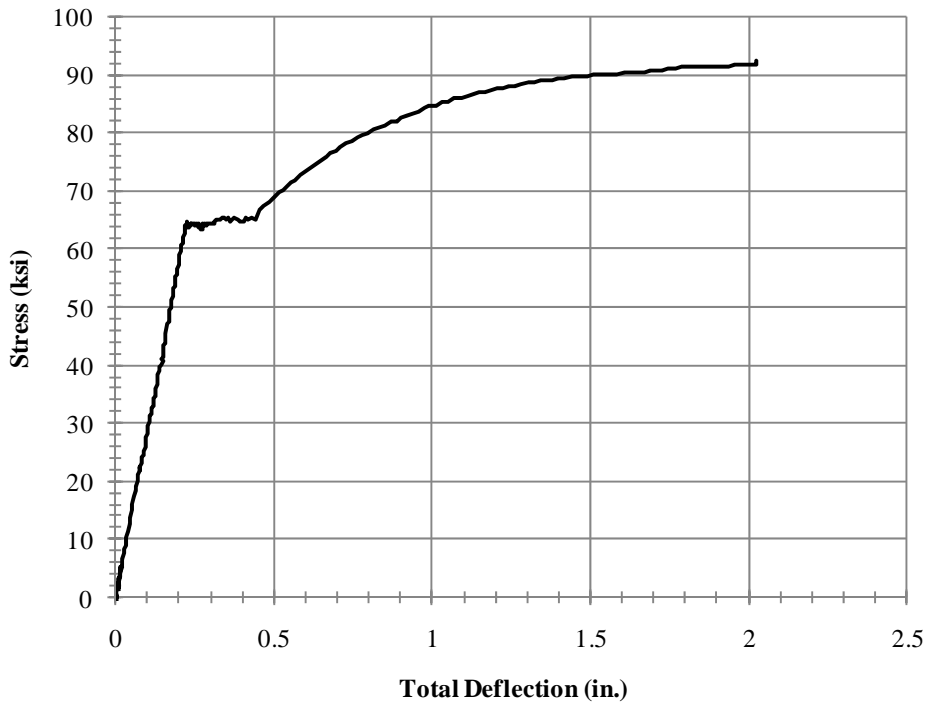


Figure B-2: Stress vs. Total Deflection for A605 Reinforcing Bars

B.2 A706 REINFORCING BARS

ASTM A706 reinforcing bars were used for the transverse reinforcement test program as well as the last longitudinal reinforcement test specimen (Section 4.7). The stress-strain curve for the No. 5 and No. 4 reinforcement is shown in Figure B-3 and Figure B-4, respectively. The total deflection was not recorded for the A706 bars; however, the ultimate strength for the No.5 and No. 4 bars is shown in Figure B-5 and Figure B-6, respectively, which plot stress against time. The yield strength of the No. 5 bars was 62 ksi with an ultimate strength of 96 ksi. The yield strength of the No. 4 bars was 65 ksi with an ultimate strength of 100 ksi.

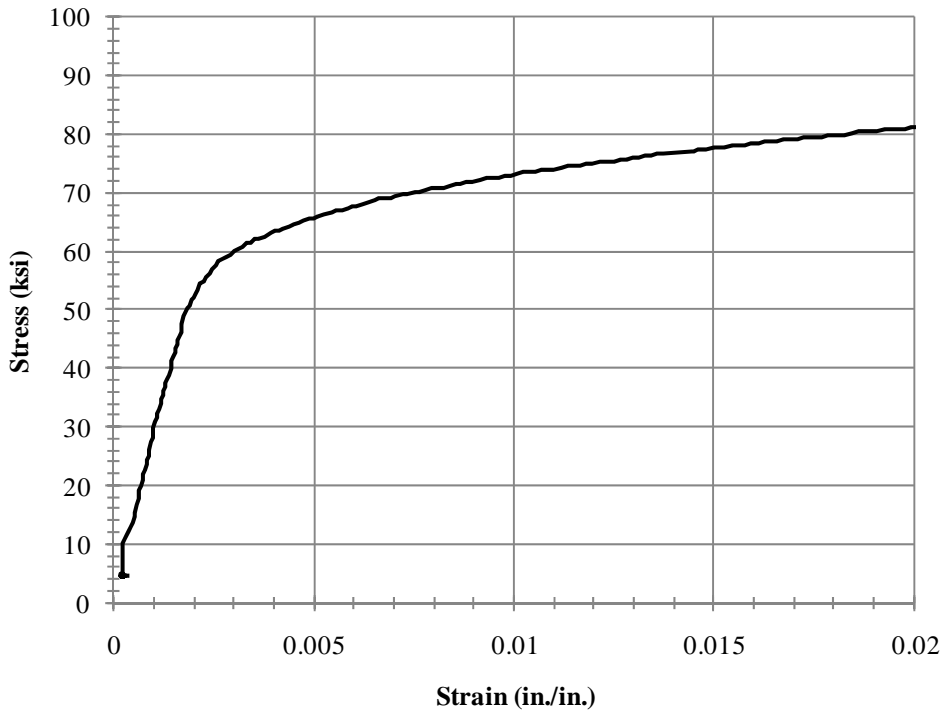


Figure B-3: Stress-Strain for No. 5 A706 Reinforcing Bars

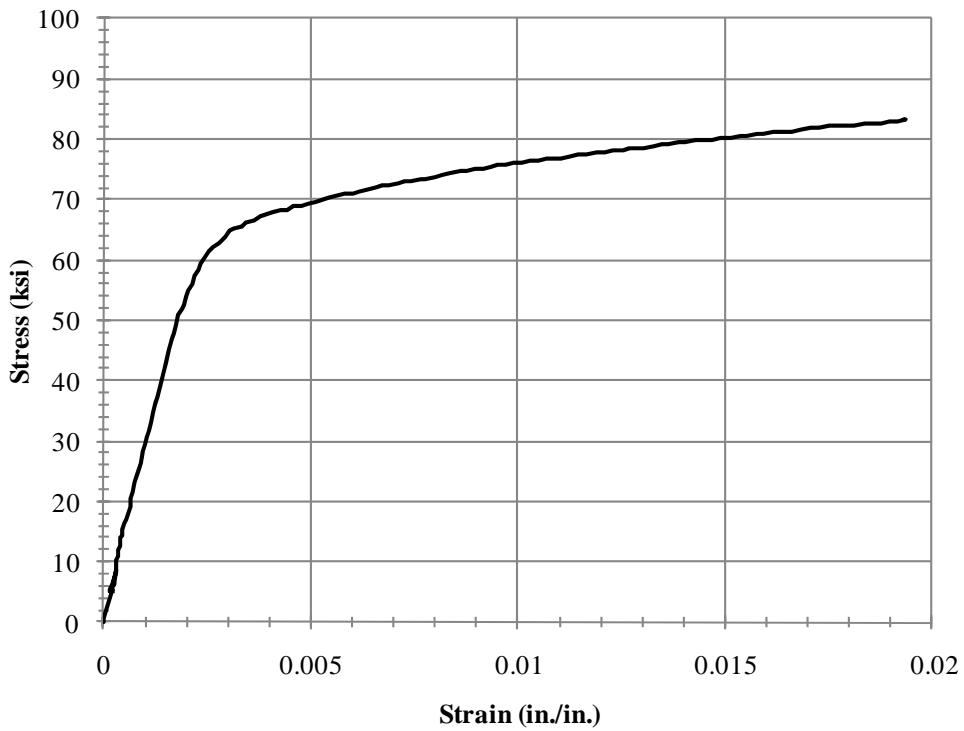


Figure B-4: Stress-Strain for No. 4 A706 Reinforcing Bars

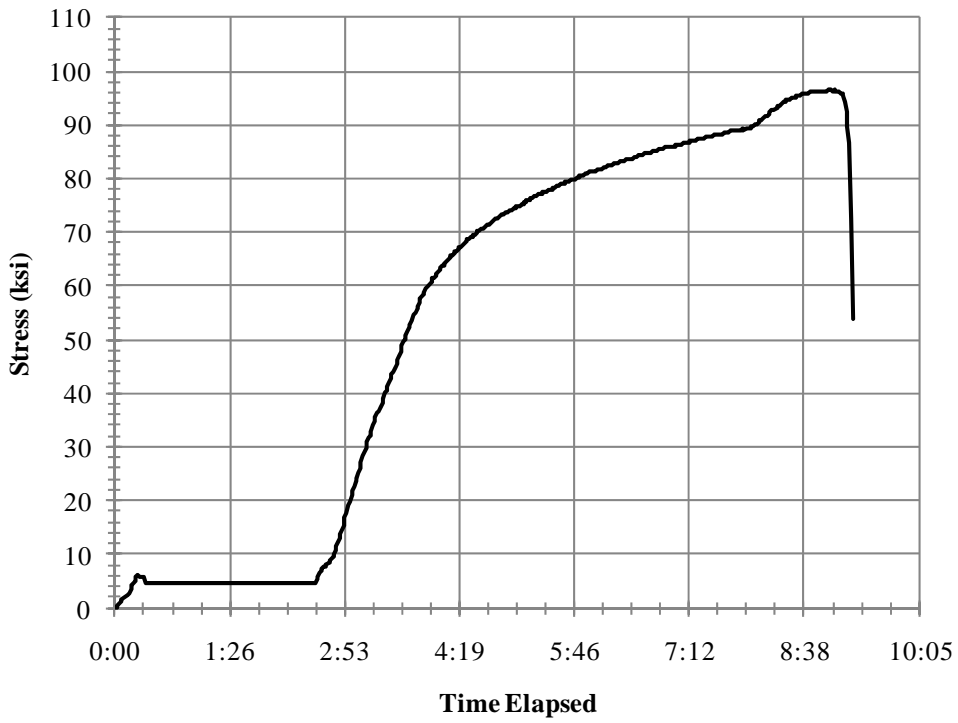


Figure B-5: Stress vs Time for No. 5 A706 Reinforcing Bars

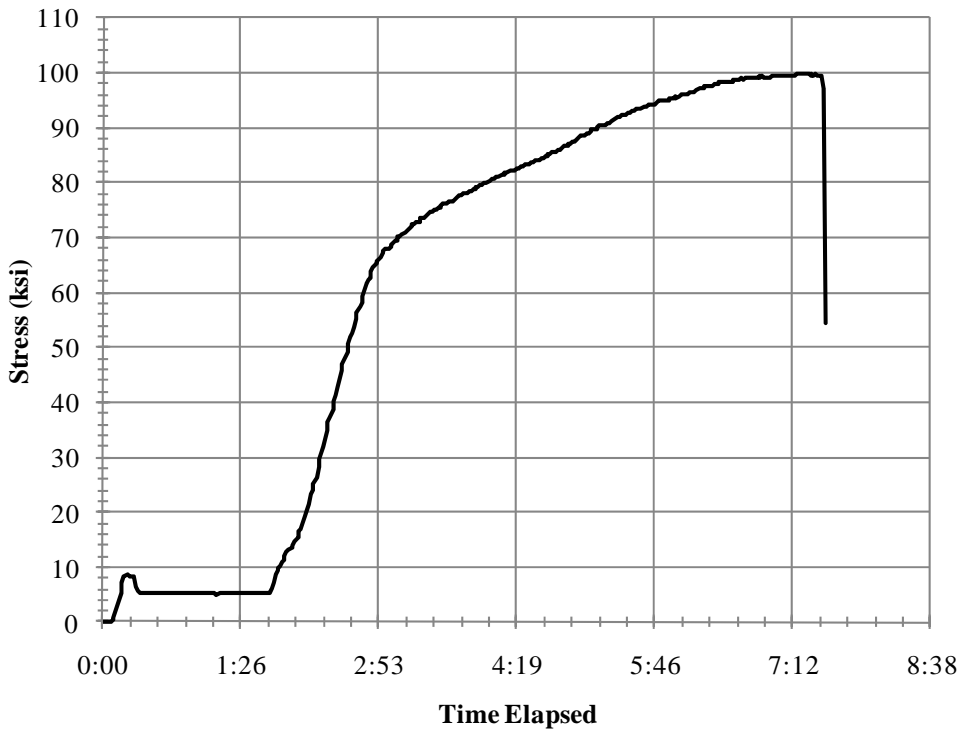


Figure B-6: Stress vs. Time for No. 4 A706 Reinforcing Bars

B.3 A185 WELDED WIRE REINFORCEMENT

ASTM A185 welded wire reinforcement was used for the transverse reinforcement test program. The stress-strain curve for the D31 and D20 reinforcement is shown in Figure B-7 and Figure B-8, respectively. The stress is plotted against total deflection of the loading head for the D31 and D20 reinforcement in Figure B-9 and Figure B-10, respectively. The yield strength of the D31 welded wire was 84 ksi with an ultimate strength of 94 ksi. The yield strength of the D20 welded wire was 92 ksi with an ultimate strength of 103 ksi.

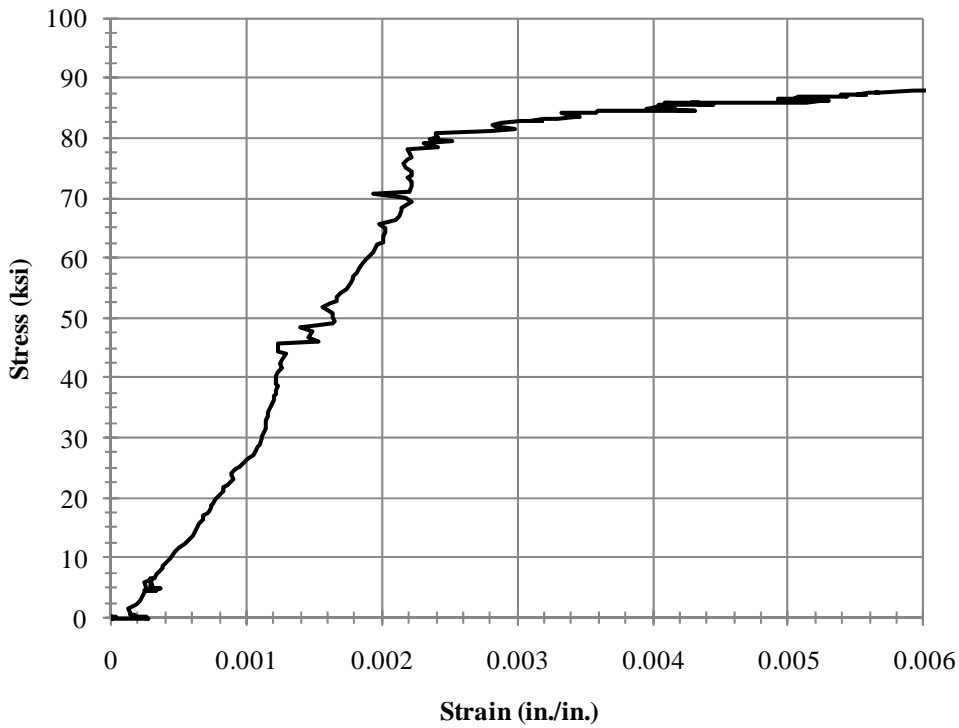


Figure B-7: Stress-Strain for D31 Reinforcement

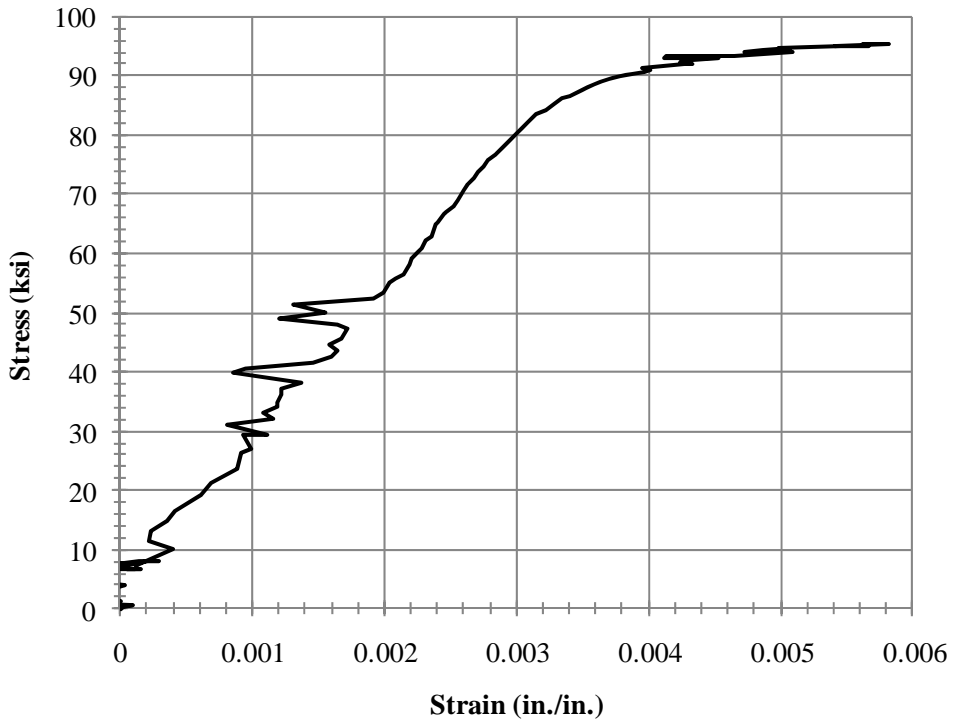


Figure B-8: Stress-Strain for D20 Reinforcement

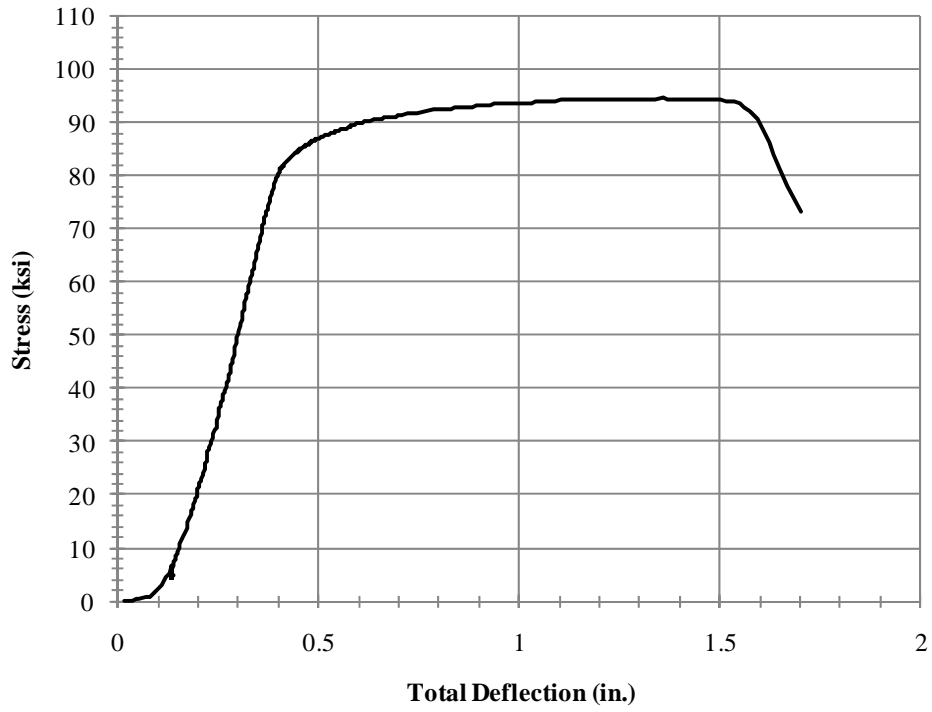


Figure B-9: Stress vs. Total Deflection for D31 Reinforcement

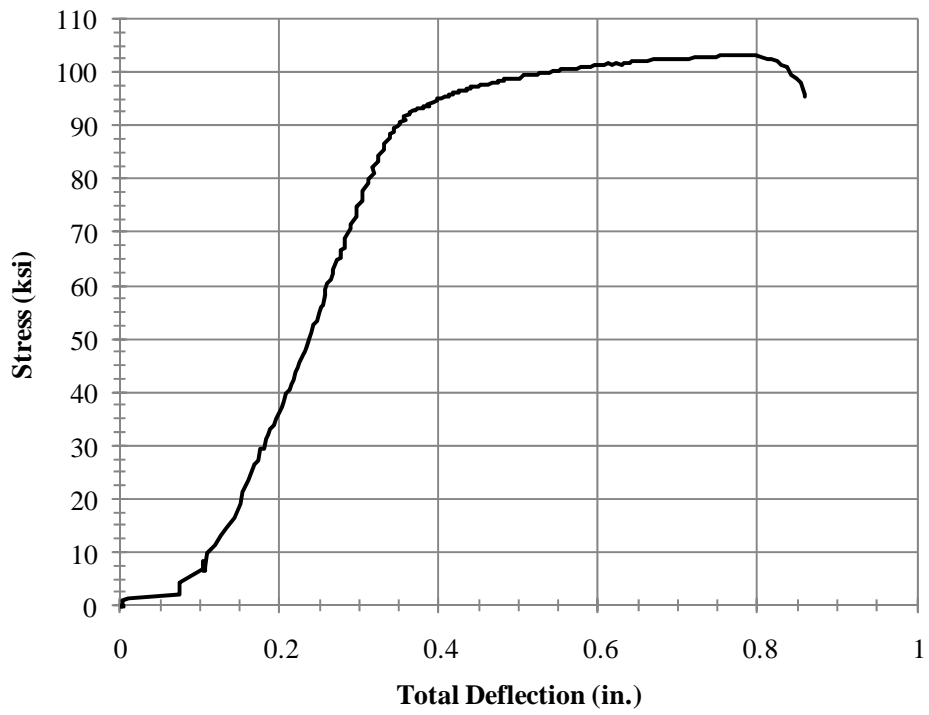


Figure B-10: Stress vs. Total Deflection for D20 Reinforcement

REFERENCES

- Abendroth, R. E. (1994). Deformations in composite prestressed concrete bridge deck panels. *Journal of Structural Engineering* , 120 (11), 3233-3242.
- ACI Committee 318. (2008). *Building Code Requirements for Structural Concrete (ACI 318-08) and Commentary (ACI318R-08)*. Farmington Hills, MI: American Concrete Institute.
- Agnew, L. S. (2007). *Evaluation of the Fatigue Behavior of Bridge Decks with Precast Panels at Expansion Joints*. Master's Thesis: The University of Texas at Austin.
- Atlas, A., Siess, C. P., & Kesler, C. E. (1965). Behavior of one-way concrete floor slabs reinforced with welded wire fabric. *Journal of the American Concrete Institute* , 62 (5), 539-555.
- Azad, A. K., Baluch, M. H., Abbasi, M. S., & Kareem, K. (1994). Punching capacity of deck slabs in ger-slab bridges. *ACI Structural Journal* , 91 (6), 656-662.
- Barker, J. M. (1975). Research, application, and experience with precast prestressed bridge deck panels. *PCI Journal* , 20 (6), 66-85.
- Barnoff, R. M., & Rainey, D. E. (1974). *Laboratory Test of Prestressed Concrete Deck Planks and Deck Plank Assemblies*. The Pennsylvania Transportation Institute. Research Project No. 71-8 An Experimental Prestressed Concrete Bridge Report No. 2.
- Batchelor, B. d., & Hewitt, B. E. (1976). Tests of model composite bridge decks. *ACI Journal* , 73 (6), 340-343.
- Beeby, A. W. (2006, Dec.). The influence of the parameter ϕ/p_{eff} on crack widths. *Structural Concrete* , 137-142.
- Bieschke, L. A., & Klingner, R. E. (1982). *The Effect of Transverse Strand Extensions on the Behavior of Precast Prestressed Panel Bridges*. Center for Transportation Research, Summary Report 303-1F(S).

- Black, M. S. (1975). Ultimate strength of two-way concrete slabs. *ASCE Journal of the Structural Division* , 101 (ST1), 311-324.
- Boswell, C. A. (2008). *Simple Design Details using Precast Concrete Panels at Skewed Expansion Joints*. Master's Thesis: The University of Texas at Austin.
- Broms, B. B. (1965). Crack width and crack spacing in reinforced concrete members. *Journal of the American Concrete Institute* , 62 (10), 1237-1255.
- Brotchie, J., & Holley, M. (1971). Membrane action in slabs. *ACI Special Publication 30: Cracking, Deflection, and Ultimate Load of Concrete Slab Systems* , pp. 345-377.
- Buth, E., Furr, H. L., & Jones, H. L. (1972). *Evaluation of a Prestressed Panel, Cast-in-Place Concrete Bridge*. Texas Transportation Institute, Research Report 145-3.
- CEB-FIP. (1978). *Model Code for Concrete Structures: CEB-FIP International Recommendations, 3rd ed.* Paris: Comite Euro-International du Beton.
- Christiansen, K. P. (1963). The effect of membrane stresses on the ultimate strength of the interior panel in a reinforced concrete slab. *The Structural Engineer* , 41 (8), 261-265.
- Collins, M., & Mitchell, D. (1997). *Prestressed Concrete Structures*. Toronto, Canada: Response Publications.
- Coselli, C. J. (2004). *Behavior of Bridge Decks with Precast Panels at Expansion Joints*. Master's Thesis: The University of Texas at Austin.
- Coselli, C. J., Griffith, E. M., Ryan, J. L., Bayrak, O., Jirsa, J. O., Breen, J. E., et al. (2006). *Bridge Slab Behavior at Expansion Joints*. Center for Transportation Research, TxDOT Research Report 0-4418-1.
- Csagoly, P., Holowka, M., & Dorton, R. (1978). The true behavior of thin concrete bridge slabs. *Transportation Research Record* (664), 171-179.
- Desayi, P., & Kulkarni, A. B. (1977). Load-deflection behavior of restrained r/c slabs. *ASCE Journal of the Structural Division* , 103 (ST2), 405-419.
- DeStefano, R. J., Evans, J., Tadros, M. K., & Sun, C. (2003). Flexural crack control in concrete bridge structures. *Proceedings of the 3rd International Symposium on High-Performance Concrete*. Orlando, FL.

- Donnelly, K. S. (2009). *Influence of Precast Concrete Panel Surface Condition on Behavior of Composite Bridge Decks at Skewed Expansion Joints*. Master's Thesis: The University of Texas at Austin.
- Dowell, R. K., & Smith, J. W. (2006, March-April). Structural tests of precast, prestressed concrete deck panels for California freeway bridges. *PCI Journal* , 2-13.
- Ebeido, T., & Kennedy, J. B. (1996). Punching strength of deck slabs in skew composite bridges. *Journal of Bridge Engineering* , 1 (2), 59-66.
- Felber, A. J. (1990, April 12). RESPONSE. *Version 1.0*. Department of Civil Engineering, University of Toronto.
- Folliard, K., Smith, C., Sellers, G., Brown, M., & Breen, J. E. (2003). *Evaluation of Alternative Materials to Control Drying-Shrinkage Cracking in Concrete Bridge Decks*. Center for Transportation Research, TxDOT Research Report 0-4098-4.
- Frosch, R. J. (2001). Flexural crack control in reinforced concrete. *Design and Construction Practices to Mitigate Cracking (ACI SP-204)* , 135-154.
- Gamble, W. L., Sozen, M. A., & Seiss, C. (1969). Tests of a two-way reinforced concrete slab. *ASCE Journal of the Structural Division* , 95 (ST6), 1073-1096.
- Gergely, P., & Lutz, L. A. (1968). Maximum Crack Width in Reinforced Concrete Flexural Members. *Causes, Mechanisms, and Control of Cracking in Concrete (ACI SP-20)* , 87-117.
- Graddy, J. C., Kim, J., Whitt, J. H., Burns, N. H., & Klingner, R. E. (2002). Punching-shear behavior of bridge decks under fatigue loading. *ACI Structural Journal* , 99 (3), 257-266.
- Hon, A., Taplin, G., & Al-Mahaidi, R. S. (2005, May-June). Strength of reinforced concrete bridge decks under compressive membrane action. *ACI Structural Journal* , 1-11.
- Ivy Steel & Wire. (2009). *How to Specify*. Retrieved February 10, 2010, from Ivy Steel & Wire Web site: http://www.ivysteel.com/how_to_specify.htm

- Jones, H. L., & Furr, H. L. (1970). *Study of In-Service Bridges Constructed with Prestressed Panel Sub-Decks*. Texas Transportation Institute, Research Report 145-1.
- Kluge, R. W., & Sawyer, H. A. (1975). Interacting pretensioned concrete form panels for bridge decks. *PCI Journal* , 20 (3), 34-61.
- Krauss, P. D., & Rogalla, E. A. (1996). *NCHRP Report 380: Transverse Cracking in Newly Constructed Bridge Decks*. Washington, D.C.: National Academy Press.
- Kuang, J., & Morley, C. (1992). Punching shear behavior of restrained reinforced concrete slabs. *ACI Structural Journal* , 89 (1), 13-19.
- Lee, S. L., Mansur, M. A., Tan, K. H., & Kasiraju, K. (1987, Nov.-Dec.). Cracking behavior of concrete tension members reinforced with welded wire fabric. *ACI Structural Journal* , 481-491.
- Liebeberg, A. C. (1966). Arching action in concrete slabs. *National Building Research Institute, Council for Scientific and Industrial Research: Report 234* .
- Lloyd, J. P., Rejali, H. M., & Kesler, C. E. (1969, May). Crack control in one-way slabs reinforced with deformed welded wire fabric. *ACI Journal* , 366-376.
- Merrill, B. D. (2002). *Texas' Use of Precast Concrete Stay-in-Place Forms for Bridge Decks*. 2002 Concrete Bridge Conference. TxDOT.
- Miller, R. A., Aktan, A. E., & Shahrooz, B. M. (1994). Destructive testing of decommissioned concrete slab bridge. *Journal of Structural Engineering* , 120 (7), 2176-2198.
- Nawy, E. G. (1968, October). Crack control in reinforced concrete structures. *ACI Journal* , 825-836.
- Ockleston, A. J. (1958). Arching action in reinforced concrete slabs. *The Structural Engineer* , 36 (6), 197-201.
- Ockleston, A. J. (1955). Load tests on a three storey reinforced concrete building in Johannesburg. *The Structural Engineer* , 33, 304-322.

- Park, R. (1965). The lateral stiffness and strength required to ensure membrane action at the ultimate load of a reinforced concrete slab and beam floor. *Magazine of Concrete Research* , 17 (50), 29-38.
- Park, R., & Gamble, W. L. (2000). Membrane action in slabs. In *Reinforced Concrete Slabs* (2nd Edition ed., pp. 636-694). John Wiley & Sons, Inc.
- Quinn, K. (2009, May 8). FINAL PROJECT: CE 383P. *Version 1.0*. Department of Civil Engineering, University of Texas at Austin.
- Tammo, K., & Thelandersson, S. (2009). Crack behavior near reinforcing bars in concrete structures. *ACI Structural Journal* , 106 (3), 259-267.
- Taylor, S. E., Rankin, B., Cleland, D. J., & Kirkpatrick, J. (2007). Serviceability of bridge deck slabs with arching action. *ACI Structural Journal* , 104 (1), 39-48.

VITA

Stephen Wroe Foster was born in Houston, Texas on April 23, 1986, the son of Michael Chisholm Foster and Colleen Marie Foster, the brother of Michael Chisholm Foster, Jr. After completing his work at James E. Taylor High School in Katy, Texas in 2004, Stephen entered The University of Texas at Austin and received a Bachelor of Science in Architectural Engineering in May 2008. After marrying his wife Jill Valerie Foster on May 24, 2008, he enrolled in the graduate program in structural engineering at the University of Texas at Austin and graduated with a Master of Science in Engineering in May 2010.

Permanent Address: 19615 Emerald Ridge Lane
 Houston, Texas 77094

This thesis was typed by the author.